

STRUCTURE AND KINETICS OF GLASS CORROSION

BY

DAVID M. SANDERS

A DISSERTATION PRESENTED TO THE GRADUATE COUNCIL
OF THE UNIVERSITY OF FLORIDA
IN PARTIAL FULFILLMENT OF THE REQUIREMENTS FOR THE
DEGREE OF DOCTOR OF PHILOSOPHY

UNIVERSITY OF FLORIDA

1973

To my wife, Marilyn

ACKNOWLEDGEMENTS

The author thanks R. Condrate for sparking an interest in materials spectroscopy while at Alfred. At the University of Florida, the author became indebted to W. B. Person for the use of his spectrometers and for aid in the interpretation of many of the results of this work related to infrared spectroscopy. The author is especially indebted to his advisor, L. L. Hench, who provided invaluable encouragement, advice, and assistance throughout the entire study. Finally, the author wishes to thank his wife, Marilyn, without whose help and encouragement this research would not have been possible.

This work was supported in part by the Office of Naval Research and in part by the Glass Container Corporation.

TABLE OF CONTENTS

	Page
ACKNOWLEDGEMENTS	iii
LIST OF TABLES	vi
LIST OF FIGURES	vii
ABSTRACT	xii
Chapter	
I INTRODUCTION	1
II METHODS FOR STUDYING GLASS CORROSION KINETICS	10
Infrared Reflection	10
Continuous Atomic Emission	12
The Optical System	12
The Minirig System	17
The Automated System	24
Continuous Atomic Emission	33
III QUANTITATIVE ANALYSIS OF GLASS STRUCTURE USING INFRARED REFLECTION SPECTRA	37
Methods	38
Results	40
Discussion of Results	49
Conclusions	68
IV ANALYSIS OF SILICA-RICH GELS FORMED DURING GLASS CORROSION	70
Methods	76
Results	78
Discussion	93
Conclusions	101

TABLE OF CONTENTS (continued)

Chapter	Page
V CORROSION OF A LITHIA-SILICA GLASS IN VARIOUS AQUEOUS ENVIRONMENTS	103
Methods	104
Results	105
Discussion	117
Conclusions	131
VI SURFACE ROUGHNESS EFFECTS ON GLASS CORROSION	133
Results	135
Discussion of Results	152
Conclusions	154
VII CONCLUSIONS AND NEW STUDIES	156
BIBLIOGRAPHY	162
BIOGRAPHICAL SKETCH	167

LIST OF TABLES

Table		Page
1	Examples of General Corrosion Conditions and Sample States Which Might Influence Corrosion Behavior	5
2	X-ray Analysis of Corroded and Auto- claved 33L Glass	114

LIST OF FIGURES

Figure		Page
1	The ray diagram for the optical system used in reflection studies made using the expanded sample compartment of the Perkin-Elmer model 621 spectrometer	14
2	Sample-holding device ("minirig") shown mounted in aluminum holder, which is in turn permanently fixed to the Plexiglas mounting block	16
3	Minirig sample holder showing a sample mounted under stress being applied through the loading bars	19
4	Infrared reflection spectra of a corroded and of a freshly abraded glass of a composition corresponding to lithium disilicate	21
5	Corrosion cells used in this study as described in the text	23
6	"Automated system" showing one sample rotated from the corrosion bath position into the position for reflectance measurement	26
7	Reflectance at 985 cm^{-1} of a lithium disilicate glass (Δ) as a function of time, compared to that from a standard composed of non-corroding vitreous silica	30
8	Schematic drawing of atomic emission sampling techniques used in this study . .	34
9	Compositional dependent changes in infrared reflection spectra in the lithia-silica system	42
10	Compositional dependent changes in infrared reflection spectra in the soda-silica system	44

LIST OF FIGURES (continued)

Figure		Page
11	Compositional dependent changes in infrared reflection spectra in the potash-silica system	46
12	A comparison of infrared spectra of 50 mole % $\text{Na}_2\text{O-SiO}_2$ glasses	48
13	The reflectance of the silicon-oxygen stretching maximum as a function of composition for the three systems studied	51
14	The reflectance of the silicon-oxygen rocking maximum as a function of composition for the three systems studied . . .	52
15	The reflectance of the silicon non-bridging oxygen vibration associated with alkali ion as a function of composition	53
16	The comparison between the recorded and calculated spectra of phase separation in a 25 mole % $\text{Li}_2\text{O-SiO}_2$ glass as described in the text	56
17	Spectra of the silicon-oxygen rocking peak for the three systems studied showing reflectance due to lithium vibration (L) as described in the text	62
18	Plot of the difference in reflectance at 520 cm^{-1} between the spectrum of vitreous silica and those of lithia-silica glasses.	64
19	Infrared spectrum of a 50 mole % SiO_2 glass	67
20	Two simplified models of the composition profile of the silica-rich corrosion layer	74
21	An example of data obtained from solution analysis of glass corrosion and its relation to the calculated quantities α , ϵ , and β	80

LIST OF FIGURES (continued)

Figure		Page
22	Changes in infrared reflection spectra of 33L glass on exposure to static water at 40°C	82
23	A comparison of the corroded and non-corroded glass spectra in the soda-silica system	84
24	A summary of the plots of ϵ and α calculated from all the solution analysis data reported in this work	86
25	An S.E.M. micrograph of the edge of the corroded layer of 33L glass exposed to static water for 350 minutes at 79.5°C . .	88
26	A composition profile of the corroded 33L glass film obtained with an electron microprobe	91
27	A comparison of normalized infrared reflectance plots with normalized ϵ behavior for corrosion of 33L at 40°C . .	92
28	A comparison of normalized infrared reflectance plots with normalized ϵ behavior for corrosion of 33L at 79.5°C .	94
29	Plots of the various reaction coordinates described in this work to obtain apparent activation energies	96
30	Changes in the infrared spectrum of 33L glass with exposure to 100% relative humidity at room temperature	107
31	Comparison of the extent of possible reaction determined by the reflectance of the stretching (S) and non-bridging oxygen (NSL) peaks of 33L glass exposed to both 0.9 ml of static liquid water and 100% relative humidity .	110
32	Infrared spectra of 33L glass given the crystallization treatments shown . . .	112

LIST OF FIGURES (continued)

Figure		Page
33	Changes in the infrared reflection spectra of 33L glass on exposure to 85% relative humidity	116
34	Comparison of the extent of reaction, determined by the magnitude of the stretching peak reflectance (S), for 33L glass exposed to water under static and flowing conditions	119
35	Changes in infrared reflection spectra upon exposure of 33L to water containing corrosion cells of different volumes and to the residual water present in a desiccator filled with Drierite	121
36	Changes in infrared reflection spectra upon exposure of 33L glass to hydrochloric acid, to a basic solution used to corrode 33L powder, and to hydrofluoric acid	123
37	S.E.M. micrographs of 33L glass having the following corrosion histories: A. freshly abraded with dry 600 grit SiC B. 4.5 hours with 0.9 ml static water C. 120 hours with 0.9 ml static water D. 216 hours with 0.9 ml static water E. 195 hours with 100% R.H. F. 239 hours with 100% R.H. The corrosion temperature was 23.5°C and all surfaces were initially abraded with dry 600 grit SiC	125
38	Variation of β and concentration of dissolved SiO ₂ with corrosion time for 33L glass abraded with dry 120, 320, and 600 grit SiC	137
39	Variation of ϵ with corrosion time for 33L glass abraded with dry 120, 320, and 600 grit SiC	140
40	Variation of α with corrosion time for 33L glass abraded with dry 120, 320, and 600 grit SiC	142

LIST OF FIGURES (continued)

Figure		Page
41	Variation of pH with corrosion time for 33L glass abraded with dry 120, 320, and 600 grit SiC	144
42	S.E.M. micrographs of freshly abraded and corroded 33L glass. The initial surface was abraded with dry 600 grit SiC and the corrosion treatment was with static water at 79.5°C in a 0.9 ml cell	147
43	S.E.M. micrographs of freshly abraded and corroded 33L. The initial surface was abraded with dry 320 grit SiC and the corrosion treatment was with static water at 79.5°C in a 0.9 ml cell	149
44	S.E.M. micrographs of freshly abraded and corroded 33L glass. The initial surface was abraded with dry 120 grit SiC and the corrosion treatment was with static water at 79.5°C in a 0.9 ml cell	151

Abstract of Dissertation Presented to the Graduate Council
of the University of Florida in Partial Fulfillment of the
Requirements for the Degree of Doctor of Philosophy

STRUCTURE AND KINETICS OF GLASS CORROSION

By

David M. Sanders

June , 1973

Chairman: L. L. Hench

Major Department: Materials Science and Engineering

A general procedure is established for studying the effects of chemical reactions on the structure of glass surfaces. This work is designed to serve as a basis for future studies relating corroded glass structures with mechanical behavior, biological applications, and the design of amorphous materials having greater chemical resistance.

To accomplish these goals, a systems approach is used to establish the variables required to completely specify a corrosion reaction. New techniques including infrared reflection spectroscopy are introduced and a theoretical basis provided for interpretation of results obtained from these techniques. In contrast to most previous work in glass corrosion, a variety of techniques are used to observe both morphological and chemical changes in the glass surface during exposure. Corrosion conditions systematically varied

include pH, solution composition, relative humidity, solution replenishment, temperature, and pressure. The effect of surface roughness is also studied. Details of glass corrosion mechanisms are discussed and related to the effects of sample state and corrosion condition on resulting corroded structures.

The infrared reflection techniques developed are sensitive measures of both silica and alkali concentrations of the gel formed on the glass surface by the corrosion process. These concentrations, used in conjunction with new parameters obtained from solution data, define a composition profile which determines future corrosion behavior of glasses. It is shown that infrared reflectance is proportional to the concentration of the reflection species. This result has general application in the use of reflection spectroscopy for analytical as well as for structural studies. Both glass surface roughness and the corrosion condition used are seen to strongly influence the chemical and morphological nature of the corroded surface in addition to affecting the kinetics of the corrosion process.

CHAPTER I

INTRODUCTION

Reactions of silicate glass surfaces with aqueous solutions are important as an engineering design parameter for many applications. The mechanical strength,⁽¹⁾ optical properties,⁽²⁾ surface electrical conductivity,⁽³⁾ and resistance to structural deterioration are all influenced by the nature of these reactions. In addition, liquids whose beneficial properties are destroyed by the release of ions are frequently stored in glass containers. One example of a problem area which has occurred in the past is the leaching of certain lead glass glazes by acidic fruit juices causing lead poisoning; another is the destruction of human blood by defective glass containers.⁽²⁾

Reactions of glasses with aqueous solutions can also have beneficial effects. Recently a calcium and phosphate containing glass⁽⁴⁾ was discovered which becomes chemically bonded to living tissues, promising to make possible the design of a new generation of rejection-free prosthetic devices. This behavior is intimately connected with chemical reactions between the glass surface and its surroundings. In addition, certain corrosion reactions increase resistance

to further attack of the glass.⁽²⁾ Related reactions have been proposed to lead to the formation of low index of refraction antireflection films,⁽³⁾ although other methods are normally used commercially to produce these films. Finally, the soluble silicate cement industry and the detergent industry depend on an intimate knowledge of the conditions under which binary silicates dissolve.⁽⁵⁾

The traditional approaches used to study the corrosion kinetics of glasses have been based either on the rate at which ions from the glass are taken into solution⁽⁶⁻⁸⁾ or on the rate of change of corrosion film thickness, surface roughness, or some other property associated with the bulk material.⁽⁹⁻¹³⁾ The first approach is exemplified by the work of Rana and Douglas,⁽¹³⁾ who chose to follow the corrosion reactions of a series of binary glass compositions with water by measuring changes in both the alkali and the silicon concentrations in the corrosion media. These workers frequently used powdered samples in order to increase the surface area exposed to the corrosion media, thereby increasing the sensitivity of their measurements. One of the most informative studies using the second approach was made by Charles,⁽¹⁴⁾ who found that superheated steam and water cause layers of corroded glass to form on soda lime glass. These layers are of sufficient thickness that they could easily be measured on sectioned samples.

Some of the difficulties encountered by workers using the first approach are related to the need for sufficient ion concentration in the corrosion solution for accurate measurement. The use of powders and grains to increase the surface area of the corroding glass complicates the interpretation of the results obtained when applying these results to the bulk systems frequently encountered in normal use. Also, using powders and grains as the starting material makes it difficult to take surface roughness of the freshly prepared glass into account. In addition, the need for a solution for analysis eliminates the possibility of studying the corrosion of glass surfaces by gas phase reactants such as water vapor.

Both conventional approaches share additional drawbacks. One of the most serious is the lack of information concerning the chemical makeup of the corroded glass surface. The techniques used to measure film thickness based on optical interference or microscopic inspection do not yield this information at all and the solution analysis experiments only supply indirect evidence. As a result, both the distribution and bonding of the atoms at the corroded glass surface have remained open to speculation.⁽²⁾ Another difficulty with all the approaches used previously is the use of single techniques for corrosion studies. It is unusual in the corrosion literature for more than one tool to be applied to a corrosion problem. As a result, much of the

careful solution analysis data was carried out using simple model glasses,⁽¹⁵⁾ most of the film thickness measurement using a wide variety of commercial glasses,⁽³⁾ and the B.E.T. pore structure analysis using phase separated borosilicate glasses.⁽¹⁶⁾ In addition, there is scant information about the effect of the corrosion condition adopted and the sample state chosen on the resulting corrosion reactions. Finally, no workers, to the author's knowledge, have applied a systems approach to determine the variables which must be controlled and explored to completely understand the corrosion process of even one glass composition.

An ideal corrosion study would involve the use of multiple experimental approaches to obtain complete information about the effect of all possible corrosion variables on all possible resulting corrosion structures and kinetics. Some of the corrosion conditions requiring specification are listed in Table 1. The size, shape and distribution of microstructures and chemical species produced in the corroded glass surface, as well as the concentration of the ions released into the corrosion solution, are all needed to specify the resulting corrosion structures and kinetics.

At the initiation of this research it was found that there was no satisfactory experimental tool in current use to obtain direct information about the concentration and bonding of atoms present in the corroded glass surface. Early results by Pfund⁽¹⁷⁾ and later results by Anderson⁽¹⁸⁾

Table 1

Examples of General Corrosion Conditions and
Sample States Which Might Influence Corrosion Behavior

Corrosion Conditions

Ratio of glass surface to corrosion solution volume
Replenishment rate
Solution volume
Flow patterns at glass surface
Initial solution composition
Initial solution pH
Relative humidity exposure
SO₂ exposure
SnCl₄ exposure
Temperature
Pressure

Sample States

Phase separation
Cords
Initial composition of glass
Roughness
Stress
Prior corrosion

suggested that infrared reflection spectroscopy might provide such a tool. Since the infrared absorption spectra contain information about the concentration, position, and strength of chemical bonds,⁽¹⁹⁾ and since reflectance spectra can be related to absorption spectra,⁽²⁰⁾ it follows that it should be possible to obtain the same information from reflection spectroscopy. Consequently, suitable techniques were developed in this research to enable infrared spectroscopy to be applied to kinetic and structural studies of glass surfaces. These techniques are discussed in detail in Chapter II.

Also of interest is the initial stage of reaction of glass surfaces with water. Since corrosion reactions can be very rapid in the first few minutes of exposure compared to later corrosion times, it was necessary to develop automated techniques to monitor these early stages to see if there was any unusual behavior. One of the techniques developed was based on atomic emission spectroscopy, while the other was based on infrared reflection spectroscopy. These techniques are also discussed in Chapter II.

Chapter III describes the relationships between infrared reflection spectra and glass structure. Reflection spectra were recorded for a series of glasses to determine spectral trends as a function of glass composition. Several observations are made about the structure of silicate based glasses, independent of corrosion responses. As with all

succeeding chapters, the literature pertinent to this chapter is reviewed there. The effect of glass corrosion is only mentioned in passing in Chapter III, but that work forms the basis for all the infrared related corrosion studies which follow. In Chapter IV the structural relations developed in Chapter III are applied to the glass corrosion problem in a systematic manner.

In addition to the new techniques developed to supply specific information about the corrosion process, the more conventional solution and microscopy techniques were also applied where appropriate. At the onset it was clear that it would not be possible to explore all of the variables possible and several of these variables were held constant throughout the entire study in order to explore the others. One of these variables was the composition of the starting glass which was chosen to be 33 mole % lithia and 67 mole % silica (33L). This particular composition was chosen because it was found to have an intermediate chemical resistance compared to a variety of glass compositions prepared in an exploratory study. Also, the glass was not phase separated and its glassy structure has been studied extensively.⁽²¹⁾ One additional glass composition, 22 mole % soda and 78 mole % silica, was chosen for a preliminary comparison and its behavior was found to be qualitatively similar as discussed in Chapter IV.

Another variable held constant throughout the study was the bulk planar surface of the glass to be corroded as discussed in Chapter II. This surface was prepared by abrading the glass with dry silicon carbide paper, a treatment which is thought to produce scratches similar to those produced during normal use.⁽²²⁾ With these constraints, some of the other possible corrosion parameters listed in Table 1 were explored and the results discussed in Chapters V and VI.

In Chapter V various modes of corrosion are explored using the techniques developed earlier. Various corrosion conditions are chosen to be models for actual exposure environments and, while the full analysis described in Chapter IV is not possible, it is possible to project results from that analysis to the more realistic cases found in Chapter V. This trend toward applications is continued in Chapter VI, where the effect of surface roughness on the corrosion behavior is explored. This is of practical interest because glass in most uses becomes scratched. Therefore surface roughness must be studied to relate experimental results to actual corrosion problems.

While no attempt was made to explore the silicate glass corrosion problem in its entirety, an attempt was made to define what would be required to make such a study. Then specific areas of the total problem were chosen to form a foundation upon which a more complete study could be based.

Rather than varying glass composition as many previous workers have done,⁽²³⁾ composition was held constant and both the corrosion conditions and surface roughness were varied in ways designed to model actual systems. The use of the new techniques developed in this work in combination with techniques used more conventionally in glass corrosion studies is quite general and should be applicable to other glass compositions and corrosion conditions.

CHAPTER II

METHODS FOR STUDYING GLASS CORROSION KINETICS

Infrared Reflection

Actual reflection can be described in terms of two idealized components. In the first (specular reflection) all the reflected light leaves an ideally smooth surface at an angle equal to the angle of incidence; in the second (diffuse reflection) the light is reflected from an ideally matte surface with equal intensity in all directions.⁽²⁴⁾ Because of the manner in which samples were prepared (to be described in a later section), the spectra obtained in this study are largely specular in nature with a very small diffuse component. This can be demonstrated experimentally by comparing the reflection spectrum of a glass sample polished to 600 grit with the reflection spectrum of the same sample polished to 1/4 μ diamond paste. The resulting spectra have peak positions that are identical, with the reflectance of the maxima for the two spectra differing by less than 0.8% because of light scattering in the 600 grit sample.

General discussions of the reasons for resorting to infrared specular reflection as opposed to infrared

absorption were given by Harrick⁽²⁵⁾ and Simon.⁽²⁶⁾

Briefly, there are three primary reasons why the reflection method is especially useful in corrosion studies. The most obvious is that with strongly absorbing materials the reflection method eliminates the necessity of preparing very thin samples. In addition, the area of investigation is limited to a depth of penetration determined by the large extinction coefficient of silica-based glasses in the wavelength region studied. Using an equation given by Born and Wolf,⁽²⁷⁾ this depth at normal incidence is estimated to be on the order of 0.5μ at $1,000\text{ cm}^{-1}$. As one increases this angle, approaching grazing incidence, the penetration depth decreases to a very small fraction of this value. A logical extension of the present work is to use a variable angle of incidence in order to vary this depth of penetration and to increase the specular component reflected from rougher surfaces.⁽²⁸⁾ Thirdly, the spectra, as in the case of absorption spectra, are characteristic of the vibrations of certain bonds. Thus the reflection spectra can be used both to determine the rate of reactions taking place in the reacting layer and, at the same time, to provide information about the structural changes that take place as a result of these reactions. Also, whenever there may be an advantage in interpretation, reflection spectra can be converted to absorption spectra via methods discussed in detail by Simon and others.^(29,30)

Continuous Atomic Emission

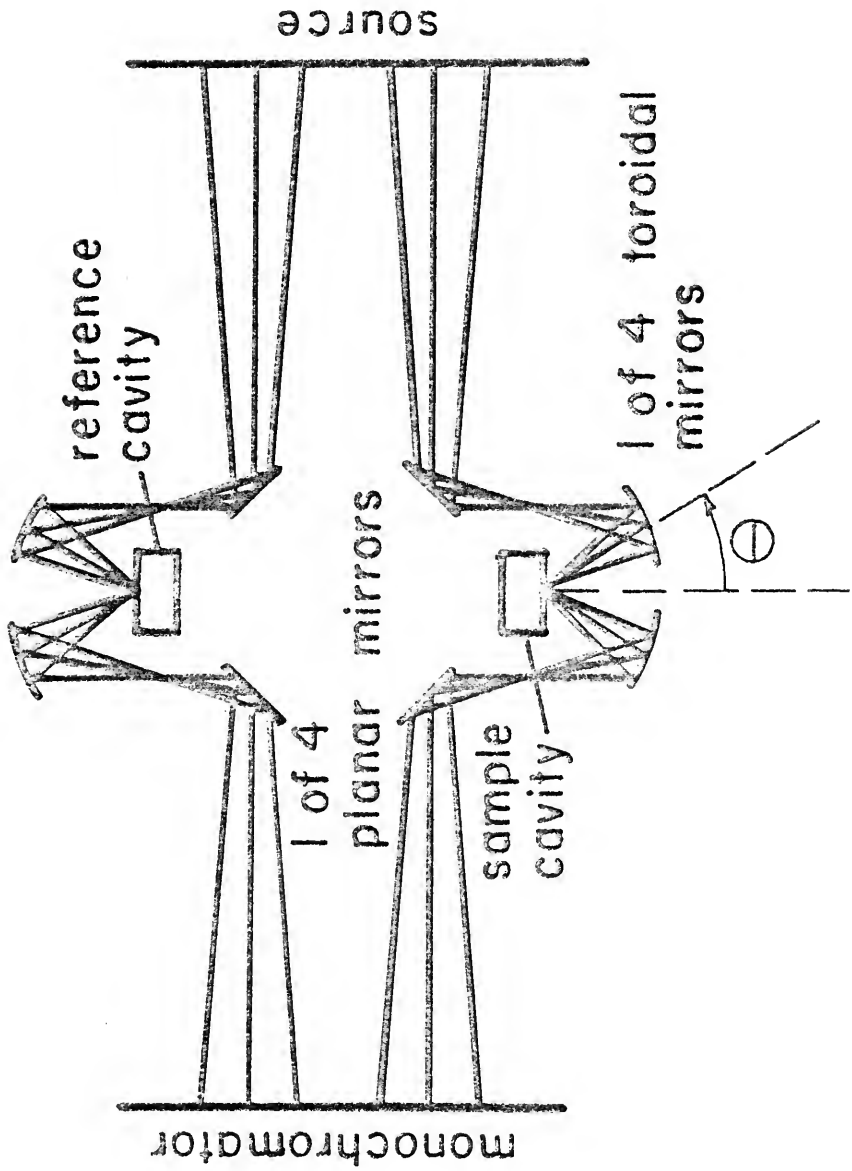
Atomic emission spectroscopy has been used by many investigators to study the amount of alkali ion corroded from powdered glass samples as a function of time. A recent review of these investigations was given by Das.⁽³¹⁾ In contrast to most of the work done in this area, the samples used in this study were in bulk form. The planar surfaces were ground with silicon carbide paper to simulate the abrading effect of normal use on the glass surfaces.

Atomic emission measures the concentration of alkali ion taken into solution, which is a direct reaction coordinate for one phase of the corrosion process. Understanding the alkali ion loss rate aids in the interpretation of the changes which occur in the infrared reflection spectra due to corrosion. Also, the use of continuous or semicontinuous atomic emission sampling, described later in this chapter, allows one to see subtle changes in the early stages of the corrosion process that are characteristic of the state of the surface before it begins to corrode to be compared with the corresponding changes in the infrared reflection.

The Optical System

The optical system used for the infrared reflection study in a Perkin-Elmer 621 spectrometer with an expanded sample compartment is shown in Fig. 1. It consists of a

Fig. 1. The ray diagram for the optical system used in reflection studies made using the expanded sample compartment of the Perkin-Elmer model 621 spectrometer.



double beam configuration of mirrors that focus a source image onto the sample and reference surfaces with a reduction in image size by approximately four times. The angle of reflection, θ , was fixed at 25° in this system.

It was soon discovered that special means were needed to permit repositioning of the front surfaces of the glass samples at the exact point of focus after each corrosion treatment. Two alternative experimental designs have been employed for this purpose -- one providing greater precision (especially in rapid reactions), the other providing more versatility. This positioning was accomplished by milling a cavity into the plate supporting the sample beam optics. This cavity accepts identical Plexiglas mounting blocks (Fig. 2) for the different positioning systems.

The reference beam has a holder similar to the one in Fig. 2 to accept interchangeable sample-holding devices, called "minirigs." In most of the experiments, a plane front-surfaced aluminum mirror was placed in a minirig which in turn was placed in the reference beam position (Fig. 1). However, it was at times desirable to place a glass in the minirig in the reference beam in place of the mirror in order to take "difference" spectra.

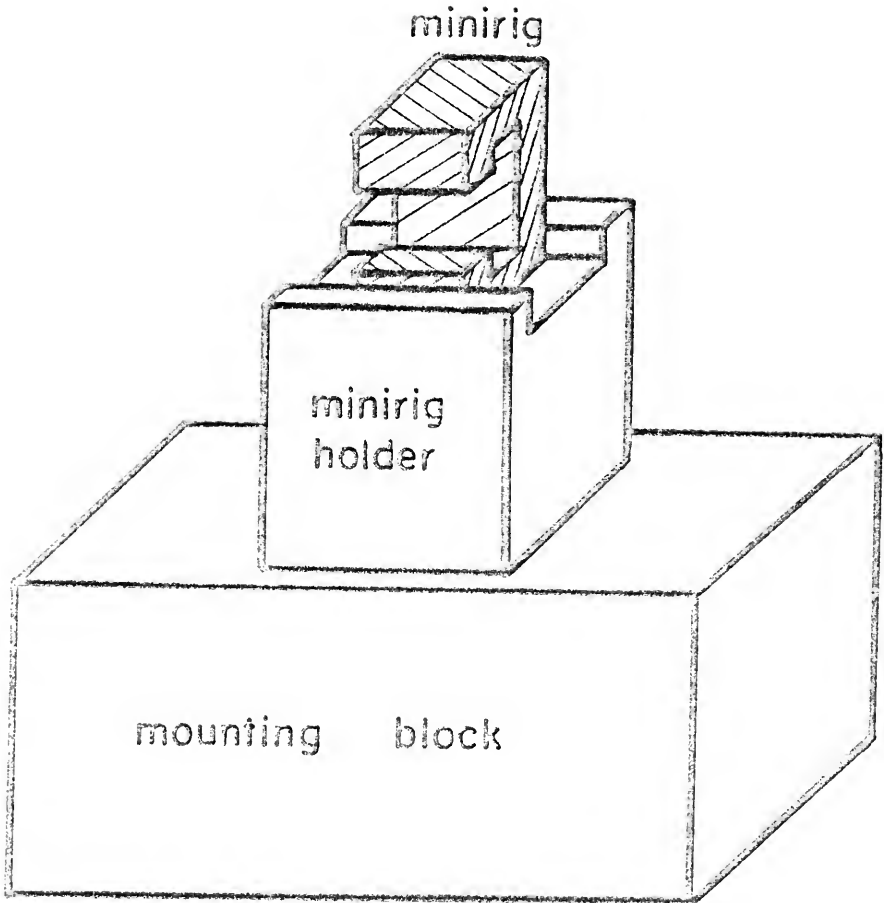


Fig. 2. Sample-holding device ("minirig") shown mounted in aluminum holder, which is in turn permanently fixed to the Plexiglas mounting block.

The Minirig System

Further detail of the minirig sample holder is shown in Fig. 3. The holder is designed to hold a glass plate under various loads to determine the effects of strain on the corrosion process. The load is applied using the set screw located in the back of the minirig, and the level of strain in the glass is determined using standard stress-optical methods. In the experiments described in this work, however, the minirig was used without the loading rods and therefore served simply as a means of holding the sample glass and reference glass or mirror in the infrared beam between corrosion treatments. The results of the study of the effects of stress on corrosion will be reported in a later work. The minirigs, in conjunction with the "minirig holder" shown in Fig. 2, comprise what will be termed the "minirig system."

As an example of the application of this minirig system we show in Fig. 4 two sample reflection spectra obtained from a glass initially of lithium disilicate composition (53 mole % Li_2O -67 mole % SiO_2). The detailed assignment of the peaks will be discussed in a later work, but one can see the extent of spectral change which can be expected. (32) Briefly, the sharp reflection peak forming at the higher frequency ($1,090 \text{ cm}^{-1}$) upon corrosion is attributed to a transformation of a part of the reactive layer to a

Fig. 3. Minirig sample holder showing a sample mounted under stress being applied through the loading bars.

FRONT VIEW OF MINIRIG WITHOUT LOADING FIXTURE

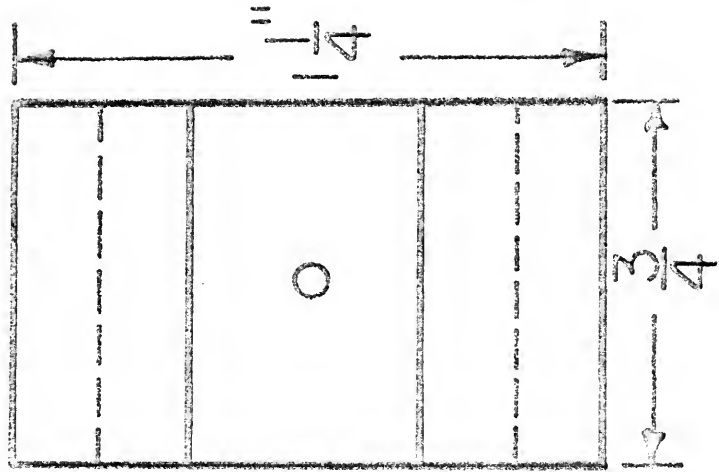
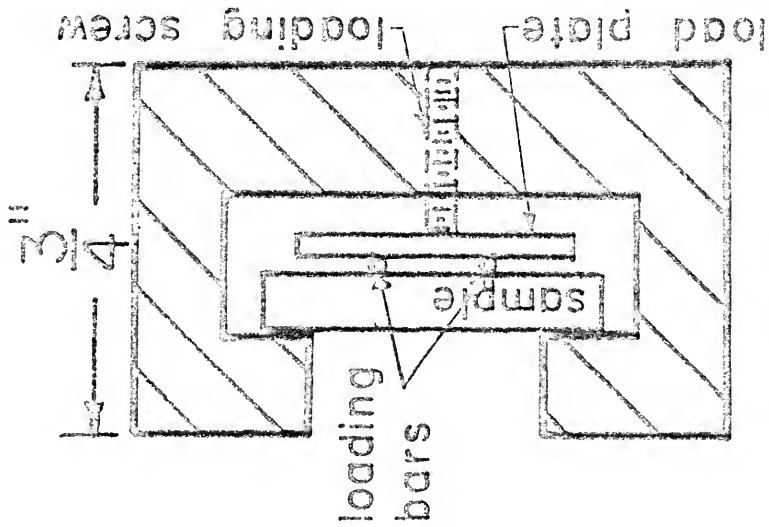
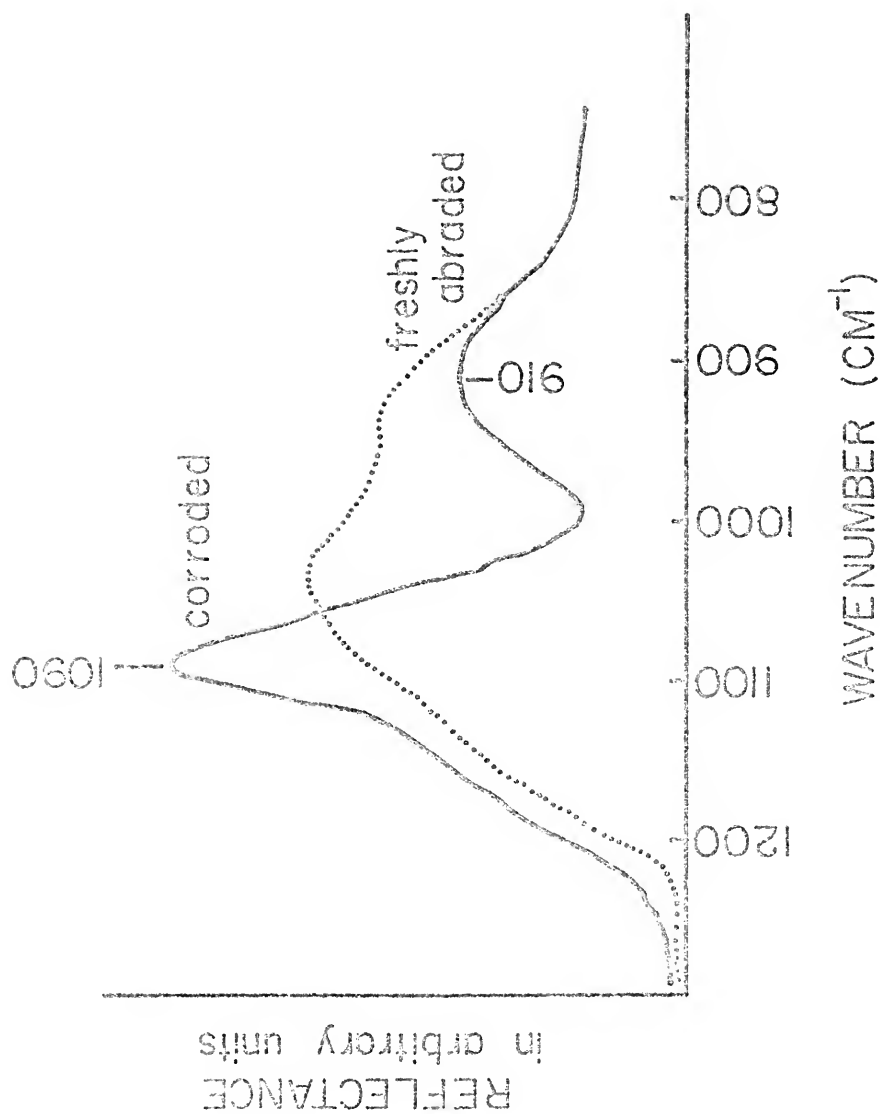


Fig. 4. Infrared reflection spectra of a corroded and of a freshly abraded glass of a composition corresponding to lithium disilicate. The freshly abraded sample was prepared by grinding the glass surface with dry silicon carbide paper. The corroded sample was prepared by subjecting the surface of a freshly abraded glass sample to distilled water in the corrosion cell described in Fig. 5A for 24 hours at 23°C.



configuration more closely resembling vitreous silica, while the peak at 910 cm^{-1} is attributed to a lithia-rich compound. The spectrum of a sample subjected to corrosion for a short time can be changed to that of the freshly polished sample by several 6-inch strokes over 600 grit silicon carbide paper, confirming the statement above that the reflection spectrum is characteristic of a surface layer less than a few microns thick. For the over-all study, many pairs of spectra similar to those in Fig. 4 were recorded under differing experimental conditions. Each pair consisted of a spectrum of a corroded glass sample and reference spectrum of the same glass sample before corrosion, recorded consecutively.

The corrosion cells employed in the minirig system are shown in Fig. 5. The cell labeled A, used with corrosive still media, is a Teflon block with a cavity containing the medium. Figure 5B shows how this cell is clamped against the glass sample during the corrosion treatment. Only a known and reproducible portion of the glass surface (determined by cavity shape) is exposed to the corrosive medium, which can be replenished at predetermined time increments if desired.

The continuous flow cell, shown in Fig. 5C, consists of a Teflon block with two perpendicular holes. Two minirigs containing glass samples that have had identical previous treatments are pressed against the cell as shown in

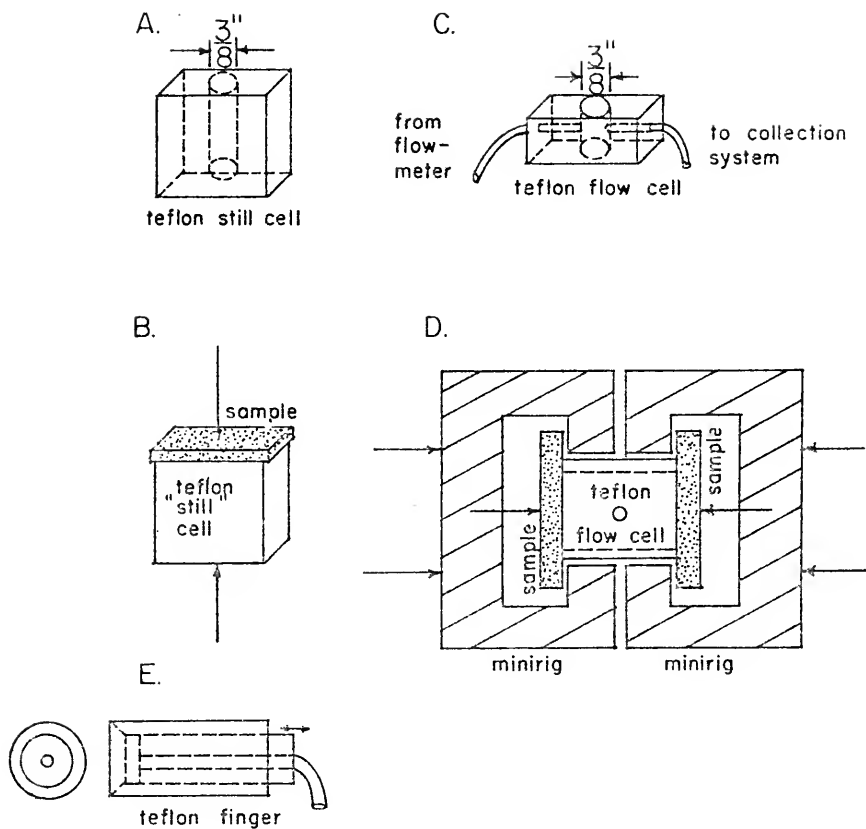


Fig. 5. Corrosion cells used in this study as described in the text.

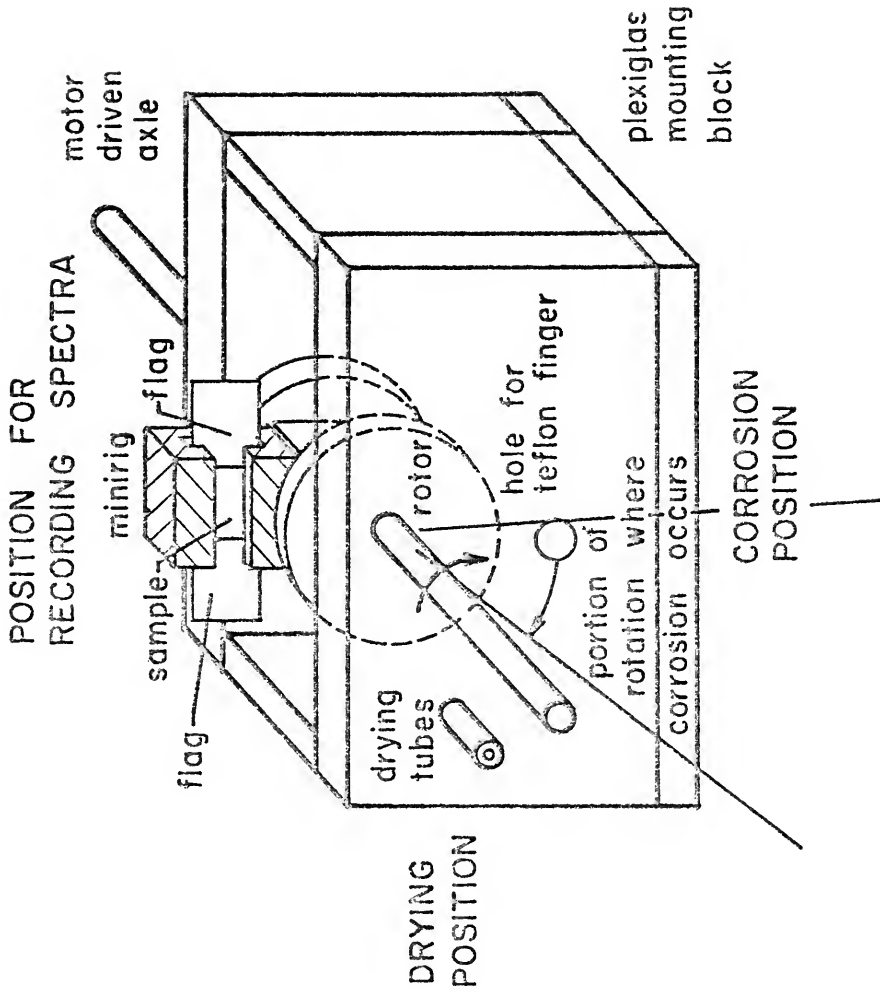
Fig. 5D. A controlled flow of water or other corrosive fluid is then introduced through the tube to the sample surfaces as indicated. The fluid can be collected from the outflow tube for studies in atomic emission spectroscopy using procedures described below. After a specified length of corrosion time, the minirig is removed from the cell and mounted in the spectrometer to record the spectrum.

The Automated System

It is sometimes desirable to compare the spectral changes with time occurring upon corrosion for several samples subjected to different applied stresses, or subjected to different surface treatments. Also, the kinetics of the rapid corrosion reactions that occur at elevated temperatures are of interest. A system that permits such studies is pictured in Fig. 6 and is termed the "automated system" in the following discussion.

The automated system consists of a "Ferris-wheel" type of arrangement (Fig. 6) where the glasses under study are alternately subjected to a corrosion treatment, dried, and placed in the sample beam of the spectrometer automatically. This is accomplished by means of the rotor which holds up to four minirigs. The rotor is mounted in a Plexiglas block of dimensions allowing it to be placed snugly in the cavity of the optical bench in Fig. 1. The rotor is driven at 1 rpm by a Hurst synchronous motor.

Fig. 6. "Automated system" showing one sample rotated from the corrosion bath position into the position for reflectance measurement.



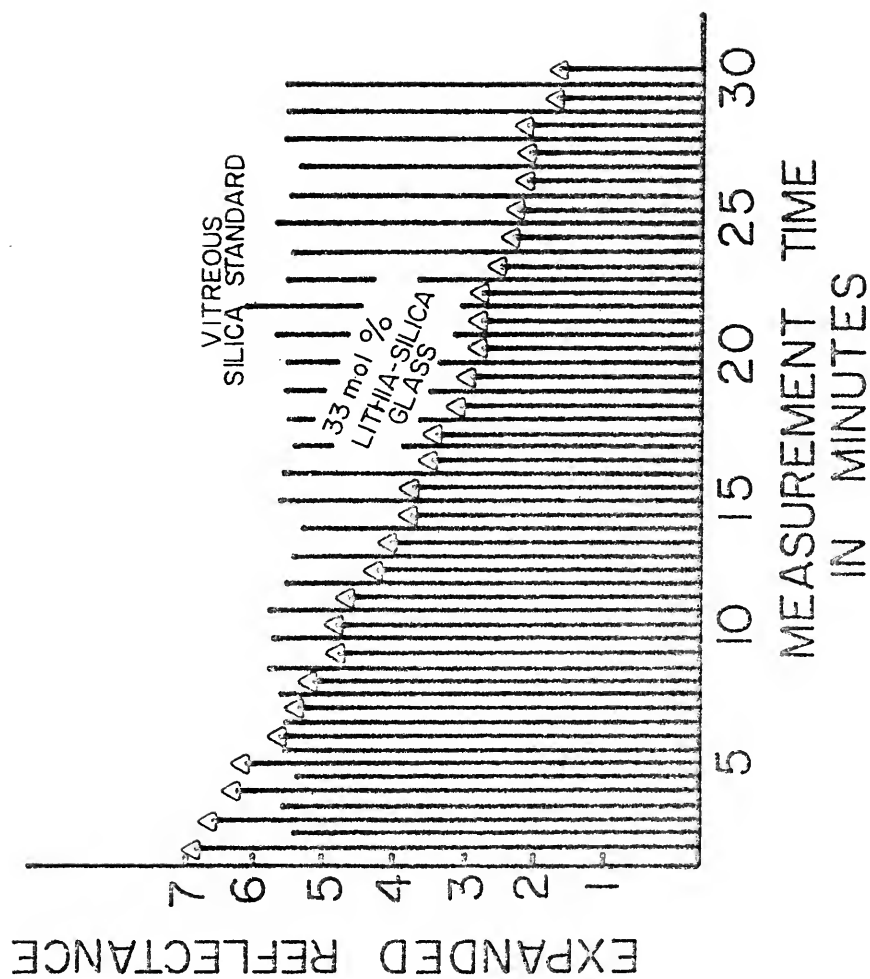
When a glass sample in the minirig is covered by the corrosive medium in the "down" (or corrosion) position, the corrosion reaction occurs for a small increment of time, controlled by the angle ϕ in Fig. 6. This angle can be varied with the different modes of corrosion to be discussed shortly. As the minirig rotates to the drying position, the corrosion reaction stops as the glass is dried (and cooled) by blowing a stream of dry nitrogen or air onto the surface. When the minirig reaches the "up" (or recording) position, the intensity of reflection at a particular wavenumber is recorded by the spectrometer. Blinds or flags on the minirigs block the infrared beam when the rotor is not positioned so that one of the minirigs is exactly vertical, in order to eliminate stray reflections from the minirig holders.

The wavenumbers chosen for the reflectance study are held constant during the entire kinetic study, so that there is a maximum change in reflectance from the sample for the particular reaction under study. This wavenumber is chosen prior to any kinetic study after examining the spectra from a corroded specimen and from a freshly polished sample of the same material (as shown in Fig. 4). The spectrometer gain is adjusted so that when the minirig reaches the "up" position the pen rises to its maximum with an "overshoot" (refer to PE manual) and then falls to zero when the minirig goes out of the recording position. The chart speed is

adjusted so that these maxima occur next to one another to result in a record of intensity as a function of time. Results are shown in Fig. 7 for the reflectance at 985 cm^{-1} from an experimental lithium disilicate glass in a minirig mounted on the rotor opposite a minirig containing a standard glass, in this case vitreous silica. This particular wavenumber (985 cm^{-1}) was selected because the variation in the reflectance was relatively large after very short periods of time, as seen in Fig. 4.

The relatively constant intensity spikes in Fig. 7 indicate the reflectance from vitreous silica, the standard chosen because it does not corrode on exposure to water. This set serves the twofold purpose of marking the exact time of recording and of indicating the noise level of the spectrometer. The spikes which monotonically decrease in height form the corrosion envelope for the experimental sample of lithium disilicate glass. The changes in reflectance are amplified by using a scale expansion of five times, and, as shown in Fig. 7, the noise is still at an acceptable level. For the spectrum shown in Fig. 7, the sample was corroded by water at approximately 90°C flowing through a Teflon tube, as described later. The actual corrosion time added on each revolution was 10 seconds, indicating that the corrosion causing the changes occurred in less than 5 minutes, causing a drop in absolute reflectance

Fig. 7. Reflectance at 985 cm^{-1} of a lithium disilicate glass (Δ) as a function of time, compared to that from a standard composed of non-corroding vitreous silica. This corrosion curve was obtained using the automated system described in the text and shown in Fig. 6. The reflectance scale is expanded five times with respect to that shown in Fig. 4.



intensity of roughly 1%. The fluctuation in the absolute reflectance of the standard is seen to be less than 0.15%.

This illustration shows both the advantages and disadvantages of the technique. It is clearly most useful for studies of the detailed structures of kinetic curves of very rapid reactions. The fact that it took 30 minutes to obtain 5 minutes of reaction time makes the method less desirable for studying reactions that take greater than 1 h. By increasing the angle of the arc (ϕ in Fig. 6), the length of time the sample is exposed to the corroding fluid can be increased to about 20 seconds of each revolution. However, other methods to be described shortly are more appropriate for kinetic studies of slower reactions.

If all of the positions in the rotor of Fig. 6 are filled, reflectance measurements from four different samples are recorded each revolution. One of the four minirigs always contains a standard glass for reference, chosen so that its reflectance at the wavenumber in question is nearly identical with that of the glasses of interest and so that its reflectance does not change when subjected to the corrosive medium.

Several possible modes of corrosion of the glass samples can be chosen depending on the conditions required. In the example cited in Fig. 7, a Teflon tube shown in Fig. 5E was held with its end just touching the glass surface of the minirig in the "down" position. As the rotor

revolved, the glass surface was exposed for roughly 10 seconds to water from the tube and then to the blast of air that dried the surface prior to the reflectance measurement. This configuration is useful for several reasons. It allows the study of the effect of flow rates of the corrosive media from 0.05 ml/min to more than 10 ml/min. The cell area is identical with the other corrosion cells described in Fig. 5. Small increments of corrosion are possible because the corrosion time for each cycle of the rotor is small.

One of the disadvantages of the automated system is that the spectrum is monitored at only one wavenumber for the entire experiment. This disadvantage is not serious if peak frequencies do not shift during the corrosion process, or if the extent of shift is known. Another disadvantage is that the automated system ties up the infrared spectrometer for the duration of the corrosion experiment.

For slightly slower reactions, the cell shown in Fig. 6 is used in a somewhat different mode. The entire spectrum of the untreated glass sample is recorded first. The rotor is then turned manually so that the sample dips into the corrosion solution. After an accurately determined corrosion time, the rotor is again turned quickly to place the sample in the infrared beam, the glass is wiped dry, and the reflection spectrum of the corroded sample is then recorded. This procedure is repeated at appropriate intervals to establish a set of reflection spectra as a function

of corrosion time. From these spectra one can plot reflectances at individual wavenumbers as a function of time.

Continuous Atomic Emission

The last two procedures for studying corrosion to be described here involve modifications of standard atomic emission techniques, using the Teflon cell shown in Fig. 5B . A schematic drawing of both techniques is shown in Fig. 8. In the first procedure (option 1), the corrosion fluid is drawn by the suction produced by the atomizer of the atomic emission machine. The fluid is pulled successively through a flow meter, a metering valve, and finally through the corrosion cell before reaching the instrument. The whole sample assembly is submerged in a water bath with temperature controlled to $\pm 0.1^{\circ}\text{C}$. The concentration of analyte is recorded continuously on a chart recorder connected to the photomultiplier output.

In this experiment it is necessary to monitor and control the flow rate carefully since it controls the amount of dilution experienced by a given quantity of lithium ion leached from those surfaces, and the flow into the atomizer influences the intensity of emission due to a given concentration of analyte. It has been found experimentally that fluctuations must be controlled to about $\pm 1\%$ of the flow rate to avoid these difficulties. A continuously variable

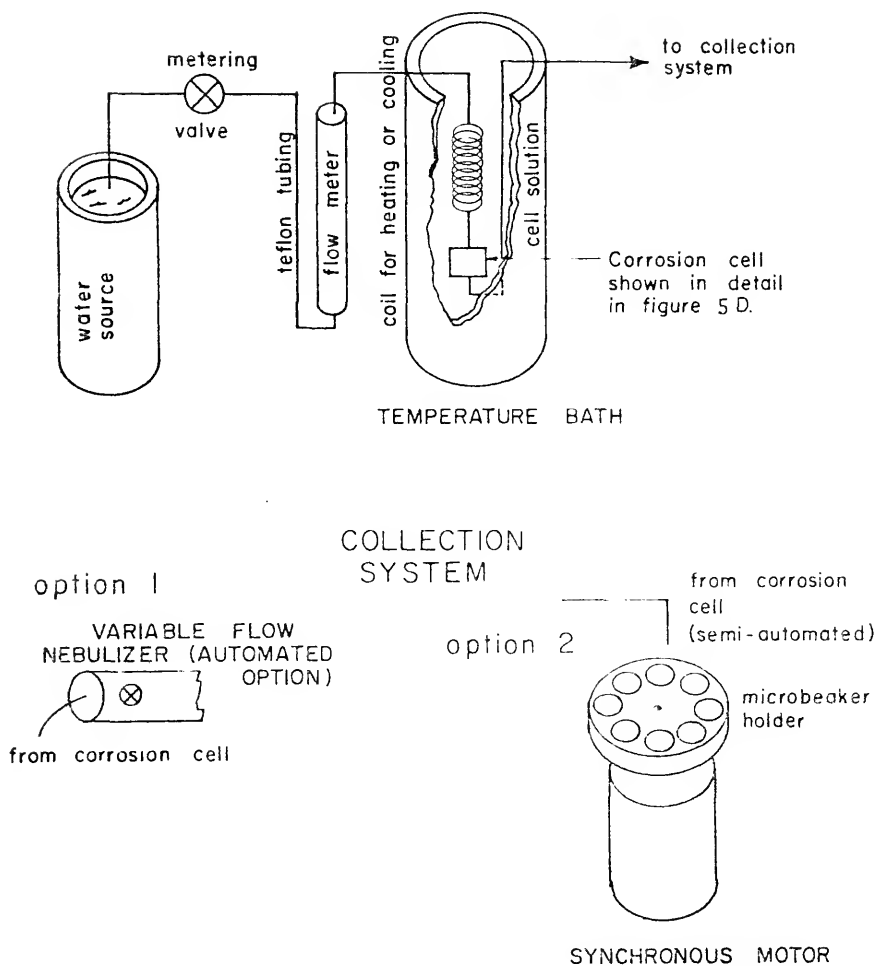


Fig. 8. Schematic drawing of atomic emission sampling techniques used in this study.

atomizer and a micrometer valve provide the necessary control. Since all of the corrosion solution is analyzed continuously, this method is particularly useful for rapid reactions in their initial stages.

For longer periods of time and slower reaction rates a second technique is used. This involves a positive pressure head established by an elevated fluid supply with automatic collection of the corrosion microbeakers (Fig. 8, option 2). The microbeakers are rotated by a synchronous motor under the outlet from the corrosion cell at a rate determined by the flow rate chosen for the corrosion treatment. Each beaker collects a sample of the analyte that is an average of the solution concentrations over the time required for collection. If the concentration is changing very rapidly, the previous technique is to be preferred; if not, the technique involving microbeakers provides certain advantages.

The use of this second option in Fig. 8 allows a blank, in most cases distilled water, to be aspirated between the measurement of each microbeaker solution, in order to help eliminate the errors due to machine drift. Also, solutions flowing at rates too slow to be measured directly using the technique involving option 1 of Fig. 8 can be collected in microbeakers, thus alleviating somewhat the problem of flow rate sensitivity discussed earlier. Finally, this second option permits one to analyze for more

than one element, and to measure pH and electrical conductivity of each solution. Thus, as is the case with the infrared techniques, the automatic measurement of corrosion is best suited to short experiments while the semiautomatic method is more versatile.

CHAPTER III

QUANTITATIVE ANALYSIS OF GLASS STRUCTURE USING INFRARED REFLECTION SPECTRA

Infrared spectroscopy has been used extensively in the study of glass largely because it is sensitive to the local positioning of atoms and the strength of the chemical bonds between them.⁽¹⁹⁾ An excellent review article by Simon⁽²⁹⁾ shows that traditional emphasis has been on the study of hydroxyl groups in glass. However, there is considerable current interest in quantitative studies of the vibrations of the atoms making up the glassy network, as reviewed by Wong.⁽³³⁾ This shift in emphasis has been encouraged by the introduction of infrared spectrometers having greater spectral wavelength ranges⁽³⁴⁾ and by the widespread use of laser Raman spectrometers permitting the study of vibrations not seen in infrared.⁽³⁵⁾ Recent theoretical studies by Bell and Dean,⁽³⁶⁾ and Gaskell⁽³⁷⁾ greatly facilitate the interpretation of spectra from simple silicate glasses having compositions corresponding to stoichiometric crystalline compounds.

The first objective of this chapter is to introduce the use of plots of reflectance vs. composition for the analysis of the concentrations of specific vibrational species present

in three series of binary silicate glasses. It will be demonstrated experimentally that reflectance is proportional to the concentration of the vibrational species causing it. Breaks in this linear behavior can be explained in terms of abrupt changes in the nature of the species involved.

A second objective is the re-examination of the spectra of the binary lithia-silica, soda-silica, and potash-silica glass systems to include the silicon-oxygen rocking vibrations. The spectrometers used by earlier workers who investigated these systems did not have sufficient wavelength range to observe these peaks. (33)

In addition, it has been found that infrared reflection spectra from glass surfaces are extremely sensitive to the attack of the surface by water vapor and aqueous solutions as discussed later. Therefore, a third objective of this study is to examine the influence of various preparation conditions on the infrared spectra of binary alkali silicate glasses.

Methods

The glasses, except for vitreous silica and the 10 mole % lithia composition, were prepared in platinum crucibles as described in an earlier work by one of the authors. (38) The glasses were cast between graphite blocks, and given a minimal anneal between 400°-500°C for 4 hours. Glass

compositions of 45 and 50 mole % Na_2O and 38 % Li_2O were quenched between steel blocks to prevent crystallization. Infrared analysis of specimens with and without annealing and with the different quench rates showed equivalent IR spectra.

The vitreous silica samples, GE125, were obtained from the General Electric Company. The 10 mole % lithia-silica samples were prepared by presintering a compact of lithium carbonate, methyl cellulose and 5 micron silica at 1250°C and fusing the compact using an oxyacetylene torch, a method similar to that used by Kumar.⁽³⁹⁾

The samples were wet ground with 600 grit silicon carbide paper. The resulting corroded layer was removed immediately before taking the reflection spectrum using dry silicon carbide 600 grit paper. It was found that for the 50 mole % $\text{Na}_2\text{O-SiO}_2$ glass this procedure did not produce an uncorroded surface due to the presence of water vapor in the air. It was therefore necessary to grind the samples of that composition in a glove box sealed to the spectrometer while continuously purging both with nitrogen obtained by boiling liquid nitrogen. This method excluded even momentary exposure to atmospheric water. Only in this way was it possible to obtain the true spectrum for the 50 mole % $\text{Na}_2\text{O-SiO}_2$ glass composition.

Selected glass compositions sent to Sharp-Schurtz Company for wet chemical analysis produced measured compositions

within 1 mole % of the nominal composition. The 50 mole % glass was analyzed twice in this lab using the well-known ammonium molybdate colorimetric analysis for silicon.⁽⁴⁰⁾ These determinations were also within 1 mole % of the nominal composition.

Results

Infrared reflection spectra of glasses having selected compositions in the lithia-silica, soda-silica, and potash-silica systems are given in Figs. 9, 10, and 11. This three-dimensional mode of representation has been chosen to illustrate trends in spectral band shapes with increasing alkali addition. The grid network drawn on each spectrum permits the determination of both reflectance and wavenumber for any point on a given spectrum. In Fig. 9 the spectra of the compositions 20, 25, 30, and 35 mole % lithia are shown broken for increased clarity. In Fig. 10 the spectrum of 16 mole % is shown broken for the same reason.

The three figures reveal similarities in the changes which take place on the addition of alkali ions to vitreous silica. The vitreous silica peaks tend to broaden and to decrease in intensity. In addition, a new peak between 900 and 950 cm^{-1} forms on the low frequency side of the prominent reflection peak near $1,100\text{ cm}^{-1}$.

Fig. 9. Compositional dependent changes in infrared reflection spectra in the lithia-silica system.

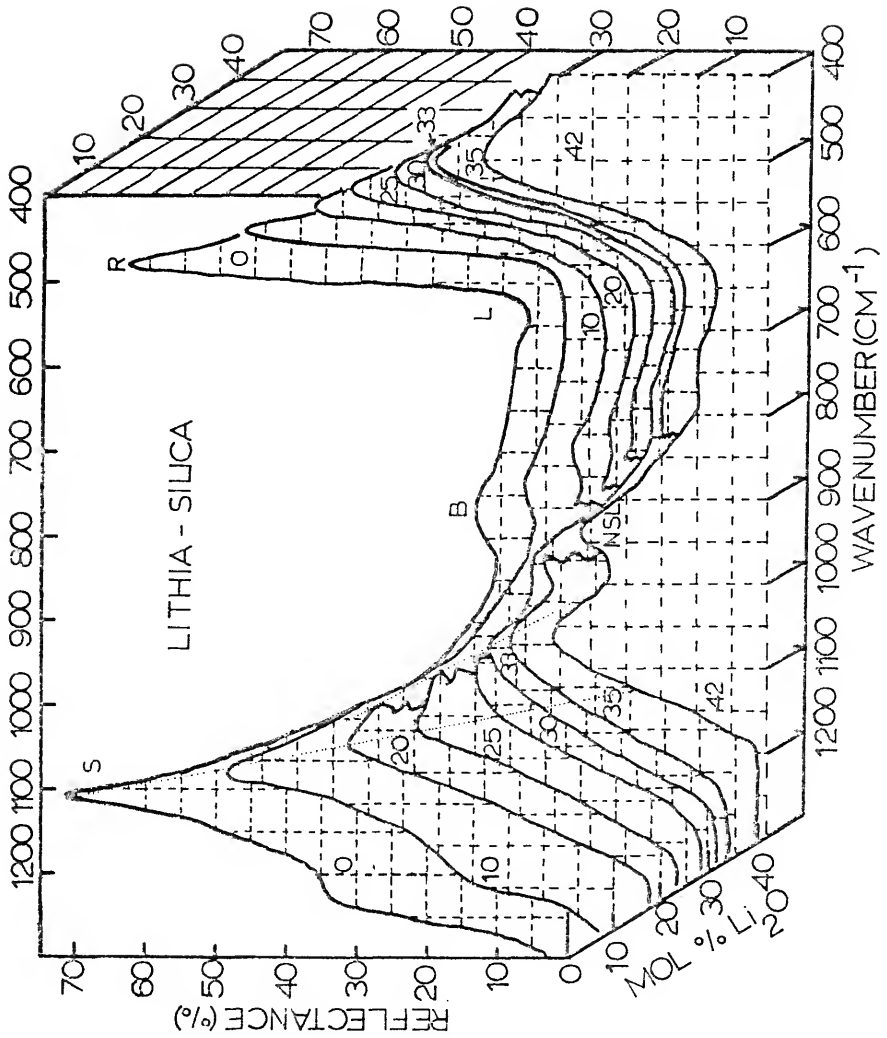


Fig. 10. Compositional dependent changes in infrared reflection spectra in the soda-silica system.

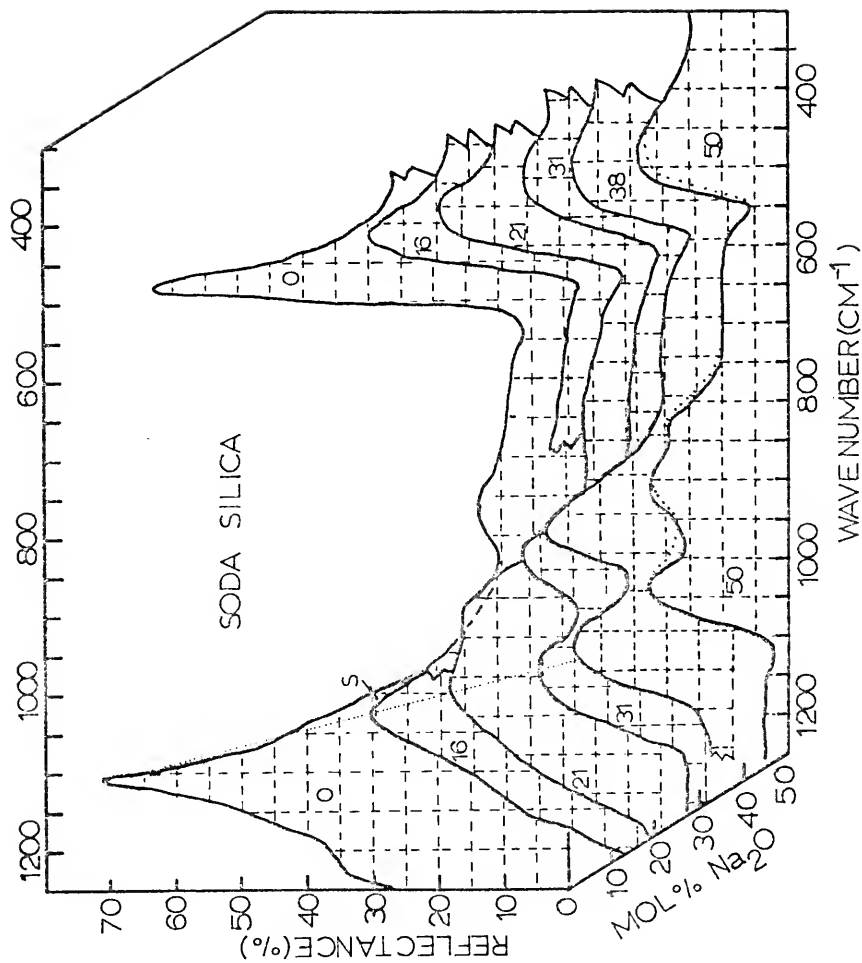
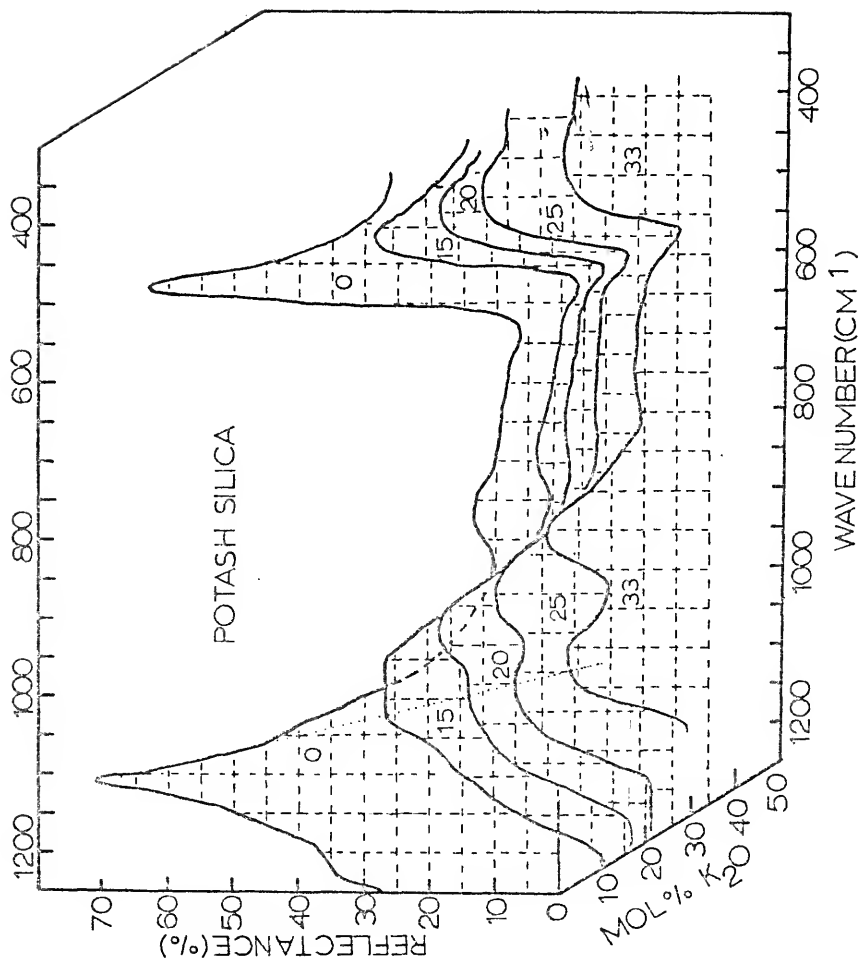


Fig. 11. Compositional dependent changes in infrared reflection spectra in the potash-silica system.



There are also subtle differences in the trends seen in Figs. 9-11 depending upon the kind of alkali ion which is introduced. It can be seen that the exact amount of change from the spectrum of vitreous silica occurring for a given mole % of alkali ion increases in the order $\text{Li} < \text{Na} < \text{K}$.

Two spectra are shown in Fig. 10 for the 50 mole % soda-silica glass. The dotted line is the spectrum obtained from a sample whose surface is ground with dry 600 grit silicon carbide paper immediately before taking the spectrum. The solid line is the spectrum obtained using the dry nitrogen technique described in the methods section. It can be seen that there are significant changes in both peak position and peak intensity due to the brief two-minute exposure of the first sample to air at 50% relative humidity, thus emphasizing the importance of careful control of the environment during the study.

As can be seen in Fig. 12, the spectrum reported for the 50 mole % soda-silica glass kept in the dry nitrogen atmosphere differs from the two spectra reported in the literature for glasses of that nominal composition. (37,41) We originally thought that this difference could be explained in terms of reactions caused by trace amounts of water present in the grinding media used by the other authors. A sample of 50 mole % soda-silica glass was therefore ground under wet acetone to see the nature of the change in the resulting spectrum. As can be seen in Fig. 12, the reaction

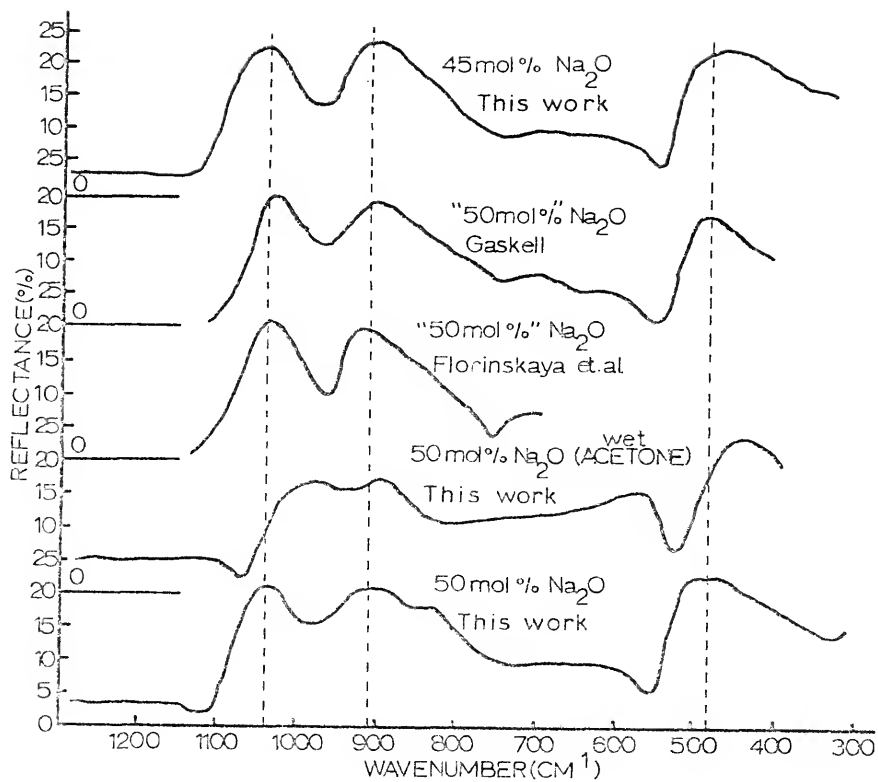


Fig. 12. A comparison of infrared spectra of 50 mole % Na₂O-SiO₂ glasses.

explains not only the disappearance of the third hump near 800 cm^{-1} , but it also causes a shift of the silicon-oxygen stretching vibration to lower frequencies. A glass of 45 mole % soda composition was then prepared and its spectrum (see Fig. 12) was found to be quite similar to the spectra of the nominal 50 mole % soda samples presented by the other authors. We suggest, therefore, that the procedure used by the other workers⁽⁴²⁾ of melting the glass samples in quartz crucibles produced glasses whose actual compositions were richer in silica than the nominal compositions by as much as 5 mole %. This postulate is consistent with the findings of Vogel⁽²¹⁾ that binary glasses having alkali concentrations greater than 33 mole % tend to dissolve quartz crucibles.

Discussion of Results

The assignment of each of the prominent features in the alkali-silicate glass reflection spectra is possible using results from recent investigations. The high frequency peak in vitreous silica near $1,100\text{ cm}^{-1}$ (S) is attributed to the silicon-oxygen stretching vibration.⁽⁴³⁾ The new peak that forms between 900 and 950 cm^{-1} on the low frequency side of the S peak as the concentration of alkali ion increases is assigned to the silicon non-bridging oxygen stretching vibration (NSR).⁽⁴⁴⁾

The peak found between 400 and 600 cm^{-1} is due to rocking motions of the silicon-oxygen bonds and the peak near

800 cm^{-1} is due to bending motions of the same bonds. The last two assignments are based upon the lattice dynamical calculations of a vitreous silica model developed by Bell and Dean.⁽³⁶⁾

In previous work done on binary silicate glasses, the frequencies of various peaks for a given binary system have been plotted as a function of composition, yielding irregular curves. The discontinuities in these plots have been interpreted as indicating heterogeneous structures.⁽⁴²⁾ In the present work, the reflectance of an individual peak maximum rather than its wavenumber has been emphasized because it has been found to be directly proportional to composition. However, when frequencies are plotted against composition and compared to those obtained by Cherneva and Florinskaya,⁽⁴⁵⁾ the agreement is excellent. Differences in the 50 mole % soda glass are also present, as discussed earlier.

Plots of the maxima of the spectra found in Figs. 9, 10, and 11 vs. composition are given in Figs. 13, 14, and 15. It can be seen that in all cases the behavior of the reflectance is linear with composition of bulk glass. In each case breaks occur in the otherwise linear plots. It is argued that if reflectance can be shown to be proportional to the concentration of the species causing it and that it is additive, then these breaks imply abrupt changes in the nature of the species causing the reflectance.

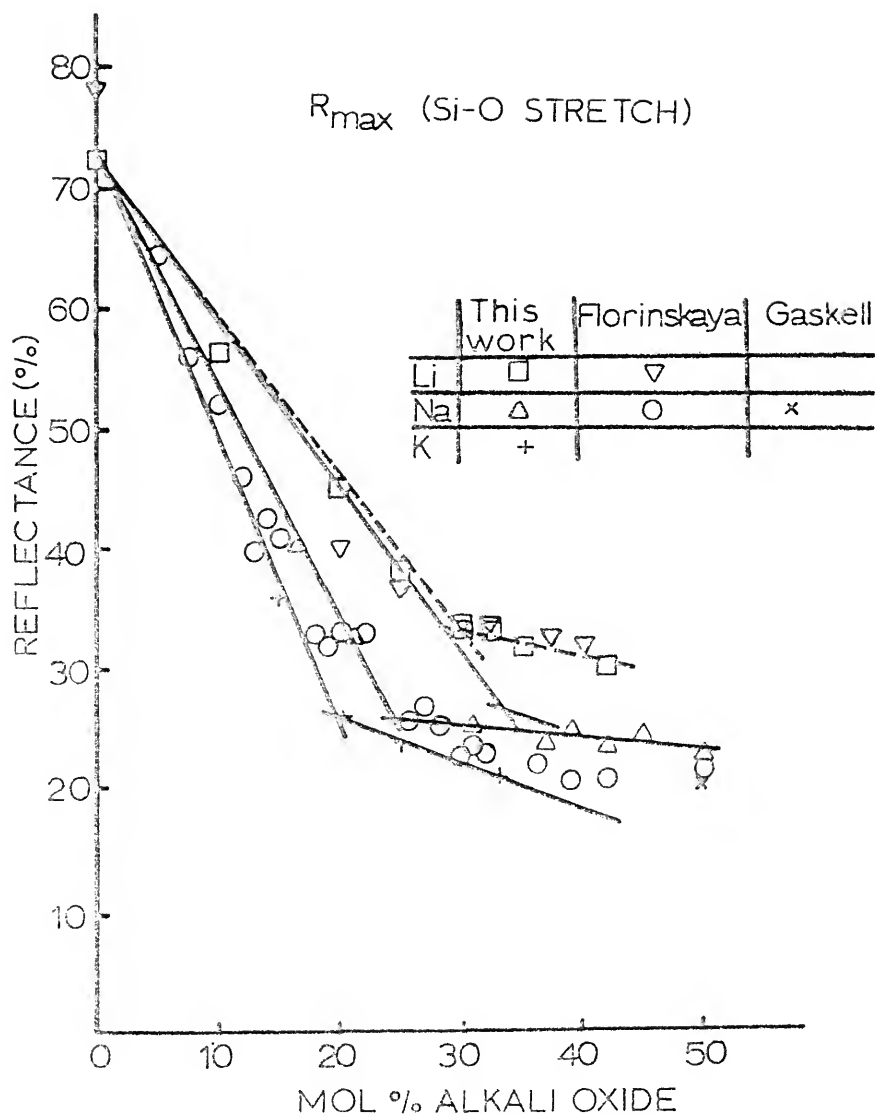


Fig. 13. The reflectance of the silicon-oxygen stretching maximum as a function of composition for the three systems studied.

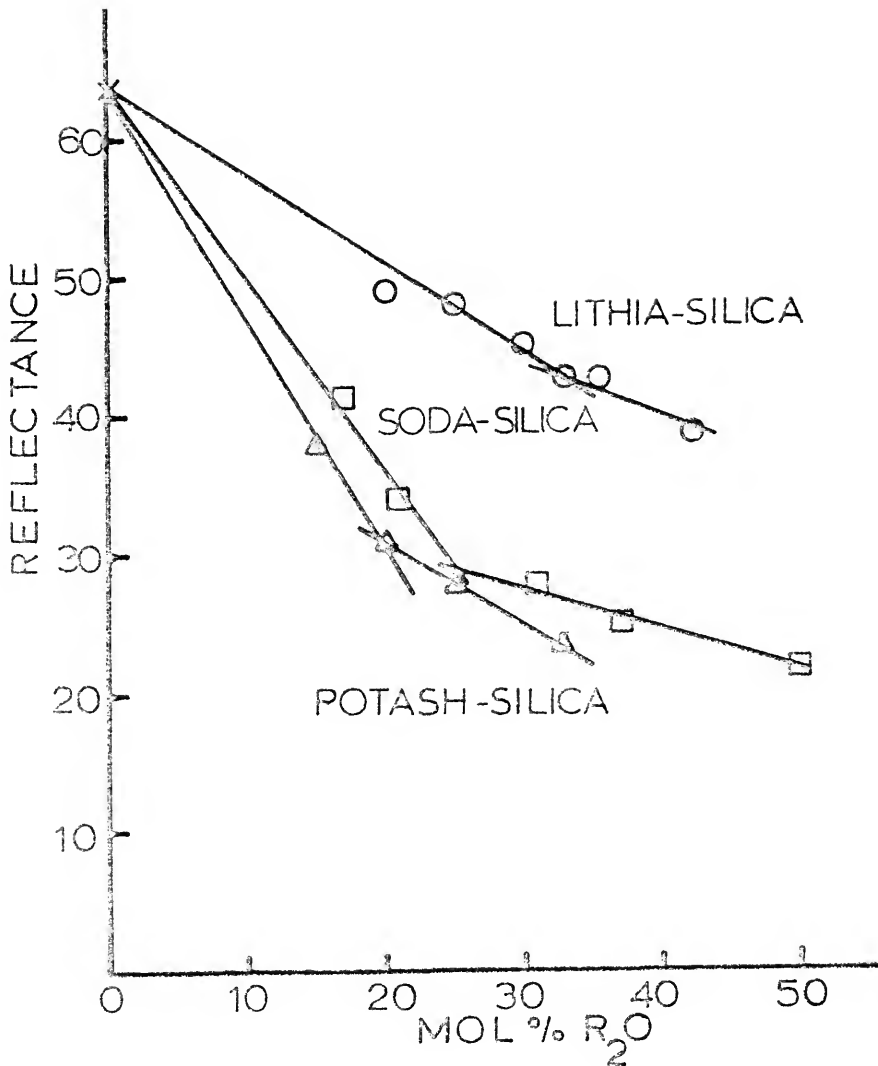


Fig. 14. The reflectance of the silicon-oxygen rocking maximum as a function of composition for the three systems studied.

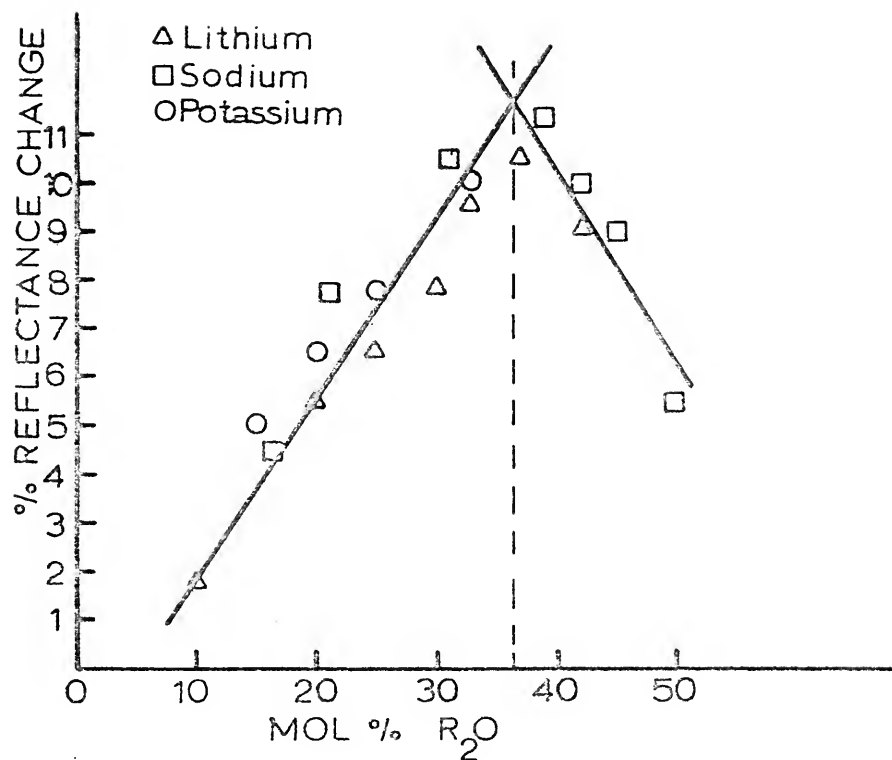
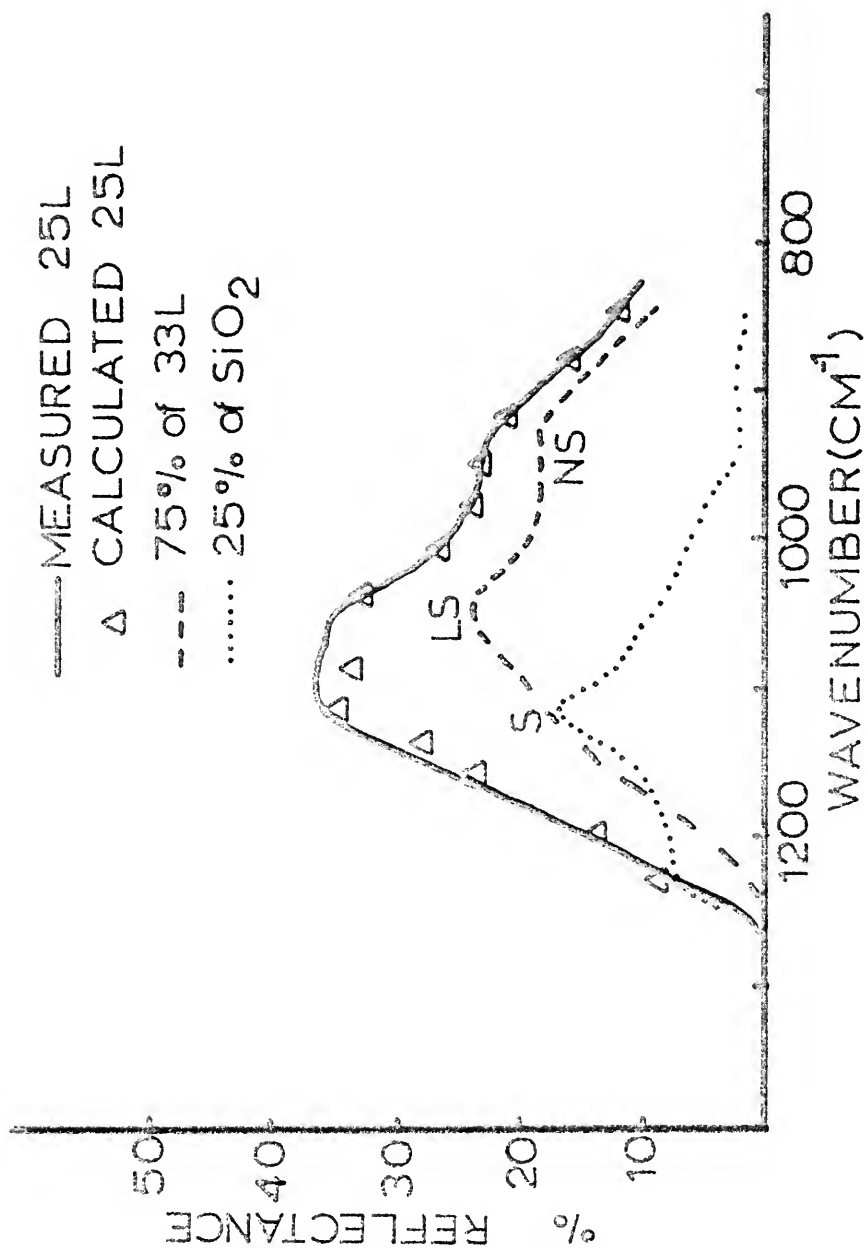


Fig. 15. The reflectance of the silicon non-bridging oxygen vibration associated with alkali ion as a function of composition.

Figure 16 is a demonstration of an analysis which is possible using the principles introduced above. The solid line is the measured spectrum of 25 mole % lithia-silica glass. This glass is phase-separated and known to contain, using the lever principle on the miscibility dome, approximately 75% of the reflectance of 33 mole % lithia-silica glass and 25% of the reflectance of vitreous silica. The dotted curve was obtained by multiplying the spectrum reflectance of vitreous silica by .25 , while the dashed line was obtained by multiplying the reflectances of 33 mole % lithia-silica glass (33L) by .75. The triangles are obtained by adding, at each wavenumber, .25 times the reflectance of SiO_2 plus .75 times the reflectance of 33L. It is seen that the agreement between the calculated and measured spectra of 25 mole % lithia-silica glass is excellent. The slight discrepancy that is seen may be due to the fact that the end points of the miscibility gap at the annealing temperature are not exactly those given. Also, the errors in the calculated spectrum may be due to errors in measured reflectances compounded by the addition process used to obtain it.

By separating the 25 mole % lithia-silica glass spectrum into its component parts, as described in the previous paragraph, it is seen that the recorded spectrum is simply the sum of two simpler spectra. The peaks in the simpler spectra have already been assigned. Thus, the prominent peak in the

Fig. 16. The comparison between the recorded and calculated spectra of phase separation in a 25 mole % $\text{Li}_2\text{O-SiO}_2$ glass as described in the text.



recorded spectrum is the combination of the stretching peaks due to 33L and silica. The shoulder at 950 cm^{-1} is largely due to the silicon non-bridging oxygen stretching vibration of 33 mole % lithia-silica glass.

In Fig. 13 the reflectance of this combination band comprised of two stretching peaks for the three systems studied is plotted against composition. The two stretching peaks are the S peak already discussed and a new LS peak which is the silicon-oxygen stretching peak of lithium disilicate glass. The data of Gaskell⁽³⁷⁾ and Cherneva and Florinskaya⁽⁴⁵⁾ are also plotted for comparison. It can be seen in Fig. 13 that the reflectance of the bridging silicon-oxygen stretching band varies linearly with the addition of alkali with an abrupt change in slope between 18 and 35 mole % alkali depending on the kind of alkali ion added. This linear behavior makes the technique an excellent non-destructive analytical tool for the determination of the alkali concentration of high-silica glass; the basis of a technique used to follow the progress of glass corrosion reactions discussed in Chapter II.

The break in the lithia-silica plot in Fig. 13, denoted by the dashed line, is due to the domination of the combination band by the LS vibration as seen in Fig. 16. At high silica concentrations, this combination band is controlled by the S peak because the proportional contribution from vitreous silica is higher. The S and LS contributions to

the combination band are illustrated in Fig. 9 with straight lines drawn through the portions of the combination band due to each respective peak. In the lithia-silica system, the break in the plot of the reflectance of this combination band vs. composition, designated by a dashed line, occurs when the reflectance of the hump due to the LS mode is greater than that due to the S vibration. The break is an artifact due to the way in which the reflectance of a compound band was defined. If, instead of plotting the highest reflectance of the combination band, the reflectances due to the S vibration alone are plotted, the break then occurs at 33 mole % lithia. This is taken to be the true reflectance plot for this vibration and is shown in Fig. 13 as a solid line. In the bands for the potassia-silica and soda-silica systems the two stretching peaks are not separated (see Figs. 10 and 11) and therefore do not exhibit this complication.

The breaks for the three systems occur at 18, 21, and 33 mole % alkali oxide for the potash-silica, soda-silica, and lithia-silica systems, respectively. At the transformation temperature the boundaries of the miscibility gaps of the soda-silica and lithia-silica systems are known to be 20 and 33 mole %, respectively.⁽⁴⁶⁾ Charles⁽⁴⁶⁾ argues that the consolute temperature of the potassia-silica miscibility gap is below the glass transformation temperature and hence not observable experimentally. But by the same argument,

such a gap is thermodynamically probable. The gap boundary should be closer to vitreous silica than for the soda-silica system.⁽⁴⁶⁾ The breaks in the plots of reflectance vs. glass composition are thus seen to be due to the depletion of a vibrational species, in this case, the stretching vibration of the high silica phase. The linear decrease in reflectance corresponds to the expected linear decrease in the volume fraction of the vitreous silica matrix as the total glass composition moves across the miscibility region. The fact that miscibility does not take place in the potash system for kinetic reasons does not prevent the local segregation of non-bridging oxygen around the alkali ions described by Weyl.⁽²⁾ Thus, the plots of reflectance vs. composition detect both phase separation on a macroscopic scale and the tendency towards phase separation on a microscopic scale.

Figure 14 shows plots of the maximum reflectances of the silicon-oxygen rocking peaks shown in Figs. 9, 10, and 11. The breaks occur at the same compositions as were observed for the stretching plots just discussed. The fact that the break in plots of the R peaks is not as abrupt as observed for the plots of the S peaks indicates that the effect of alkali ions on rocking vibrations is not as great as on stretching vibrations. In fact, the break in the lithia-silica plot is barely detectable in Fig. 13. The fact that the spectra of strongly phase separated 20 and 25

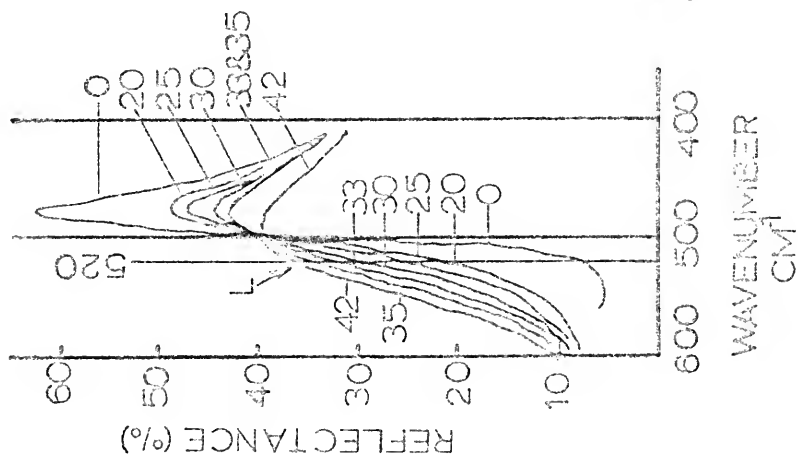
mole % lithia-silica glass (given in Fig. 9) do not have bimodal rocking peaks further strengthens the argument that the rocking vibration is quite similar in vitreous silica and lithium disilicate glass.

Figure 17 shows a detailed comparison of the rocking peaks for the three systems studied. It is seen that the spectra of all the glasses in the potash-silica and soda-silica systems exhibit a minimum near 520 cm^{-1} . The spectra of the lithia-silica glass, on the other hand, exhibit no such minima, having additional reflectance in this area (designated by the letter L). The greatest difference between the spectra of vitreous silica and 33 mole % lithia-silica glass occurs near 520 cm^{-1} . It is concluded that this maximum is due to the motion of lithium ions. The corresponding sodium and potassium-oxygen vibrations are not seen because they are found at lower frequencies and therefore buried in the continuum.⁽⁴⁷⁾ This assignment is in agreement with the work of Risen, who has reported this vibration in the same frequency range for a variety of lithium ion containing systems.⁽⁴⁸⁻⁵⁰⁾

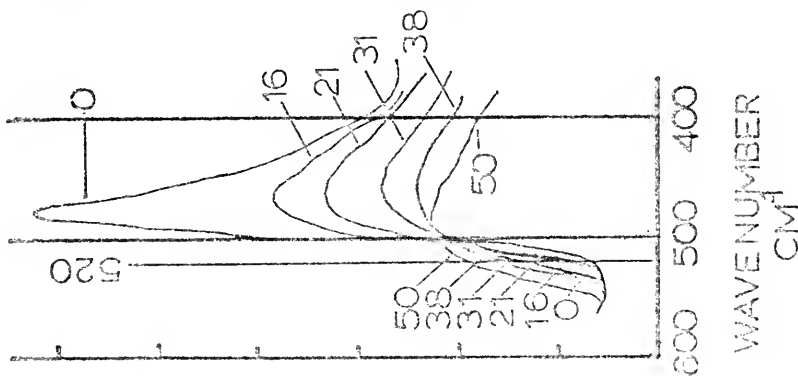
Figure 18 is a plot of the difference in reflectance at 520 cm^{-1} between the spectrum of vitreous silica and the spectra of various lithia-silica glasses. It is seen that the behavior can be approximated by straight lines having breaks at 10 and 33 mole % lithia. The breaks indicate abrupt changes in the environment around the lithium ions

Fig. 17. Spectra of the silicon-oxygen rocking peak for the three systems studied showing reflectance due to lithium vibration (L) as described in the text.

LITHIA-SILICA



SODA-SILICA



POTASH-SILICA

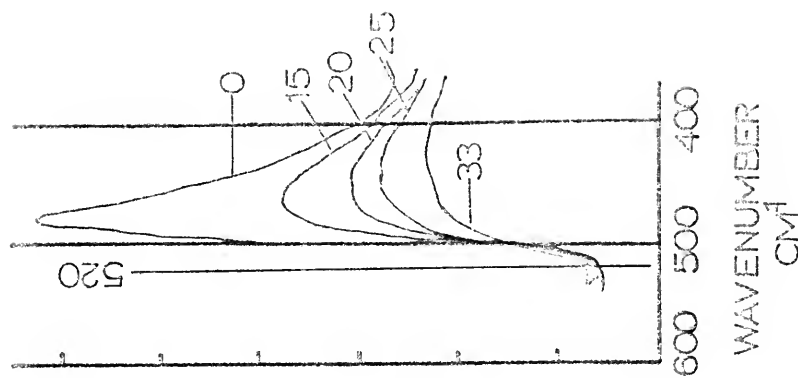
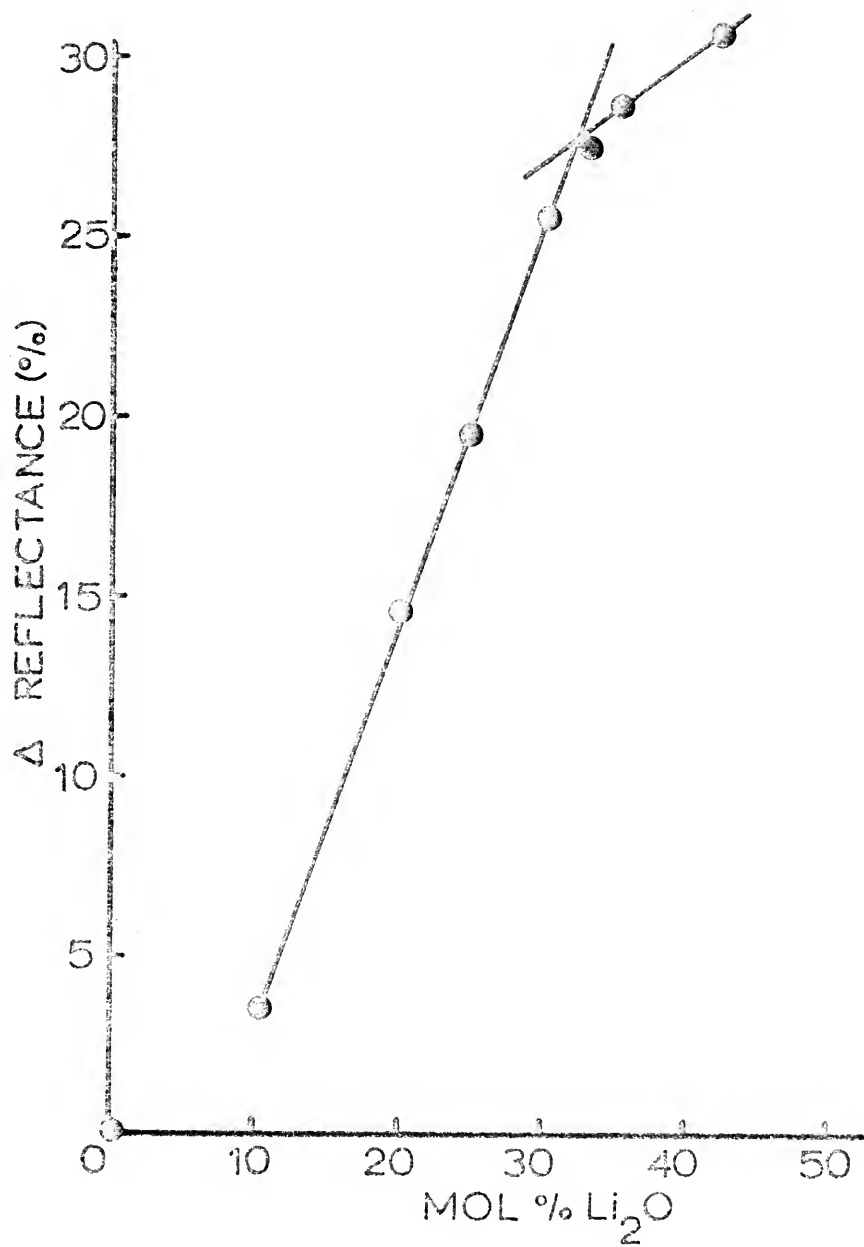


Fig. 18. Plot of the difference in reflectance at 520 cm^{-1} between the spectrum of vitreous silica and those of lithia-silica glasses.



and coincide with breaks found in plots of the activation energy for electrical conduction as a function of composition.⁽⁵¹⁾ Also, Kumar and Maitra⁽³⁹⁾ have shown that glasses having lithia concentrations less than 10 mole % do not release lithium ions into aqueous solutions, indicating that the silica-rich phase completely surrounds the small volume fraction of lithia-rich phase present in these phase separated glasses.

Again, this linear behavior of the reflectance of lithia-silica glasses at 520 cm^{-1} with mole % lithia permits the measurement of the concentration of lithium ion in lithia-silica glasses. Since lithium is not easily detected using x-ray techniques because of its low atomic number, the use of infrared reflectance spectroscopy provides a promising analytical tool for the study of lithia-based glasses.

A plot of the reflectance of the non-bridging silicon-oxygen stretching reflectance (NSR) vs. composition is given in Fig. 15. It is seen that the behavior is quite similar in all three systems with a maximum reflectance occurring at roughly 36 mole % R_2O . The explanation for this maximum illustrates the nature of the species causing this band.

It can be shown⁽⁵²⁾ that a band due to a specific vibrational species produced by the combination of two reactants can be plotted against the concentration of one of those reactants to yield a maximum. This maximum corresponds to the stoichiometry of vibrational species causing the

reflectance. In the present case, the alkali ion reacts with the silicon-oxygen network to produce non-bridging silicon-oxygen bonds. At 33 mole % R_2O , there is one non-bridging oxygen per silicon-oxygen tetrahedron. Since the maximum in the plot of the NSR peak vs. composition occurs at compositions slightly greater than 33 mole % R_2O , it is seen that the NSR peak is due to a vibrational species which, on the average, has slightly more than one non-bridging oxygen per tetrahedron.

At concentrations greater than the 36 mole %, the number of tetrahedra having more than one non-bridging oxygen becomes substantial. These tetrahedra are linked by the remaining bridging silicon-oxygen bonds forming chainlike structures. The two non-bridging oxygens in a tetrahedron can then couple to vibrate in a symmetrical and asymmetrical manner, forming peaks on either side of the non-bridging oxygen peak. This is, in fact, seen in the spectrum for 50 mole % soda-silica glass shown in Fig. 19. Coupling of the two NSR vibrations leads to the two small peaks diagrammed schematically on either side of 960 cm^{-1} . These peaks lead to both the filling in of the valley between the S and NSR peaks and the new shoulder formed on the low frequency side of the NSR peak at $\sim 820\text{ cm}^{-1}$.

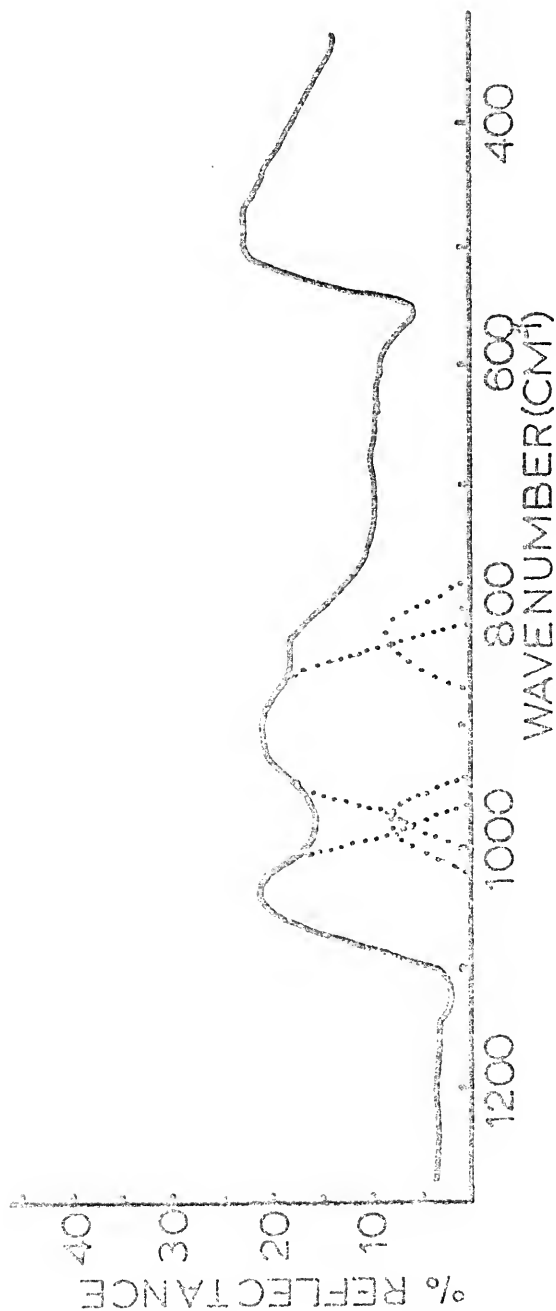


Fig. 19. Infrared spectrum of a 50 mole % SiO₂ glass. The dotted lines represent possible peaks forming this spectrum as described in the text.

Conclusions

It has been shown experimentally that infrared reflectances are proportional to the concentrations of the vibrational species causing them. Further, these reflectances can be added wavenumber by wavenumber to show more clearly the origin of the broad bands frequently encountered in the spectra of amorphous substances (see Fig. 16). These characteristics allow the extension of assignments made on stoichiometric glasses to more complex glass systems.

In addition, breaks in the linear plots of reflectance vs. bulk composition in a series of glasses imply changes in the nature of the vibrational species involved. These changes can be a depletion of a vibrational species as was seen in the stretching peak behavior near the miscibility gap boundaries (see Fig. 13), a change in the local geometry as was seen in the behavior of the lithium vibration near 10 mole %, or a partial coupling of several vibrations as was seen in the behavior of the non-bridging silicon-oxygen bond at high soda concentrations (see Figs. 15 and 19).

In the composition sequences the rocking peak follows much the same changes as does the stretching peak. This is expected because both peaks are due to different motions of the same atomic group, the silicon-oxygen tetrahedron. The phase separation seen in the lithia-silica system in the 20 and 25 mole % glasses does not cause shoulders on the

rocking peak as it does on the stretching peak (see Fig. 9). This implies that the rocking peak behavior in the lithia-silica system is not as sensitive to local composition fluctuations caused by phase separation.

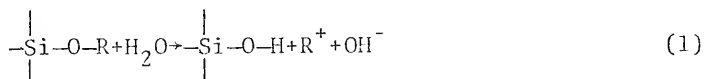
The high frequency base of the rocking peak at 520 cm^{-1} contains reflectance due to the motion of lithium ions in the glassy network. This reflectance is not seen to the same extent (see Fig. 17) in the potash and soda-silica systems due to the increased mass of those cations, which causes the peaks due to them to be buried in the continuum.

In searching for an optimal method of preparation for the glass surfaces, it was found that grinding with 600 grit dry silicon carbide paper produced a very reproducible surface free of reaction products due to the interactions of the glass surface with its environment. For 50 mole % soda-silica glass, this process had to be carried out in a totally dry environment without even momentary exposure of the sample to the water vapor in the atmosphere. For this reason, the author feels that the spectrum of 50 mole % soda-silica glass given in this work is the most accurate to date.

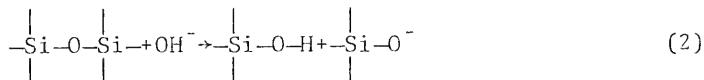
CHAPTER IV

ANALYSIS OF SILICA-RICH GELS FORMED DURING GLASS CORROSION

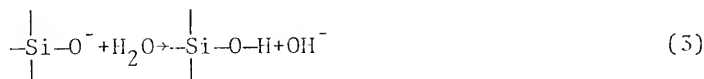
Charles described the destruction of alkali silicate glass by water in terms of three chemical reactions.⁽⁵⁴⁾ The first involved the penetration of a proton from the water into the glassy network, replacing an alkali ion which is, in turn, released into solution:



This reaction produces an OH^- ion and a non-bridging oxygen bond attached to a hydrogen ion (NSH). A second reaction, with the hydroxyl ions obtained in Equation (1), destroys silicon-oxygen-silicon bonds to form non-bridging silicon-oxygen bonds (NS) as:



The NS bond formed in Equation (2) interacts with the water molecule forming another NSH bond and a hydroxyl ion, which is free to repeat reaction 2 over again, e.g.,

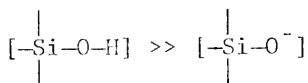


The silicic acid formed in all three reactions is soluble in water under the appropriate conditions of pH, time, temperature and ion concentrations.

Following the discussion by Douglas et al.,⁽⁵⁵⁾ the relationship between the activity of NS groups in the aqueous solution is derived as:

$$\frac{[\text{NS}]}{[\text{NSH}]} = \frac{[-\text{Si}-\text{O}^-]}{[-\text{Si}-\text{O}-\text{H}]} = 10^{-9.8} \quad (4)$$

assuming that the pH of the solution is less than nine and hence the LiOH and $-\text{Si}-\text{O}-\text{R}$ (NSR) are completely dissociated. Equation (4) shows that in acid and in neutral solutions



Also, if one assumes equilibrium conditions, [NSH] decreases rapidly with increasing pH. When [NSH] is very low, [NSL] increases and Equation (4) no longer holds. One expects, from equilibrium considerations, that the amount of R^+ release would decrease with increasing pH above pH 9. Douglas argues⁽⁵⁵⁾ that as the pH exceeds 9.8, the number of NS groups increases, leading to a net charge and breakup of the structure and increased rate of silica release.

The above relationships do not specify the location of the various corrosion species, e.g., the silanol (NSH) groups may either go into solution or form a film on the glass surfaces. Likewise, NSR groups may be present in

films on the glass surface that have been exposed to high pH values. The extent to which a glass forms a film and the coherence of that film has a strong influence on corrosion behavior.

Shmidt⁽⁵⁶⁾ introduced a parameter, α , defined as

$$\alpha = \frac{N_{\text{SiO}_2}}{m} \cdot \frac{1}{N_{\text{Na}_2\text{O}}} \quad (5)$$

where $R_2O \cdot m\text{SiO}_2$ is the composition of the glass and N is the moles/cm² of glass surface which dissolves into solution. α is a measure of the extent of selective dissolution, when $\alpha \approx 0$, compared to total dissolution, when $\alpha \approx 1.0$. At intermediate α values, a mixture of selective and total dissolution occurs concurrently. Shmidt found in binary soda-silica glasses that at a given temperature α remained unity with increasing silica concentration to a critical concentration where it decreased precipitously to zero. At higher temperatures the critical composition occurred at higher concentrations of silica. Thus, for the one-hour treatment used by Shmidt, at 100°C, only compositions having silica concentrations >80 mole % formed films.

In the present study the dependence of α on exposure time is determined for 33 mole % $\text{Li}_2\text{O-SiO}_2$ (33L) and 31 mole % $\text{Na}_2\text{O-SiO}_2$ (31N) glasses. In addition, a new parameter which is a measure of the amount of silica available for film formation is defined. This quantity, referred to as "excess

silica," or ϵ , is the difference between the amount of silica which would go into solution if the ratio between the alkali concentration and the silica concentration in the original glass were maintained (balanced silica or β) and the amount of silica which actually does go into solution. The relationships between these quantities are:

$$\alpha = \frac{Y \text{ solution}}{X \text{ solution}} \bigg/ \frac{Y \text{ glass}}{X \text{ glass}} \quad (6)$$

$$\alpha = \left(\frac{\text{PPM SiO}_2}{\text{PPM R}^+} \right) \cdot \left(\frac{\text{mwR}}{\text{mwSiO}_2} \right) \cdot \left(\frac{\text{Pm}}{1 - \text{Pm}} \right) \quad (7)$$

and

$$\beta \text{ (balanced silica)} = \left(\frac{\text{PPM SiO}_2}{\alpha} \right) = \left(\frac{\text{PPM R}^+ \cdot \text{mwSiO}_2}{\text{mwR}} \right) \cdot \left(\frac{1}{\text{Pm}} - 1 \right) \quad (8)$$

and

$$\epsilon \text{ (excess silica, PPM)} = \beta - \text{PPM SiO}_2 = \text{PPM SiO}_2 \left(\frac{1 - \alpha}{\alpha} \right) \quad (9)$$

where Y = moles SiO_2 , X = moles R_2O , Pm = mole fraction R_2O in glass, mw = molecular weight, PPM SiO_2 = concentration of silica in solution, and PPM R^+ = concentration of R^+ in solution.

Figure 20 shows two hypothetical plots of silica concentration vs. its distance from the film surface, which can be calculated from the parameters described in this work. The area under the composition profile (S) shaded in Fig. 20 is equal to one-half times the product of the ordinate and

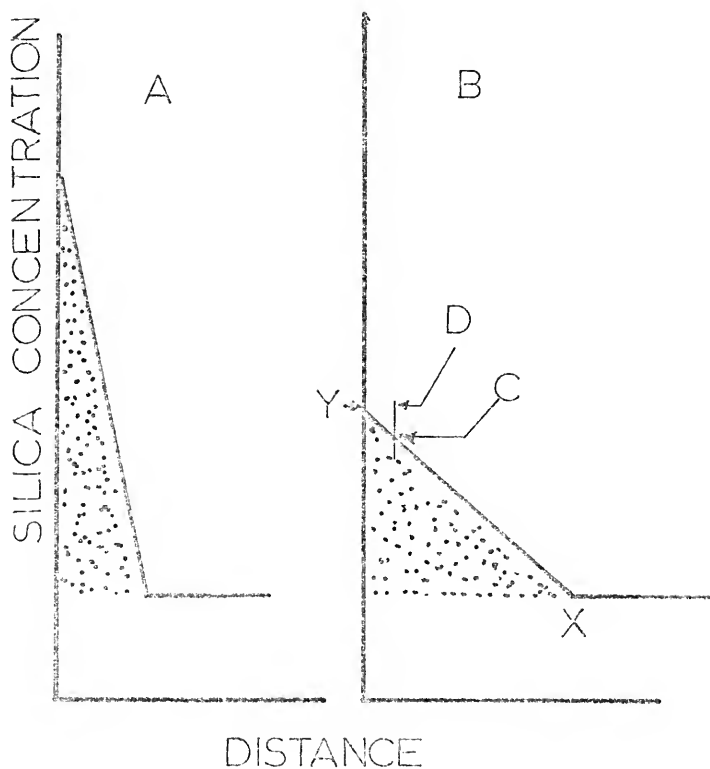


Fig. 20 Two simplified models of the composition profile of the silica-rich corrosion layer. Part A is a profile of a more resistant layer while Part B represents a less resistant layer.

abscissa of the shaded triangle. The ordinate is the difference between the measured surface silica concentration (Y) and the silica concentration of the original glass, thus having units of grams of excess silica divided by cm^3 of film volume. The abscissa is the profile thickness (X) in cm. The product, therefore, has units of grams of excess silica divided by the film surface area (A) given in cm^2 .

The quantity S can also be obtained from the parameter ϵ if the solution volume (V) and V/A ratio is known.

$$S \left(\frac{\text{grams excess silica}}{\text{cm}^2 \text{ film surface}} \right) = \left(\frac{\text{grams excess silica} \times 10^{-3}}{1,000 \text{ cm}^3 \text{ solution}} \right) \times \frac{V}{A} \left(\frac{\text{cm}^3 \text{ solution}}{\text{cm}^2 \text{ film surface}} \right)$$

In the present study, the V/A ratio is simply the depth of the cylindrical corrosion cell cavity (d) and therefore the area under the composition profile (S) is proportional to the product of ϵ and the corrosion cell depth (d) in cm, e.g., $S = \epsilon d 10^{-6}$. Both plots in Fig. 20 have the same area and hence the same ϵ values for the surface film, but the excess silica in film A is distributed much closer to the surface than in film B. Thus, film A is characteristic of a resistant film. Film B, on the other hand, is thicker because it has the same ϵ value as film A but a lower surface SiO_2 concentration, a characteristic of less resistant films.

Methods

The glass samples were corroded using the static corrosion cells as described in Chapter II. After exposure, the cell solution was immediately diluted for later analysis for lithium or sodium concentration using atomic emission spectroscopy, and for dissolved silica using the well-known molybdenum blue calorimetric method.⁽⁴⁰⁾ At low temperatures and/or short times, it was necessary to corrode a number of samples in the same manner in order to obtain sufficient concentrations of silica for analysis. The pH was determined for each run using short range pH paper (± 0.5) calibrated with a pH electrode.

The exposed glass surfaces were analyzed using IRRS as described in Chapter II. Each corroded glass sample was run with a freshly polished 33L glass for comparison. The difference in reflectance between specific features of the uncorroded glass and that of the corroded samples was measured for each spectral feature of interest. These features were the maximum value of the silicon-oxygen stretching peak at $1,100\text{ cm}^{-1}$ (S), the maximum value of the silicon non-bridging oxygen stretching peak at 425 cm^{-1} (NS), the reflectance at 520 cm^{-1} due to the lithium ion (L), and the maximum value of the rocking peak at 475 cm^{-1} (R). The greatest extent of deviation in reflectance from the uncorroded reflectance was taken as 100% reaction. Thus, the

reflectance values of corrosion events less than this maximum value were divided by the maximum value and multiplied by 100 to obtain the value of the percent reaction reported herein.

An Acton Laboratories, Model MS-67 electron microprobe was used to determine the composition profile of one of the films. The glass sample was exposed to water at 79.5°C for 17 hours. Its infrared spectra were recorded and the sample imbedded in epoxy. The imbedded sample was then cut perpendicular to the corrosion film and the resulting exposed edge polished using standard metallographic techniques to 0.25 μm diamond paste. Both the corroded section and a standard silica sample were plated side-by-side with a gold film.

The 33L sample was scanned for silicon at 10 microns per inch from the interior portion out to the edge of the sample. In addition, the film was scanned point by point manually at 2-micron intervals from the edge of the sample inward. This procedure was repeated five times and an average taken. A linear relationship between the number of counts per second and the concentration of the silica was assumed as a first approximation.

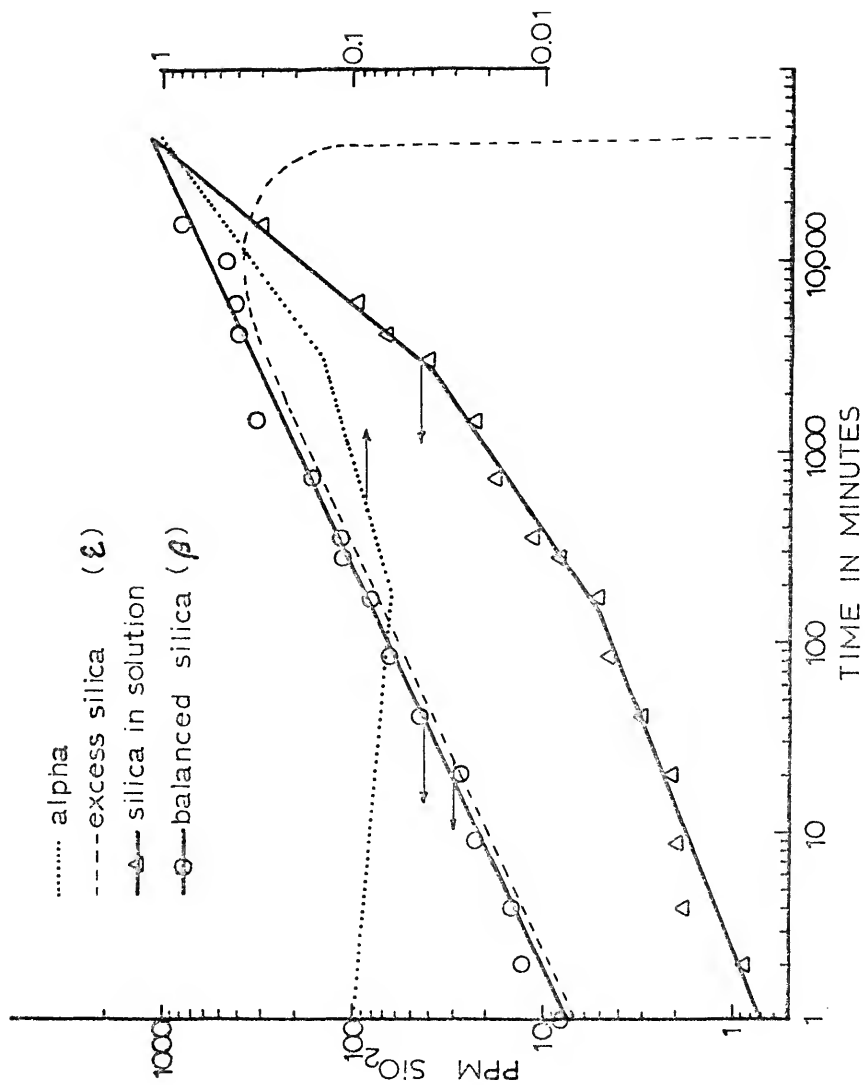
Results

Figure 21 is the solution data obtained for 33L at 40°C. It is representative of results obtained over a temperature range of 24.5 to 79.5°C. In Fig. 21 the solid line with circles is the plot of balanced silica, β , computed from the lithium concentration of the corrosion solution as discussed previously. Since β is proportional to the lithium concentration, as with lithium release, its plot is a straight line on the log-log scales as shown in this figure.

The concentration of silica in solution is best approximated by three line segments with breaks corresponding to pH values of 7 and 9. α values are shown as a dotted line. As with the behavior of silica in solution, α has three linear portions and two breaks at the same values of pH, 7 and 9. Figure 21 shows that, upon exposure of a freshly abraded 33L sample to water, the initial α value decreases with time, indicating an increasing tendency for film formation. The initially higher value of α , which implies a greater tendency for total destruction of the glassy network, is probably due to the presence of high energy silica network sites produced by the abrasion process, as discussed later.

In Fig. 21 the first break in the α curve occurs at about 170 minutes, after which the slope of the α curve becomes positive, indicating a continually decreasing tendency for film formation. Finally, at the second break,

Fig. 21. An example of data obtained from solution analysis of glass corrosion and its relation to the calculated quantities α , ϵ , and β .



occurring at 3,000 minutes, the α -time slope becomes still steeper and rapidly approaches unity. When unity is reached there is no tendency for film formation and the whole reaction is one of total dissolution of the silicon-oxygen network. However, the value of $\alpha \approx 1$ does not preclude the possibility of a high silica film being present on the glass if elsewhere in the system there are insoluble corrosion products having higher alkali content than the glass.

The ϵ curve, representing the silica that can be available for film formation, is shown in Fig. 21 as a dashed line. Because the excess silica is the difference between a relatively large quantity, e.g., balanced silica, and a relatively small quantity, silica in solution, its behavior closely parallels the former. Only when the balanced silica and the solution silica approach the same order of magnitude does ϵ deviate significantly from β , as can be seen in Fig. 21. The ϵ curve reaches a maximum when the value of α is ≈ 0.45 , indicating that roughly half of the total reaction has led to film formation.

In order to interpret the solution behavior, infrared reflection spectra of the same corroded 33L glasses were recorded and are summarized in Fig. 22. The silicon-oxygen stretching peak of 33L (LS) is seen to sharpen and increase in reflectance with corrosion time while the non-bridging silicon-oxygen peak associated with alkali ion (NSL) is seen

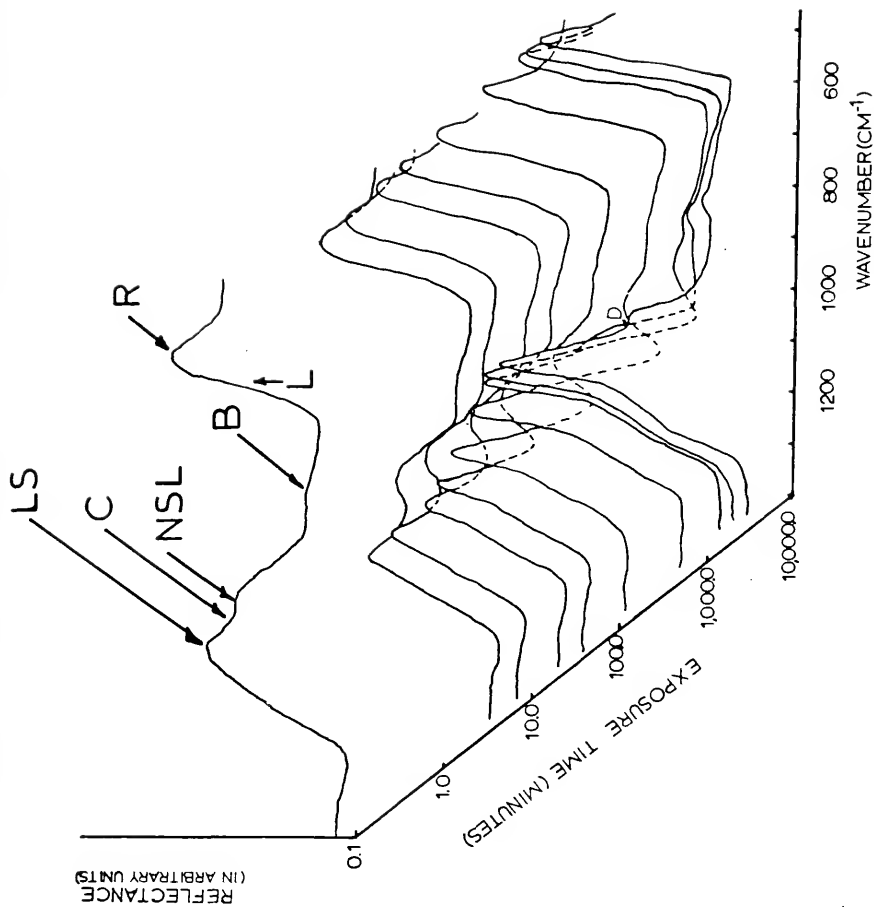


Fig. 22. Changes in infrared reflection spectra of 33L glass on exposure to static water at 40°C. The letters are explained in the text.

to decrease. Both these changes show that the corrosion process leads to a structure similar to that of vitreous silica.

The similarity of the vitreous silica reflection spectra and a 33L glass corroded in water for 22 hours at 50.5°C is shown in Fig. 23. Concurrently, the silicon-oxygen rocking peak (R) in Fig. 22 increases in reflectance and sharpens during corrosion. This change can also be attributed to an increase in the silica content of the structure sampled by the reflectance method as discussed in Chapter III. After longer periods of time, the peak B is seen to form, which is attributed to the bending mode of a silicon-oxygen bond. All of the above changes are expected in a leaching process with the increase in the silica concentration resulting from the loss of alkali ions.

Direct evidence for the decrease in alkali concentration can be seen as a decrease in reflectance at 520 cm^{-1} . This reflectance, labeled L in Fig. 22, is due to the vibration of lithium ions and its decrease signifies a decrease in the average concentration of the lithia. Another change, the decrease in reflectance between peaks LS and NSL, due to coupling between them, is also related to the loss of the lithium ions responsible for this coupling.

The shoulder (D in Fig. 22) formed at 1,010 cm^{-1} after exposure to water for 3,000 minutes at 40°C has not been conclusively assigned. It may be due to an interference

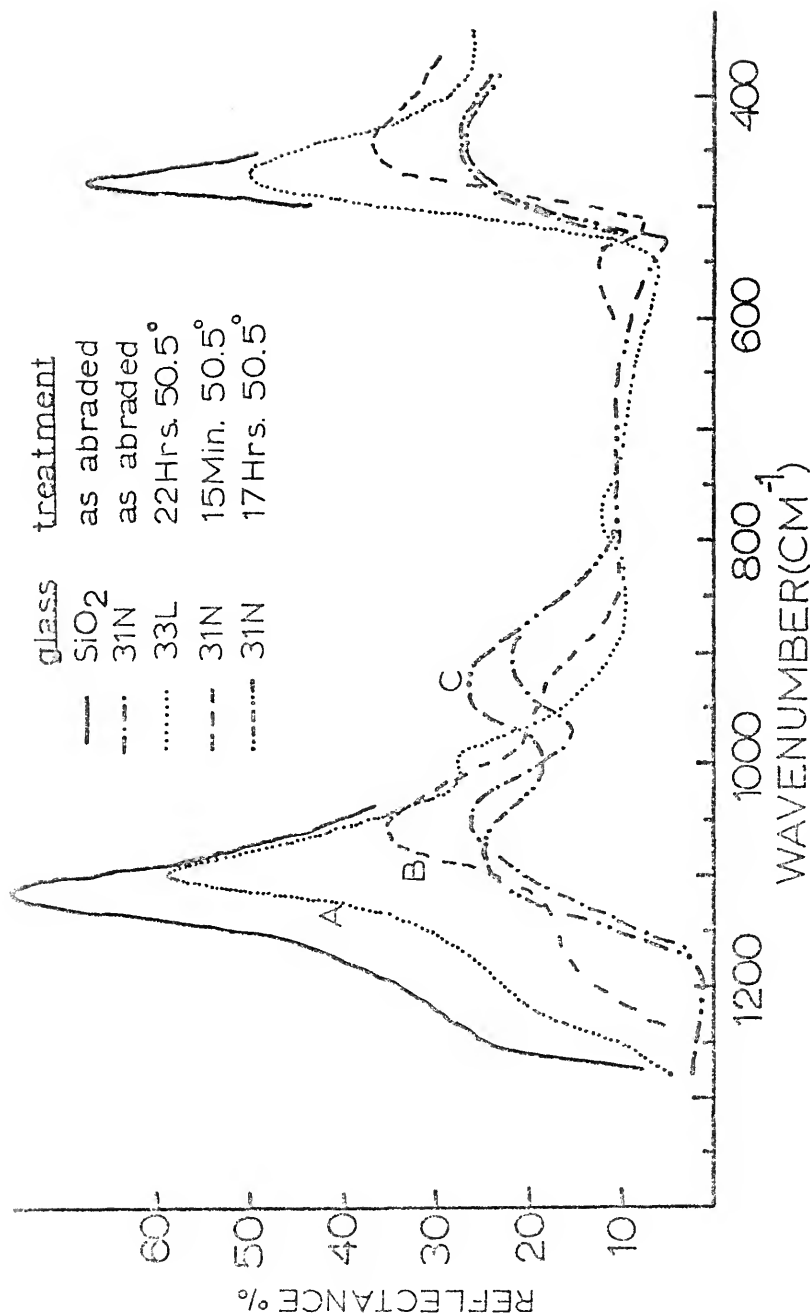


Fig. 23. A comparison of the corroded and noncorroded glass spectra in the soda-silica system. The spectra of vitreous silica and corroded 33L are included for comparison.

fringe caused by the corroded layer, but more probably is due to the silicon non-bridging oxygen vibration associated with bonded hydrogen ions in a polymerized gel structure. A similar assignment was given by Naudin for an absorption peak found at 952 cm^{-1} . (57)

Figure 24 is a compilation of the solution data obtained at four temperatures. Part II of Fig. 24 contains plots of α values for the 33L glass. Also included is a dotted line showing the behavior of α for 31N at 50.5°C . In part I of Fig. 24, the behavior of excess silica is shown for the same glass compositions and temperatures. For clarity, letters coded for the appropriate temperature are placed at the ends and break points of the solid lines for the 33L curves.

Figure 25 is a micrograph of the corroded layer of 33L treated for 350 minutes at 79.5°C . The area seen is the fractured edge of the corroded layer made by drawing a diamond stylus through the film. The gage ball marked with the arrow is 0.87 microns in diameter. The white, jagged flakes are debris produced by the diamond stylus. The corrosion layer in the foreground has grinding scratches with pits roughly 0.5 microns in diameter running along them. These pits appear to be the same depth as the corrosion film. They apparently are due to the total dissolution of the glass in the scratch valleys.

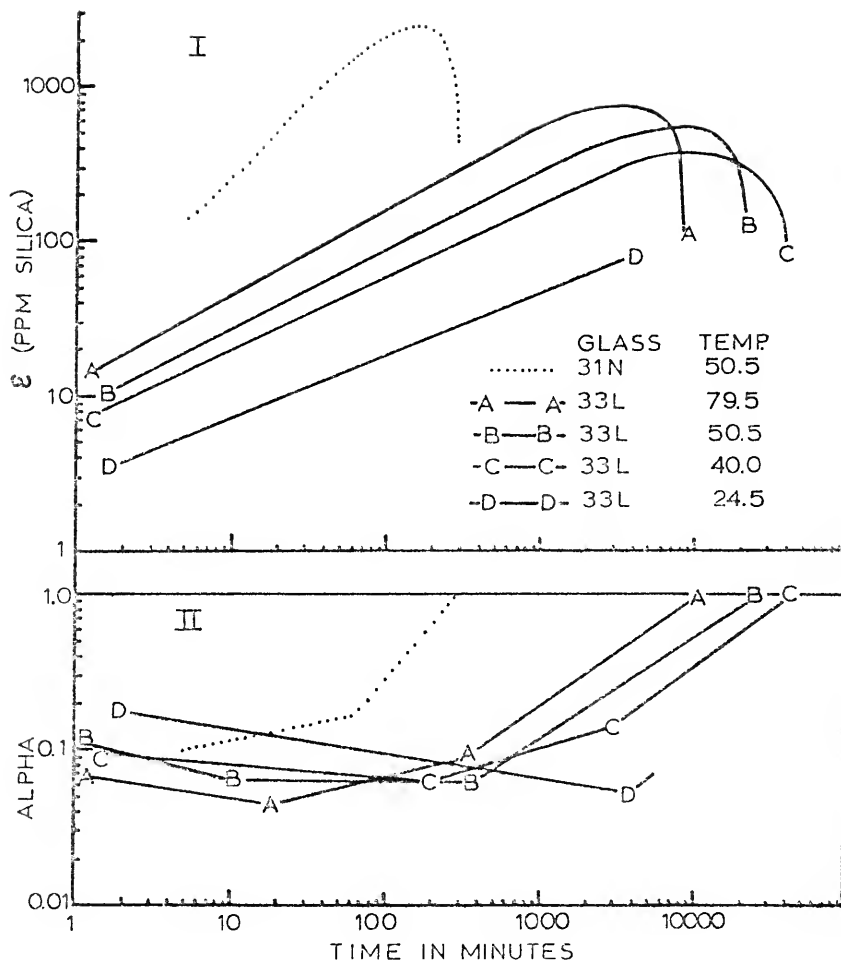


Fig. 24. A summary of the plots of ϵ and α calculated from all the solution analysis data reported in this work. The letters are used to designate the corrosion temperature involved.

Fig. 25. An S.E.M. micrograph of the edge of the corroded layer of ^{33}L glass exposed to static water for 350 minutes at 79.5°C . The gage ball is 0.87 microns in diameter.



Comparison of α (see Fig. 24) for corrosion of 33L at different temperatures reveals that, at short times, α decreases with increasing temperature, while at longer times α increases with increasing corrosion temperatures. At intermediate corrosion times, α is relatively independent of corrosion temperature. This is due to a reactive glass surface produced by the abrasion process used to prepare the corrosion samples. This reactive glass, present in the scratch valleys, dissolves completely on exposure to water, causing the pits seen in Fig. 25 and the higher values of α during initial exposure, Fig. 24. At slower reaction rates found at lower temperatures, this effect was more evident in the α plot because it represents a larger proportion of the total concentration of ions in solution.

At higher temperatures, the larger total concentration of ions in solution decreases the impact of scratches on the α behavior and hence a lower value of α is observed (Fig. 24). For longer corrosion times, the total solution concentrations are large enough that α is larger with increasing temperature.

The α curve of the 31N glass is consistently higher than that of the 33L glass (Fig. 24-II). This means that during corrosion, a larger percentage of the silicon-oxygen network is destroyed in the 31N glass than in 33L at the same temperature. Also, during corrosion of 31N, α reaches unity 10^4 minutes sooner than during corrosion of 33L. This

difference is a measure of the relative reactivity of the two compositions in aqueous solutions.

Plots of ϵ as a function of corrosion time, Fig. 24-I, reveal that at higher temperatures a higher value of ϵ is attained. From the arguments given previously, the higher ϵ value implies that the maximum film thickness attainable increases with increasing temperature. The plot of ϵ for 31N has a maximum greater than any of the maxima obtained with 33L for the temperatures shown. Thus, in the cases studied, the more rapid the film-forming process the thicker the resulting corroded layer, as illustrated in Fig. 20.

Figure 26 is a composition profile of 33L after 17 hours in H_2O at $79.5^\circ C$ obtained from a microprobe scan. The total film thickness is 15 microns with a discontinuity in the slope of the profile at 6 microns from the surface. The composition of the film at the surface is 93.5 mole % silica. The remainder of the corroded film may be composed either of porosity, hydrogen, or lithium ions. The shape of the measured profile is similar to the model film profile shown in Fig. 20.

Figure 27 shows the corrosion time dependence of the reflectances of several IR spectral features, e.g., 520 cm^{-1} and the Si-O stretch peak(s) found near $1,100\text{ cm}^{-1}$, compared to excess silica, ϵ , calculated from Equation (9) using solution data at $40^\circ C$. To permit this comparison, all quantities plotted are normalized by dividing the change due

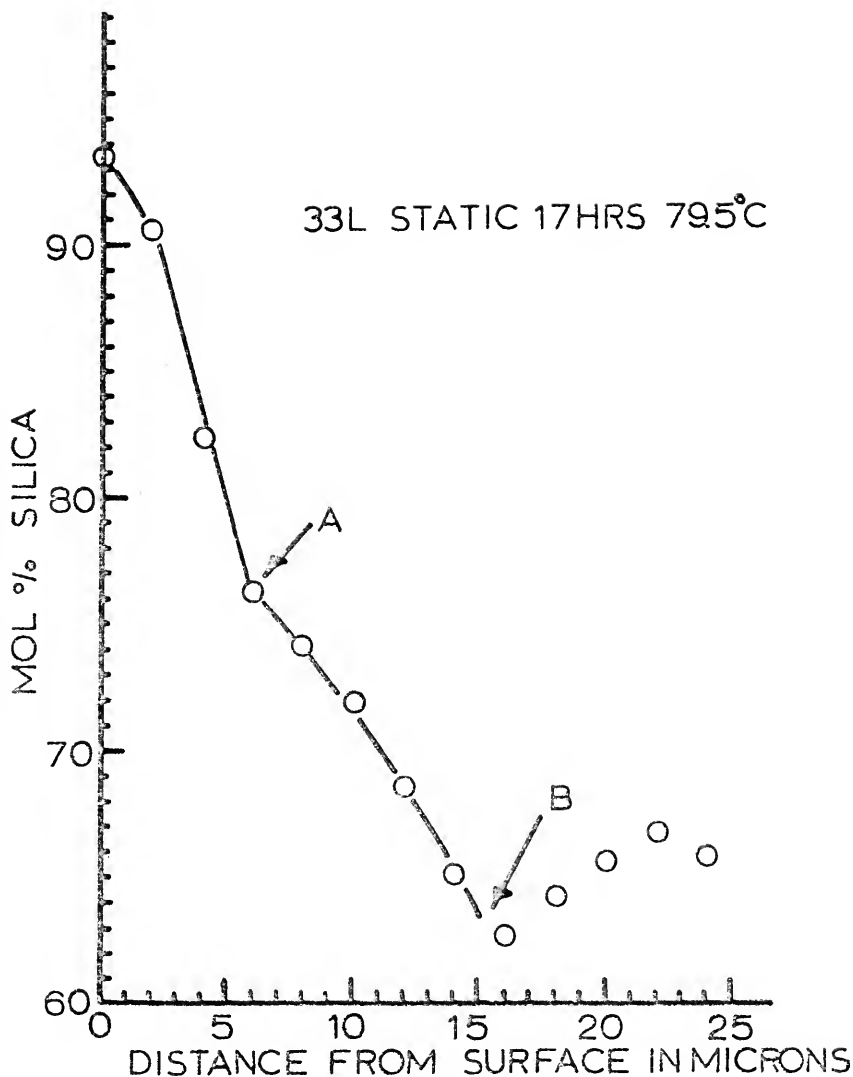


Fig. 26. A composition profile of the corroded 33L glass film obtained with an electron microprobe. This film was obtained by corroding 33L glass with 79.5°C water for 1,020 minutes.

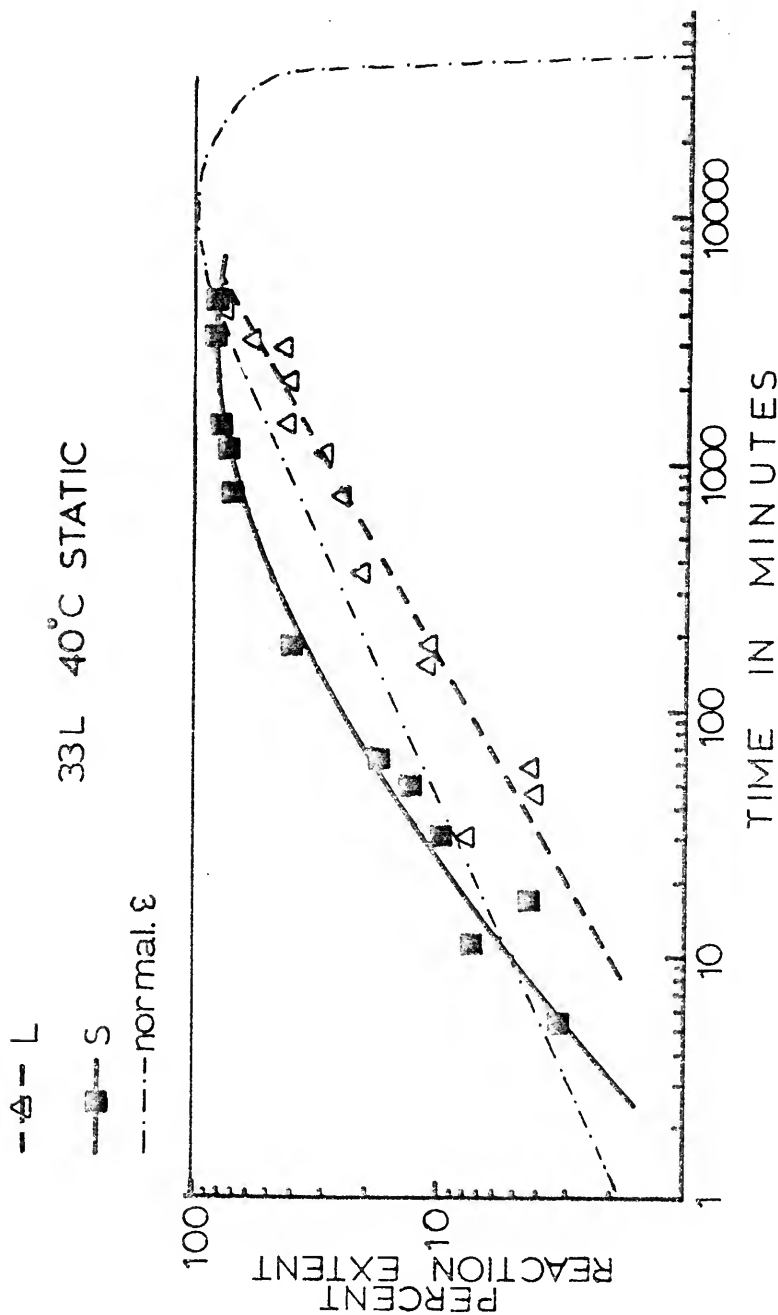


Fig. 27. A comparison of normalized infrared reflectance plots with normalized ϵ behavior for corrosion of 33L at 40°C.

to corrosion at a given time by the maximum extent of change possible for that particular reaction coordinate.

The normalized change in IR reflectance due to corrosion at various wavelengths will be designated "infrared estimators of the extent of reaction" for the rest of this work. This terminology is necessary because some of these "estimators" such as the L reflectance at the base of the Si-O rocking peak are not reflectance peaks, but rather sides of peaks which are buried under other peaks. Nevertheless, they can be used to follow the change in the silica concentration at the film-solution interface after a particular corrosion event.

Figure 28 is a comparison of infrared and solution behavior of 33L at 79.5°C. The data shows that at 79.5°C the infrared estimators lie above the excess silica curves, whereas at 40°C the infrared estimators of extent of reaction lie around the normalized silica excess curve. The reason for this difference is discussed in the next section.

Discussion

As described by Schroder⁽⁵⁸⁾ and summarized by Weyl⁽²⁾ the glass corrosion process involves a combination of the total dissolution of the whole glassy network and the partial dissolution or leaching of one of the components of that network. Total dissolution does not produce films on

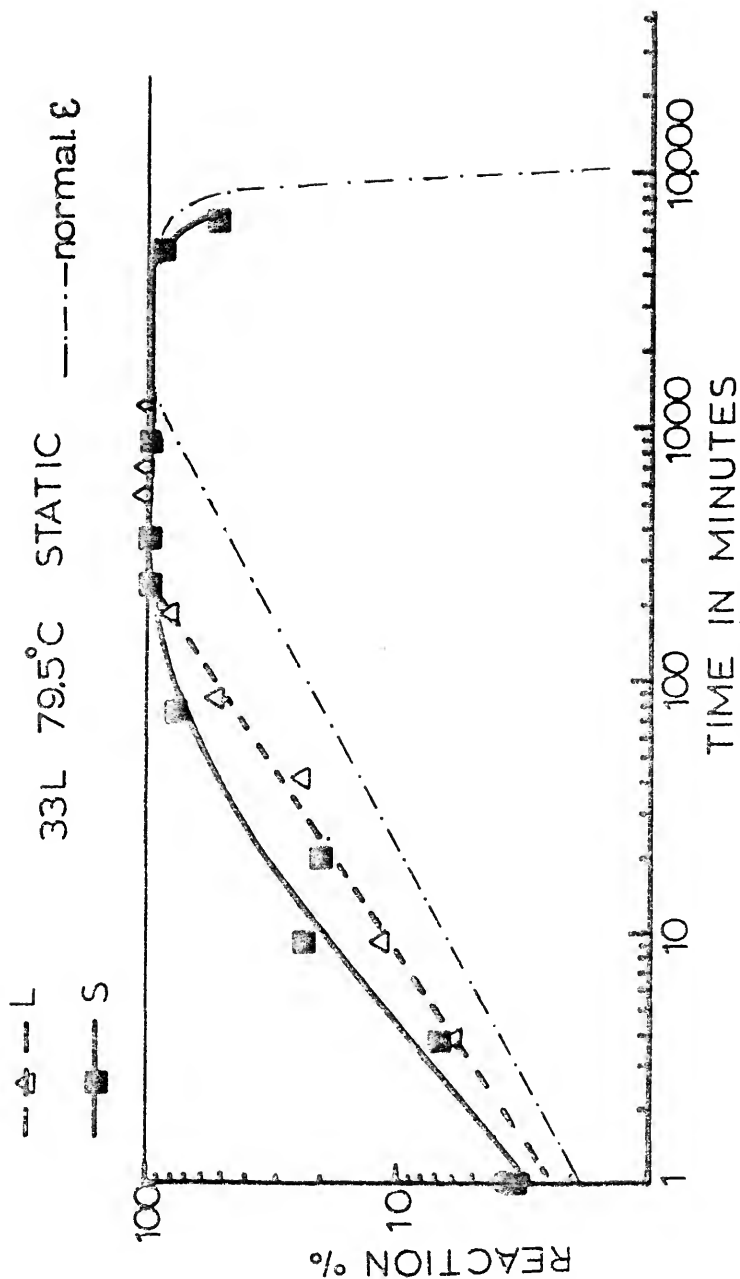


Fig. 28. A comparison of normalized infrared reflectance plots with normalized ϵ behavior for corrosion of 33L at 79.5°C.

the glass surface, while leaching produces a silica-rich layer which may have a strong influence on later corrosion kinetics.⁽²⁾ In many glass-water systems both processes occur simultaneously and the nature of the corroded layer, if present, is determined in part by the relative rates of the two mechanisms. In the present study, changes in the corrosion film are described in terms of ϵ , the amount of silica available for film formation, and the silica concentration of the film surface as determined by IRRS.

The linear relationship between IR reflectance and the concentration of the vibrational species producing the reflection spectra was established earlier in Chapter III. Since all changes in the IR spectra due to corrosion require a preferential loss of alkali ions leaving an excess concentration of silica, one would expect the activation energy for the infrared changes to be similar to that for alkali ion loss. Such is the case in Fig. 29, where the log of the time required to achieve 50% of the total change possible for a particular spectral feature is plotted against $1/T(^{\circ}\text{K})^{-1}$. The activation energy, 19 ± 2 kcal/mole, is the same as that observed for obtaining a particular concentration of Li^+ ions in the corrosion cell, Fig. 29. This result is similar to that reported for the release of alkali ion in a number of silica-based glasses,^(13,59) which is in turn similar to that required for ionic conduction in the bulk glass.⁽⁶⁰⁾

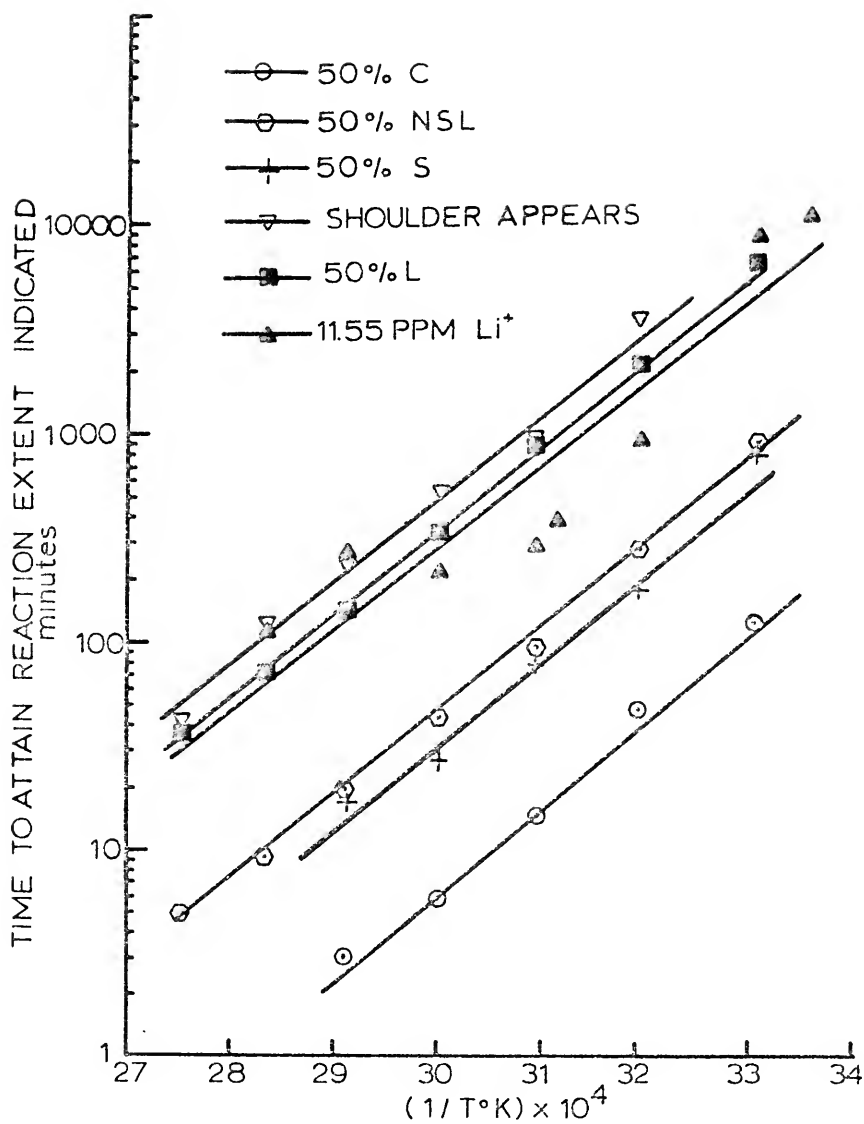


Fig. 29. Plots of the various reaction coordinates described in this work to obtain apparent activation energies.

The relative sensitivity of the various infrared estimators can be seen in Fig. 29. The coupling between the S and NSL peaks, labeled C, is the most sensitive estimator of reaction extent as it reaches half its total value, at any temperature, faster than the other estimators. Since C is due to the sum of reflectance from both S and NSL, its high sensitivity is caused by the addition of small changes in the S and NSL peaks, thus producing larger changes in the C reflectances. The S and NSL peaks have similar sensitivity and their curves in Fig. 29 almost overlap. The L peak and the appearance of the shoulder at $1,000\text{ cm}^{-1}$ have the lowest sensitivity of the estimators discussed.

With the exception of the coupling mode already discussed, the differences in the sensitivity of the IR reflectance changes (L, S, NSL) are due to a penetration depth effect. This is illustrated in Fig. 20B where D is the depth of penetration of the IR beam into the corrosion layer. The greater the depth of penetration, D, of the IR beam for a given profile, the lower the average concentration determined by that beam. Since penetration depth is proportional to the wavelength,⁽²⁷⁾ its value for the L reflectance at 19.23 microns is roughly twice as great as that for the S peak at 9.09 microns and the NSL peak at 10.5 microns. This difference is further enhanced by a contribution from the difference in index of refraction at the S, L, and NSL frequencies. This explains the consistently lower values for

the reaction extent as measured by the L reaction coordinate compared to the reaction extent measured by the S and NSL reaction coordinates.

At both 40° and 79.5° the change in S occurs more rapidly than the change in L. This is due to the effect of penetration depth on sensitivity discussed above. The difference in S and L is more pronounced at 40°C, indicating a greater slope of the composition profile (Fig. 20) for that temperature.

The combination of the depth effect and the total dissolution of the surface of the corroded layer causes the non-linear shape of the S plots in Figs. 27 and 28. As shown in Fig. 20A, the effect of dissolving the surface of the corrosion profile will be to decrease the SiO_2 concentration, Y. This in turn results in a slower rate of increase in Y with time, seen as a bending of the S plots (Figs. 27 and 28) at high extents of reaction. The L plots, on the other hand, "see" a larger percentage of the corroded film and thus are less sensitive to the dissolution of the high silica surface of the corroded layer. L plots, therefore, have a linear behavior more characteristic of the changes in the film as a whole.

The relative position of the S and L plots with respect to the ϵ plot is also informative. In Fig. 27 the ϵ plot is between the S and L plots, while in Fig. 28 both S and L lie above ϵ . This behavior is understood using the film profile

model, Fig. 20A. During the film-forming process, the area under the profile shaded in Fig. 20A increases with corrosion time. This increase may be due to an increase in the film thickness, X , an increase in the silica concentration at the film surface, Y , or a simultaneous increase in both. The S and L plots of Figs. 27 and 28 follow changes in Y as a function of corrosion time, whereas the parameter ϵ follows the area under the profile. Thus, at 79.5° most of the film-forming process involves an increase in X under a high constant value of Y , whereas at 40° the film-forming process involves a simultaneous increase in both X and Y .

This result appears contrary to the previous observation that the slope of the film profile at lower temperatures appears to be steeper than the comparable profile obtained at a higher temperature. The discrepancy is due to the greater total possible thickness of the film produced at higher temperatures as evidenced by the greater maximum value of ϵ (Fig. 24). The increasing maximum film thickness with corrosion temperature appears to be related to the rate of film formation as seen in Fig. 24. At higher temperatures or for the 31N glass, where ϵ increases more rapidly, the maximum in ϵ is greater than at lower temperatures where ϵ increases more slowly.

The presence of maxima in the ϵ plots of Fig. 24 indicates that, in general under static conditions, the corroded layer increases to a maximum thickness and then dissolves as

the rate of total dissolution exceeds the rate of selective leaching. A maximum should also occur in the reflectance plots if this interpretation is correct. Figure 28 shows that at long corrosion times the S reflectance starts to decrease, indicating a decrease in the silica concentration at the film-solution interface. A more pronounced decrease in surface silica concentration is seen in Fig. 23 for 31N glass corroded for 17 hours (spectrum C). A comparison of spectrum C with the spectrum of freshly abraded 31N shows that the corroded glass surface is almost identical to that of the original glass. After 17 hours the area of the sample exposed to the corrosive media had an indentation of roughly 1 mm in depth where the glass had been completely dissolved into solution. A corroded spectrum identical to the freshly abraded spectrum was expected because the corrosion time (see Fig. 24) exceeded the time required to reach an α of unity or an ϵ value of zero for that composition and temperature. The small difference in the infrared spectra that was observed is probably due to the fact that α does not appear to reach unity as the projection shown in Fig. 24 would suggest. Instead, as β and ppm SiO_2 become close, ppm SiO_2 deviates from its linear behavior and appears to follow β in some way which permits residual excess silica concentration. The exact nature of this behavior will require more accurate measurements of solutions because the quantity of interest, ϵ , is the difference between two large quantities, β and ppm SiO_2 .

Spectrum A in Fig. 23 is representative of a high silica concentration at the film surface corresponding to a profile similar to that pictures in Fig. 20A. Spectrum B of Fig. 23, on the other hand, is an example of the spectrum of a profile having a low silica concentration at the solution-film interface, such as Fig. 20B. The two spectra represent the maximum silica concentration that can be obtained at the solution-film interface for their respective glass compositions as determined by infrared reflection-time studies, i.e., Fig. 22. The 33L film, which is richer in silica at the film-solution interface, is found to be two orders of magnitude more resistant than the film formed on the 31N glass, which has a much lower silica concentration at its film-solution interface. This resistance comparison is made on the basis of the total ppm silica released after some arbitrary time. After 100 minutes at 50.5°C, for example, 33L releases 6.5 ppm SiO_2 compared to 1,200 ppm for 31N. Thus, the large difference in corrosion resistance of two binary silicate glasses having similar alkali concentrations, but different cations, is due at least in part to the distribution of silica in the corrosion layer.

Conclusions

The nature of silica gel films formed on glass surfaces due to selective leaching of alkali ions can be monitored by a combination of a parameter ϵ (obtainable from ion

concentrations in solution and giving the amount of silica available for film formation) and the concentration of silica at the corrosion film's surface as determined using infrared reflection spectroscopy. These two quantities can be used to define a model of the actual corrosion film profile which serves to permit the comparison of films formed on different glasses under different corrosion conditions.

With the unreplenished corrosion condition used in this study, the corrosion of 33L and 31N glasses shows similar behavior with respect to the manner in which the ions dissolve from the glass (Fig. 24). However, 33L glass corrodes two orders of magnitude slower than 31N glass. This is principally due to the formation of a corrosion film on the 33L glass which has a high surface silica concentration as determined using infrared reflection spectroscopy and the electron microprobe. The 31N sample, having a similar ϵ value and hence the same amount of silica available for film formation, has a much lower surface silica concentration. Thus, the profile of 31N glass is more like Fig. 20B, while the profile of 33L glass is more like Fig. 20A.

The effect of scratching the glass surface appears in the solution data as an unusually high silica release. This in turn produces a higher initial value of α . This effect decreases with increasing corrosion times and increasing temperatures. It produces 0.5 micron pits along the grinding scratches due to the total dissolution of chemically active glass produced by the grinding process.

CHAPTER V

CORROSION OF A LITHIA-SILICA GLASS IN VARIOUS AQUEOUS ENVIRONMENTS

Glass corrosion is a complex phenomenon and, consequently, the numerous studies conducted for specific engineering purposes resist compilation into a unified body of knowledge. Excellent reviews by Beattie,⁽²³⁾ Holland,⁽³⁾ Weyl,⁽²⁾ Das,⁽³¹⁾ Bacon,⁽⁶¹⁾ and Eitel⁽⁶²⁾ illustrate the many different approaches applied to various aspects of the glass corrosion problem. The subject can be conveniently divided into either the effects of sample state or the influence of corrosion condition on the corrosion kinetics and the structure of the corroded glass surface. Sample states important in glass corrosion include glass composition, mole fraction of a crystal phase, internal or applied stresses, surface roughness, phase separation, homogeneity, and powder or bulk form of the material. Corrosion conditions of concern include ranges of relative humidity, sulfur dioxide and other gas phase surface reactants, pH, the starting and final compositions of corrosion solutions, pressure and temperature of the corrosion solution, and the ratio of the solution volume to the corroded area.

Douglas and coworkers have conducted a systematic study of the effects of solution pH and glass composition on the ions released by glass into solution⁽⁵⁵⁾ using glass grains for the glass state and buffered and/or neutral solutions for the corrosion condition. They initially studied binary silicate glasses,⁽¹³⁾ and later more complicated ternary systems⁽¹⁵⁾ which better approximate commercial glass compositions.

In the present study, infrared reflection spectroscopy, recently adapted for quantitative glass corrosion studies of bulk glass surfaces, is used to characterize the corroded layer formed on 33 mole % lithia-silica glass under a variety of corrosion conditions. The surface of each sample was freshly abraded with dry 600 grit silicon carbide paper to provide a reproducible surface state which approximates glass damaged through normal use. The effects of other glass states on corrosion behavior are discussed in Chapter VI.

Methods

The glass samples, after being abraded with dry silicon carbide paper to remove the effects of any previous environmental reactions, were subjected to a specific environmental condition after which the infrared spectrum of the corroded surface was recorded using the "minirig" reflectance attachment described in Chapter II. The samples were treated with

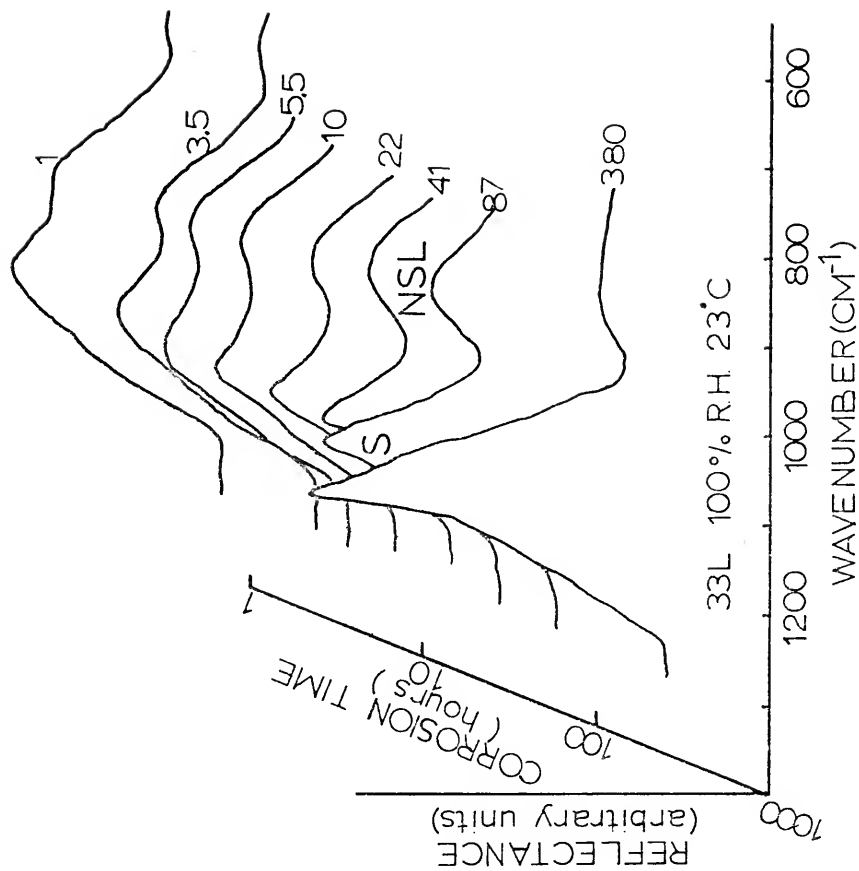
100% relative humidity by holding them in a vertical position in a container having an excess of liquid water. It was observed visually that water condensed and ran off the glass surfaces during the corrosion treatment. For the 85% R.H. treatment air bubbled through a water bath held at 38°C was passed into a chamber containing the glass samples held at 40°C.

For static and dynamic water exposures the glass samples were held against water-filled Teflon blocks, as described in Chapter II. A controlled flow of water at the rate of 2.4 ml/min, determined by a flowmeter, was passed through the Teflon blocks to study replenishment effects. Room temperature treatments were controlled to within $\pm 2^\circ\text{C}$. A high pressure corrosion condition was obtained using an Autoclave Engineers autoclave with an excess of liquid water heated to $210 \pm 5^\circ\text{C}$ for 93 hours. In addition to the infrared reflection spectrum, an x-ray diffraction pattern was recorded for the autoclaved sample using copper $K\alpha$ radiation monochromated with a primary beam monochromator. Scanning electron micrographs of various samples were taken using a Cambridge stereoscan scanning electron microscope.

Results

The changes in the infrared reflection spectrum of 33L after various stages of exposure at 100% relative humidity and at room temperature (23.5°C) are shown in Fig. 30. The

Fig. 50. Changes in the infrared spectrum of ^{33}L glass with exposure to 100% relative humidity at room temperature. The absorption peak assignments S and NSL correspond to the stretching and non-bridging oxygen vibrations, respectively.



silicon-oxygen stretching peak (S) increases in reflectance after an incubation period of approximately 1,000 minutes, while the silicon non-bridging oxygen peak associated with alkali ions (NSL) decreases. Also, the reflectance due to the overlap of the S and NSL peaks decreases faster than the NSL peak reflectance, forming a valley between the S and NSL peaks. All of these changes are due to the formation of a silica gel film on the glass surface.

Figure 31 compares the rate of silica gel film formation during corrosion by 100% relative humidity at 23.5°C with the rate due to liquid water treatments at the same temperature. The percent of the total possible reflectance change for the S and NSL peak maxima is plotted against corrosion time for both corrosion conditions. All the reaction coordinates appear to intersect at the same corrosion time, ~20,000 minutes, while the extent of reaction according to both the S and NSL plots is initially much greater for the liquid water treatment. This is due to a long incubation period for the change in the S peak reflectance with 100% humidity exposure. After the incubation period, the S plot for the 100% R.H. treatment increases more rapidly than the corresponding S plot for the water treatment, indicating a greater rate of gel formation once it has begun.

The effect of a 100% relative humidity treatment at an elevated temperature and pressure on the IR spectrum of 33L is shown in Fig. 32. Spectra of two 33L samples heated to

Fig. 31. Comparison of the extent of possible reaction determined by the reflectance of the stretching (S) and non-bridging oxygen (NSL) peaks of 33L glass exposed to both 0.9 ml of static liquid water and 100% relative humidity.

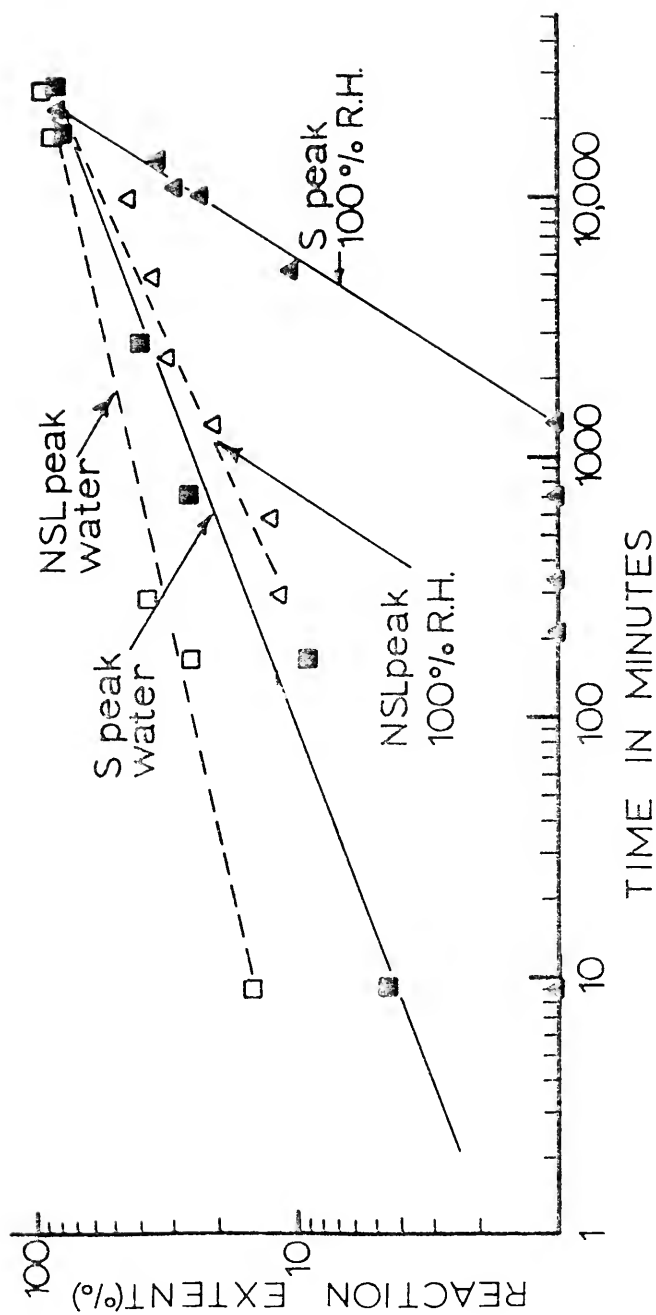
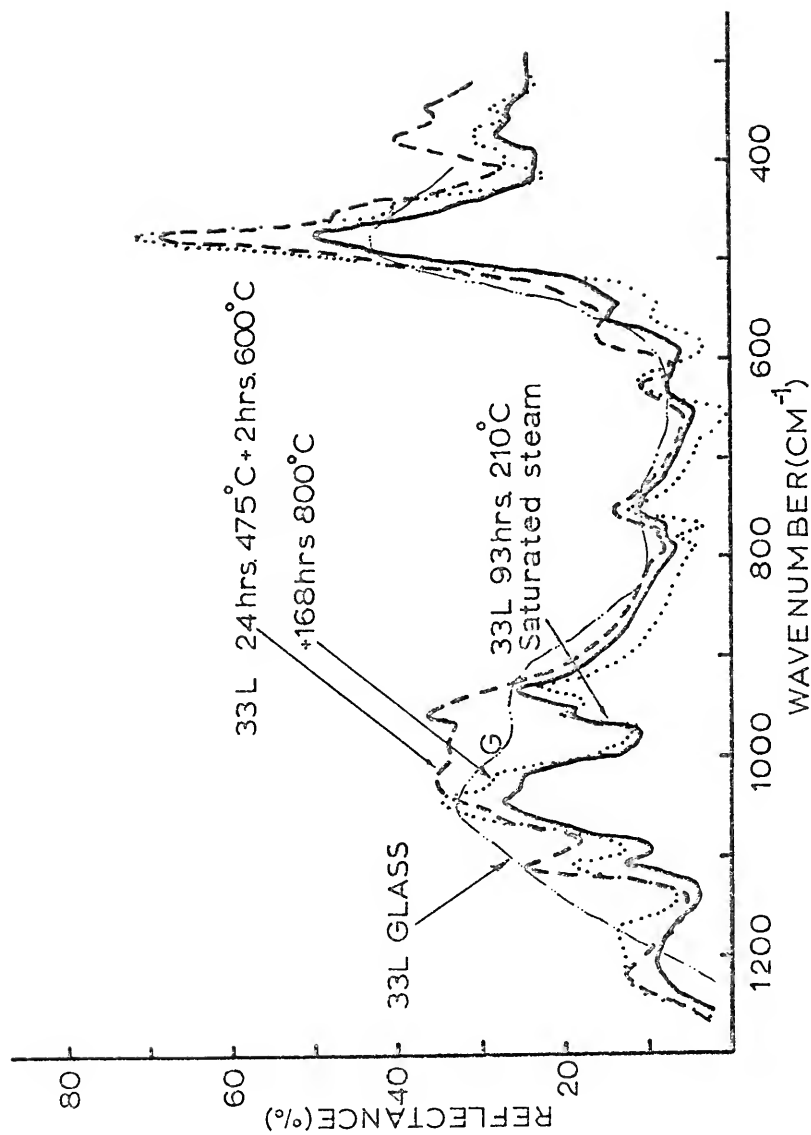


Fig. 32. Infrared spectra of 33L glass given the crystallization treatments shown. A spectrum of 33L freshly abraded with dry 600 grit SiC is included for comparison.



partially and totally crystallize the glass are shown for comparison. The 33L sample which was nucleated for 24 hours at 475°C and crystallized for 2 hours at 600°C has additional reflectance at $1,000\text{ cm}^{-1}$ in its infrared spectrum due to the 1% amorphous phase known to be present.⁽³⁸⁾ This reflectance is seen to disappear when the partially crystallized sample is reheated at 800°C for 168 hours, a treatment thought to remove residual amorphous phase. The infrared spectra of the hydrothermally treated 33L sample and the 33L sample produced by longer heat treatment at atmospheric pressure are identical. Thus crystalline lithium disilicate is produced in the autoclave treatment more rapidly than would be possible without the presence of steam. This finding is further substantiated by the identical x-ray diffraction patterns of the hydrothermally treated sample and the sample with the other heat treatment (Table 2).

In addition to the 100% R.H. treatment where water continually condensed on the glass surface, experiments were conducted at 85% R.H. at 40°C with no condensation occurring. The results of this exposure on the infrared spectra are shown in Fig. 33. The reflectance of the entire infrared spectra between 800 and $1,200\text{ cm}^{-1}$ (stretching modes) is seen to decrease with little change in the spectra between 400 and 600 cm^{-1} (rocking modes). In contrast to the behavior of the 100% R.H. exposure, Fig. 30, there is no indication of an S peak forming at $1,110\text{ cm}^{-1}$ for corrosion

Table 2

X-ray Analysis of Corroded and Autoclaved 33L Glass

33L, 93 hrs. at 210°C,
saturated steam

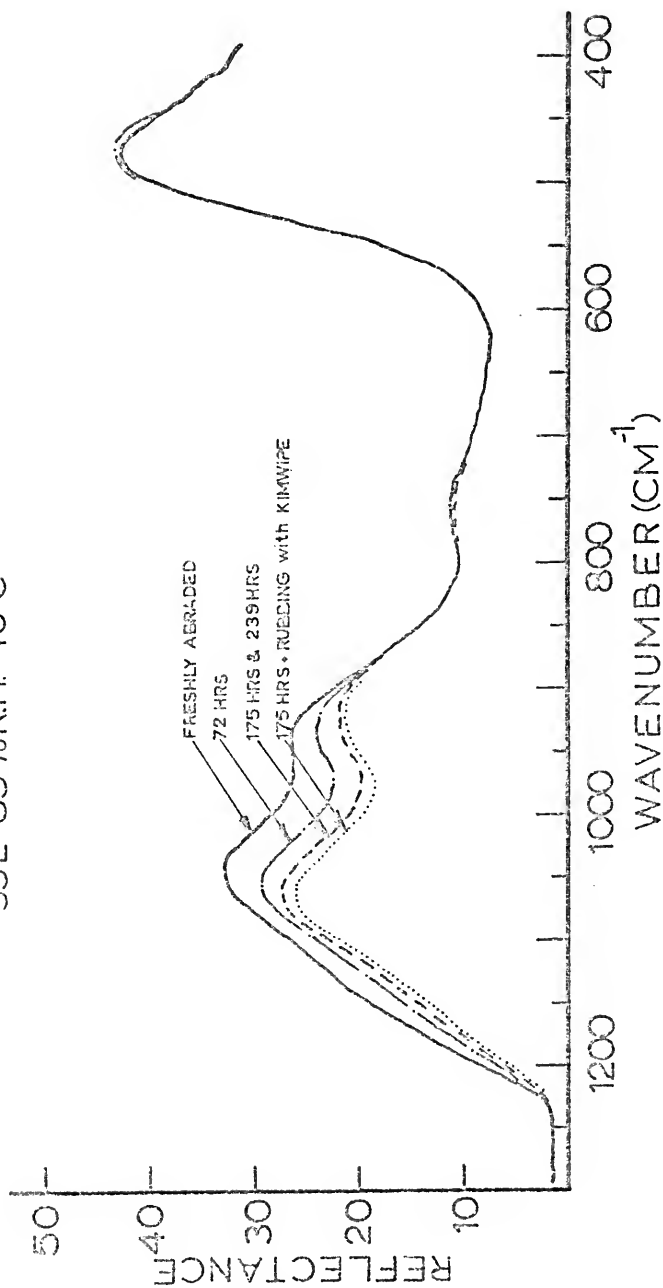
D	I
1.92	5.7
1.89	4.2
1.85	10
1.52	0.9
1.27	3.1
1.25	1.66
1.22	0.7
1.11	0.9
1.09	0.9
1.07	1.6

33L, 24 hrs. at 475°C
+ 2 hrs. at 600°C

D	I
1.91	5.2
1.89	7.5
1.85	10
1.52	1.1
1.27	3.8
1.25	0.1
1.11	0.83
1.09	0.83
1.07	1.1

Fig. 53. Changes in the infrared reflection spectra of 33L glass on exposure to 85% relative humidity. The effect of wiping an exposed sample with a Kimwipe is also shown.

33 L 85% R.H. 40°C



times up to 239 hours. The 175-hour exposure appears to form a valley between the LS and NSL peaks and this valley is made more pronounced if the treated surface is rubbed with a Kimwipe, thereby removing loose reaction products.

The effect of replenishment on the rate of corrosion film formation was studied by comparing changes in the infrared reflection spectra of 33L glass under two corrosion conditions. In the first, water was passed over the glass surface at a rate of 2.5 ml/min, while in the second, a static condition, the reaction products were allowed to accumulate in the corrosion cell. Determined by the change in reflection intensity of the S peak, the extent of film formation is greater with the replenished condition at any exposure time by a constant factor of approximately 2 as shown in Fig. 34.

To better understand the corrosion behavior under a variety of corrosion conditions the effects of cell volume, pH and HF acid treatment, and desiccator exposure on the reflection spectra are given in Figs. 35 and 36. The change in the morphology of the corroded glass surface is illustrated in Fig. 37.

Discussion

Figure 31 shows that the sequence of spectral changes due to corrosion of 33L by initially neutral water and 100% relative humidity is identical. However, the kinetics of

Fig. 34. Comparison of the extent of reaction, determined by the magnitude of the stretching peak reflectance (S), for 33L glass exposed to water under static and flowing conditions.

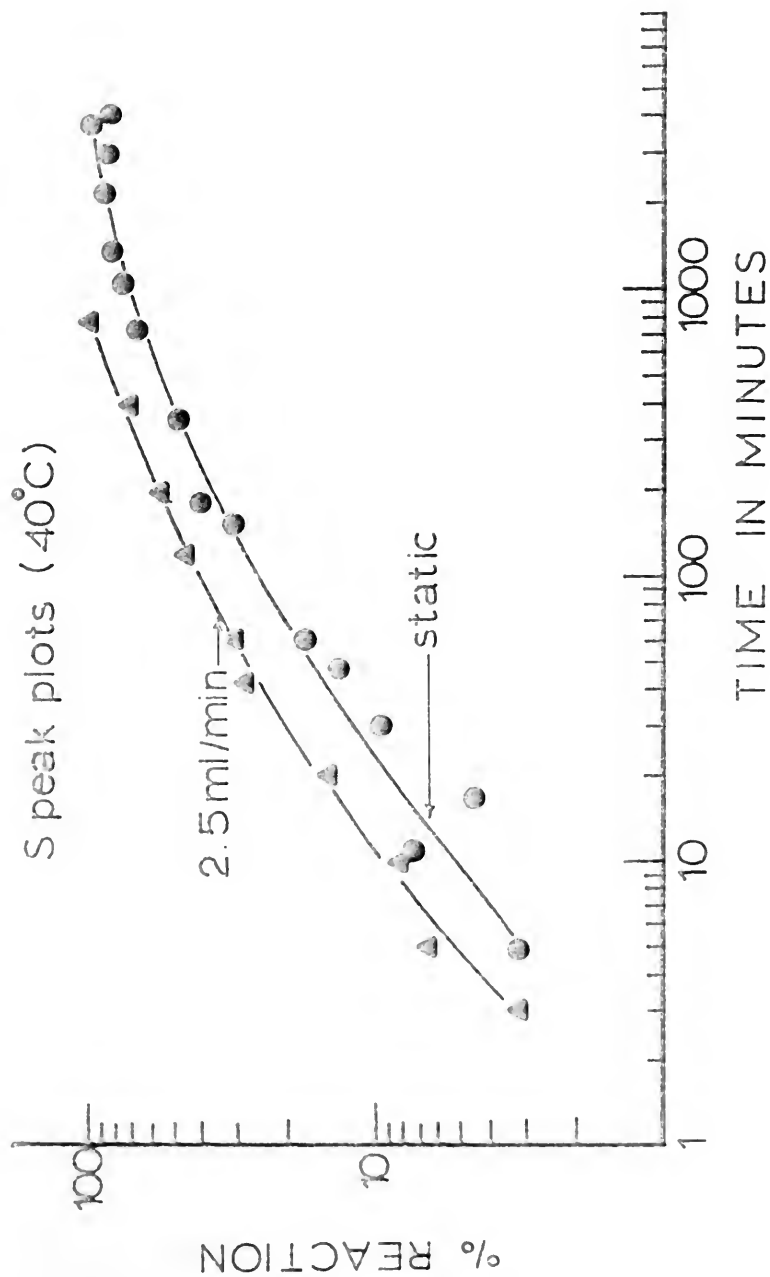


Fig. 35. Changes in infrared reflection spectra upon exposure of 33L to water containing corrosion cells of different volumes and to the residual water present in a desiccator filled with Drierite.

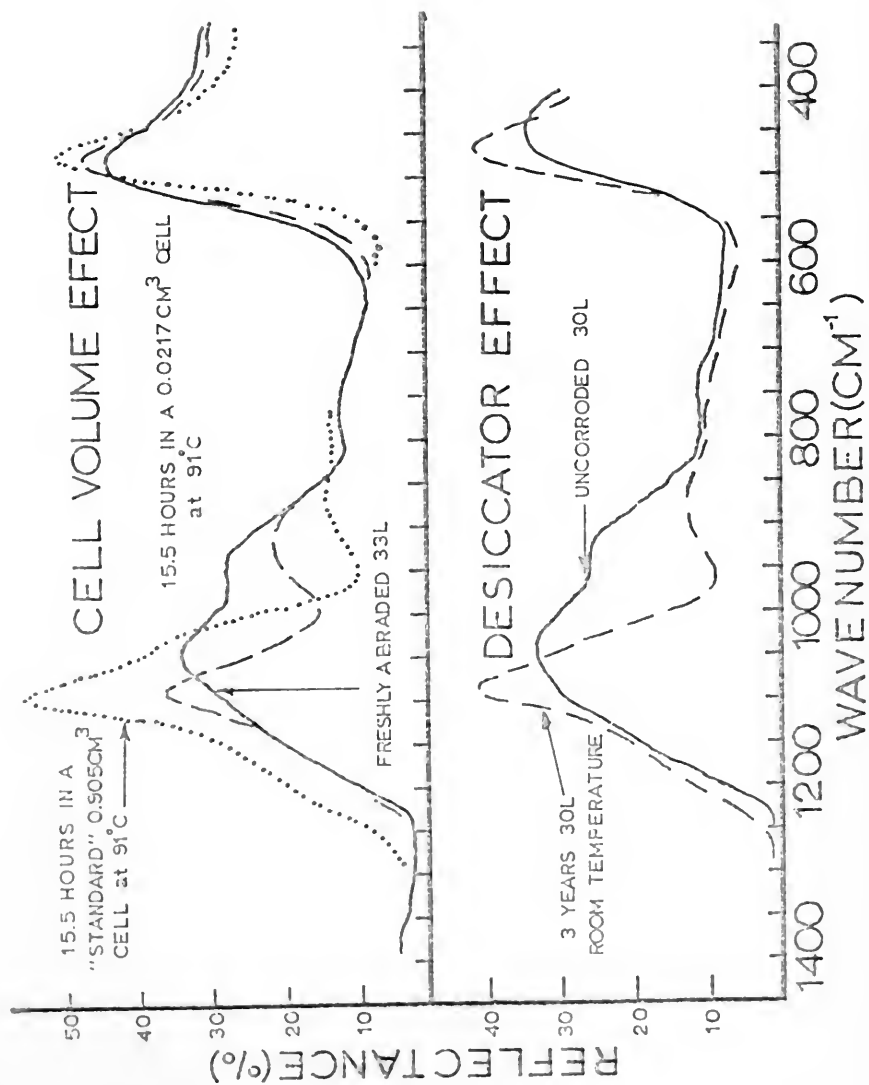


Fig. 36. Changes in infrared reflection spectra upon exposure of 33L glass to hydrochloric acid, to a basic solution used to corrode 33L powder, and to hydrofluoric acid.

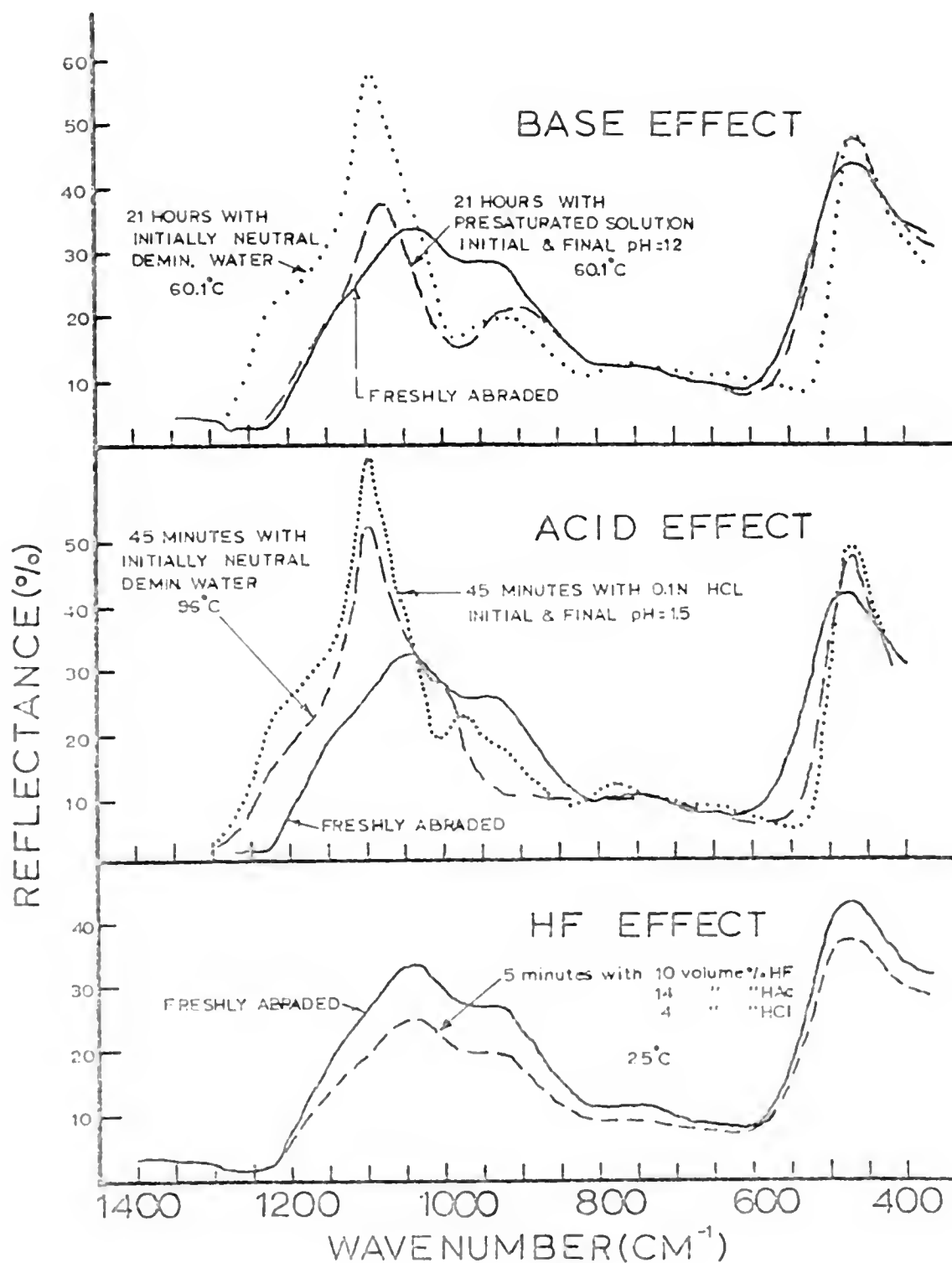
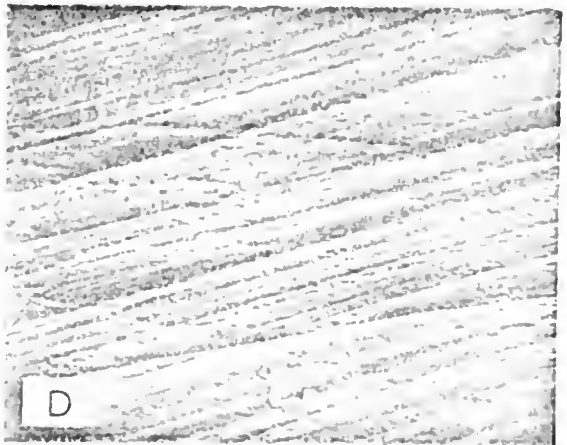
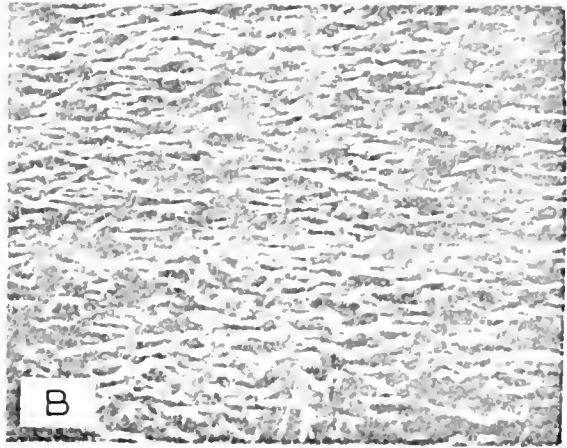


Fig. 37. S.E.M. micrographs of 33L glass having the following corrosion histories:

- A. freshly abraded with dry 600 grit SiC
- B. 4.5 hours with 0.9 ml static water
- C. 120 hours with 0.9 ml static water
- D. 216 hours with 0.9 ml static water
- E. 195 hours with 100% R.H.
- F. 239 hours with 100% R.H.

The corrosion temperature was 23.5°C and all surfaces were initially abraded with dry 600 grit SiC.



the two environments differ considerably. The change in the S peak due to the 100% R.H. treatment has an incubation period of 1,000 minutes before a measurable change occurs. After the incubation period, the film formation proceeds more rapidly than the corresponding reaction due to static liquid water exposure. Since the glass samples were held in a vertical position during the 100% R.H. treatment, liquid water condensed on the glass surface and ran off, leading to a constantly replenished situation with a very small volume of solution exposed to the glass surface at any time.

Various aspects of the complicated corrosion condition associated with the 100% R.H. attack were studied separately. Decreasing the solution volume, for instance, decreases the rate of film formation, Fig. 35A. On the other hand, Figs. 34 and 36A show that replenishment of the corrosion solution increases the extent of film formation, but does not appear to alter the slope of the S plot, the curves in Fig. 34 remaining parallel. Thus the 100% R.H. reaction behavior is only partially explained by cell volume and solution replenishment effects; the rapid film-forming rate after the incubation period is not explained by either.

One indication of the actual mechanism for the 100% R.H. is the change in the NSL peak during the incubation period. Figure 31 shows that roughly 20% of the total reaction extent for the NSL peak occurs before any increase appears in the S peak. This decrease is due to the number

of silicon non-bridging oxygen bonds associated with lithium ions decreasing during the water vapor attack, in turn due to the loss of lithium ions from the original glassy network.

It is known that the glass corrosion reactions involve the formation of silicic acid by the replacement of alkali ions in the glass by protons from the corrosion solution.⁽⁵⁴⁾ It is also known that the monosilicic acid thus formed, H_4SiO_4 , is unstable in the solid state, polymerizing rapidly to form chains, rings, and eventually three-dimensional gel structures.⁽²⁾ The polymerization results in the expulsion of water from the structure, the formation of silicon-oxygen-silicon bonds, and often results in a net contraction of the gel structure, depending on the amount of porosity produced. When solutions containing high concentrations of alkali ion are involved in the polymerization, these alkali ions become trapped in the gel structure.^(2,15)

The effect of contraction of the corrosion layer, especially on drying, is to increase the concentration of silicon-oxygen-silicon bonds at the corroded glass surface. The effect of the lithium ions trapped in the gel, on the other hand, will be to lower the surface silica concentration.

In light of this knowledge, it appears that during the 100% relative humidity exposure the lithium ions removed from the original glass structure by the ion exchange reaction migrate to the gel-air interface. Since, initially, the corrosion solution concentration of lithium ions is

quite high, the alkali ions remain in the gel and the silica concentration of this gel, as measured by the reflection spectra, does not increase. The number of silicon non-bridging oxygen bonds associated with an alkali ion, however, decreases during the ion exchange process, resulting in the observed NSL peak change during the incubation period.

With successive condensations and run-offs during the 100% R.H. exposure, the surface alkali ion is carried away from the gel and the silica concentration of the gel increases. This increase is more rapid since the rate-controlling step is the removal of alkali ion from the porous gel rather than the diffusion of alkali ion through the glass to the surface.

During corrosion by a larger volume of water, the limitation on alkali removal is less severe and both gel formation and alkali release into solution occur simultaneously at a rate determined by the diffusion of alkali ion through the glass. This is expected because the transition of alkali ion from the uncorroded glass to the surface gel should not be strongly dependent on the concentration of alkali ion in the corrosion solution.⁽¹⁵⁾

Hydrothermal treatment at 100% R.H. produces a crystalline product rather than the gel structure formed at lower temperatures (Fig. 32 and Table 2). Water can increase the mobility of atoms in glassy networks as found by Morey,⁽⁶³⁾ who observed a 544°C decrease in the melting point of a potassium disilicate glass under the influence of a

hydrothermal treatment. It is therefore likely that the hydrothermally induced crystallization reported in this work is due to a lowering of the temperature required for crystallization. An alternative explanation is a solution and redeposition mechanism. Further work is required to distinguish between these two possible mechanisms.

The corrosion of 33L at a relative humidity of 85% proceeds much more slowly than the 100% R.H. exposures. It is so slow there is some question as to the IR spectrum of the end point of this reaction. The lack of an apparent S peak increase in Fig. 33 makes one suspect that, although a gel is formed, there is sufficient lithium ion concentration in the gel to prevent an increase in surface silica concentration.

Since the 85% R.H. corroded samples appeared rough to visual inspection, the effect of light scattering on the infrared spectrum of 33L was explored by subjecting an untreated 33L sample to a standard electron microscope acid etching solution of 10% HF, 14% HAc, and 14% HCl.⁽⁶⁴⁾ The results of this treatment, shown in Fig. 36C, indicate that the shape of the reflection peaks remains the same with increasing surface roughness with only the value of reflectance decreasing. In contrast, after the 85% R.H. treatment changes in the shape of the spectral band which appears (Fig. 30) indicate a net change in the chemical makeup of the surface of the glass. Figure 35B shows that, even in a

desiccator jar containing Drierite, given sufficient time (i.e., 3 years), 30L will form a silica-rich film on its surface. In this case, lithium ion forms a powdered carbonate on the surface of the corrosion film. Thus, although the kinetics differ greatly, the spectral changes which take place under the extreme differences in corrosion condition discussed in this work are quite similar.

The increased scattering of light due to 85% humidity exposure indicates a change in the glass surface morphology during corrosion. This sequence of change, Fig. 37B, shows there is an increase in the initial surface roughness due to dissolution of active glass produced by the 600 grit grinding process used to prepare the surfaces. In the last stages of attack (Figs. 37D and F), both the water and 100% R.H. treatments appear to form a powder in the pores remaining on the glass surface. This powder is apparently a silica gel which has been redeposited from solution, as it shows no sign of crystallinity in either its infrared reflection spectrum or its x-ray diffraction pattern.

The correspondence between the infrared reflection spectrum and the surface morphology seen in this work only appears to hold for corrosion at the same temperature. The microstructures presented in Chapter IV are quite different despite similar infrared reflection spectra. Thus, both the composition profile and its morphology must be determined independently to define the state of corrosion of a glass surface.

As expected from the equilibrium equations presented in Chapter IV, the exposure to basic (Fig. 36A) and acidic (Fig. 36B) pH solutions decreased and increased the rate of film formation, respectively, while the rate was also increased by replenishing the attacking water solution. Decreasing the corrosion cell volumes decreased the rate of film formation, partially explaining the decreased film-forming rate with relative humidity exposures as compared with water exposures. In addition, it was shown that 33L forms silica-rich films under conditions where the expelled alkali ion cannot be taken into solution (i.e., in relative humidities less than 100%).

Conclusions

Silica-rich films form more readily in acidic solutions and under replenished conditions than in basic solutions and with static conditions. In a static aqueous environment, a decreased cell volume for the same surface area of the corroding glass produces a decreased rate of silica-rich film formation. A small cell volume is a model for relative humidity exposures, e.g., the same reactions take place, but at a slower rate.

The amount of water present determines the kinetics of the corrosion process and the extent of alkali release from the silica gel layer formed. Even with the small amount of water present in a desiccator, a reaction occurs after

sufficient time. In a 100% relative humidity treatment, where a small amount of water continually condenses on the glass surface and runs off, the rate of film formation is slow at first compared with static water rates. After an incubation period the rate of attack at 100% relative humidity is greater than with a static water attack, leading to an equivalent end-point of film formation.

Hydrothermal treatment causes crystallization of the glass at a temperature which is much lower than required without the presence of water. Treatment of the glass surface with a standard microscopic etching solution shows no observable change in the composition of the glass surface, but does increase its roughness. Exposure to film-forming aqueous solutions also produces pits in the glass surface as seen in scanning electron micrographs.

CHAPTER VI

SURFACE ROUGHNESS EFFECTS ON GLASS CORROSION

The mechanical strength of a glass and its resistance to corrosion are both influenced by surface roughness. Surface flaws act as stress raisers⁽²²⁾ and the glass composition of the crack tip experiencing the greatest localized stress will be most important in determining the mechanical behavior of the glass. Water reaction at the crack tip alters the composition locally and can accelerate crack propagation.⁽⁶⁵⁾ The size of surface flaws is increased and their shape is altered by the corrosion process,⁽⁶⁶⁾ which influences mechanical behavior and the development of films on the glass surface. In order to better understand the various surface flaw-environment effects of bulk glass surfaces, the corrosion of a binary 33 mole % Li_2O -67 mole % silica glass is studied as a function of surface roughness. This glass is chosen because of the simplicity of interpreting compositional changes in a binary glass, and extensive recent studies have shown its corrosion response to be similar to scratched commercial soda-lime-silica glasses.

Little is known about the influence of roughness on corrosion behavior from direct experimental evidence, but

investigations by other workers in related areas indicate the probable nature of this effect. El-Shamy and Douglas,⁽¹⁵⁾ for instance, demonstrated that alkali ion release does not seem to be affected by the ratio of corrosion solution volume to the sample surface area. On the other hand, a decrease in this ratio increases both the release of silica and the corrosion solution pH. In addition, several workers have reported an enhanced solubility of silica powder with decreasing particle size.^(67,68)

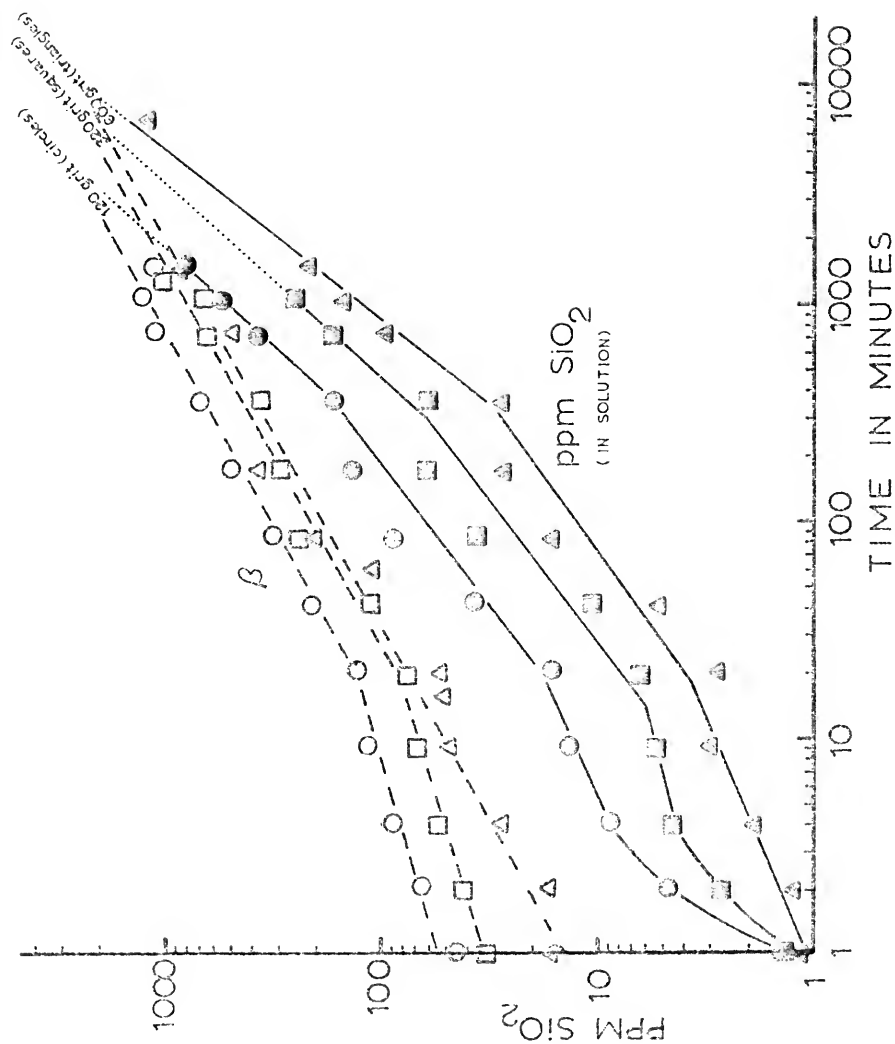
The analysis of solution concentrations used in this study follows the procedure developed in Chapter IV. Briefly, the amount of silica which would be in solution if there were no selective leaching of ions, called the balanced silica or β , is calculated from the lithium ion in solution and the ratio of alkali to silica in the initial glass. The difference between this value and the amount of silica which does actually dissolve is called the excess silica or ϵ and can be related to the amount of silica which is available to increase the silica concentration at the corroded glass surface. Finally, a parameter, α , defined by Shmidt,⁽⁵⁶⁾ is also followed as a function of corrosion time. This parameter is 1 for total dissolution and 0 for the complete selective leaching of only one ion.

Results

Figure 38 shows plots of the silica in solution and the balanced silica (β) for the 120, 320, and 600 grit surfaces investigated. The qualitative behavior of the β and solution silica pairs appears to be the same for all three surface roughnesses with the silica concentration curve converging on the β curve in each case. Each solution silica curve appears to have three portions with breaks at 20 minutes and 250 minutes. These breaks are independent of sample preparation. The actual intersection of the solution silica and β curves is known to not take place in this particular glass. The two curves converge rather than intersect, resulting in a small residual difference between the two curves which can be detected using infrared reflection spectroscopy. This detail does not affect the arguments used in this chapter.

In Fig. 38 both the 320 and 120 grit β curves have breaks at short times in contrast to the β curve of 600 grit. This deviation from the linear behavior seen at longer times is in the direction of higher initial lithium release. There are also corresponding higher solution silica values during this initial time period which are not seen in the 600 grit samples. Both the β and solution silica curves have increasing values with increasing surface roughness at any corrosion time, the difference being greater for the solution silica curves.

Fig. 38. Variation of β and concentration of dissolved SiO_2 with corrosion time for 33L glass abraded with dry 120, 320, and 600 grit SiC.



For evaluating the curves in Fig. 38, the ratio (α) and difference (ϵ) of each pair of curves have been computed and plotted in Figs. 39 and 40. The higher initial β values seen in Fig. 38 for 320 and 120 grit samples lead to corresponding breaks in the behavior of ϵ as seen in Fig. 39. At longer times ϵ curves are seen to have maximum values and to cross at approximately 1,000 minutes of corrosion time.

The α curves break at corrosion times corresponding to the solution silica curves seen in Fig. 40. Again the 120 and 320 grit samples behave in a different manner than the 600 grit samples for corrosion times less than 20 minutes. The samples with rougher surfaces have a non-linear α behavior in this initial corrosion region with the roughest surfaces having the lowest value of α . The curves cross at 3.5 minutes after which the highest α values are observed for the roughest surfaces. Since β and solution silica (Fig. 38) converge rather than intersect, the value of α does not extend to unity as discussed previously.

In addition to the concentration of alkali and silica in solution, the pH of the corrosion solution was recorded and the results are given in Fig. 41. Again the 320 and 120 grit curves are quite similar; so similar, in fact, that no attempt is made to distinguish between them. The pH curve from the 600 grit sample, on the other hand, follows an entirely different path. Also of interest is the scatter for the 320 and 120 grit samples which is not present to the

Fig. 39. Variation of ϵ with corrosion time for 33L glass abraded with dry 120, 320, and 600 grit SiC.

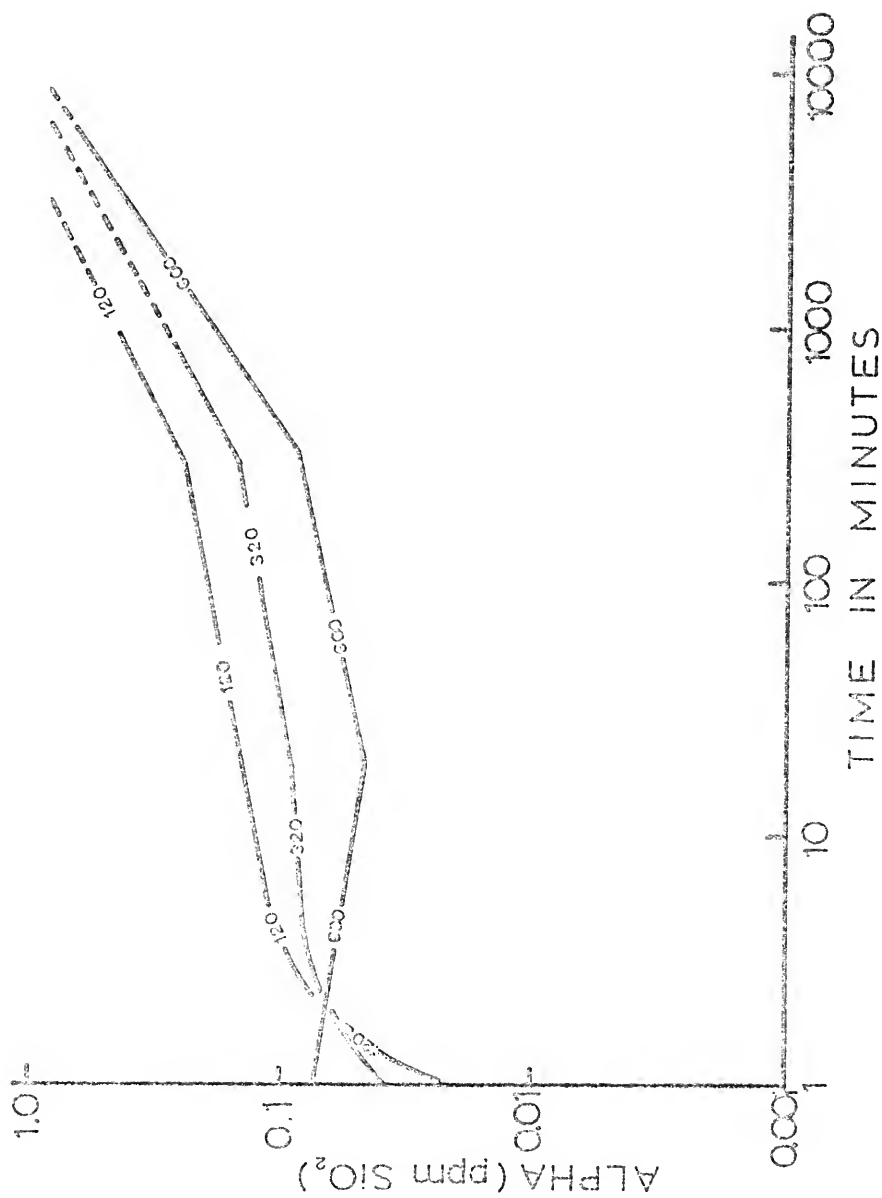


Fig. 40. Variation of α with corrosion time for 33L glass abraded with dry 120, 320, and 600 grit SiC.

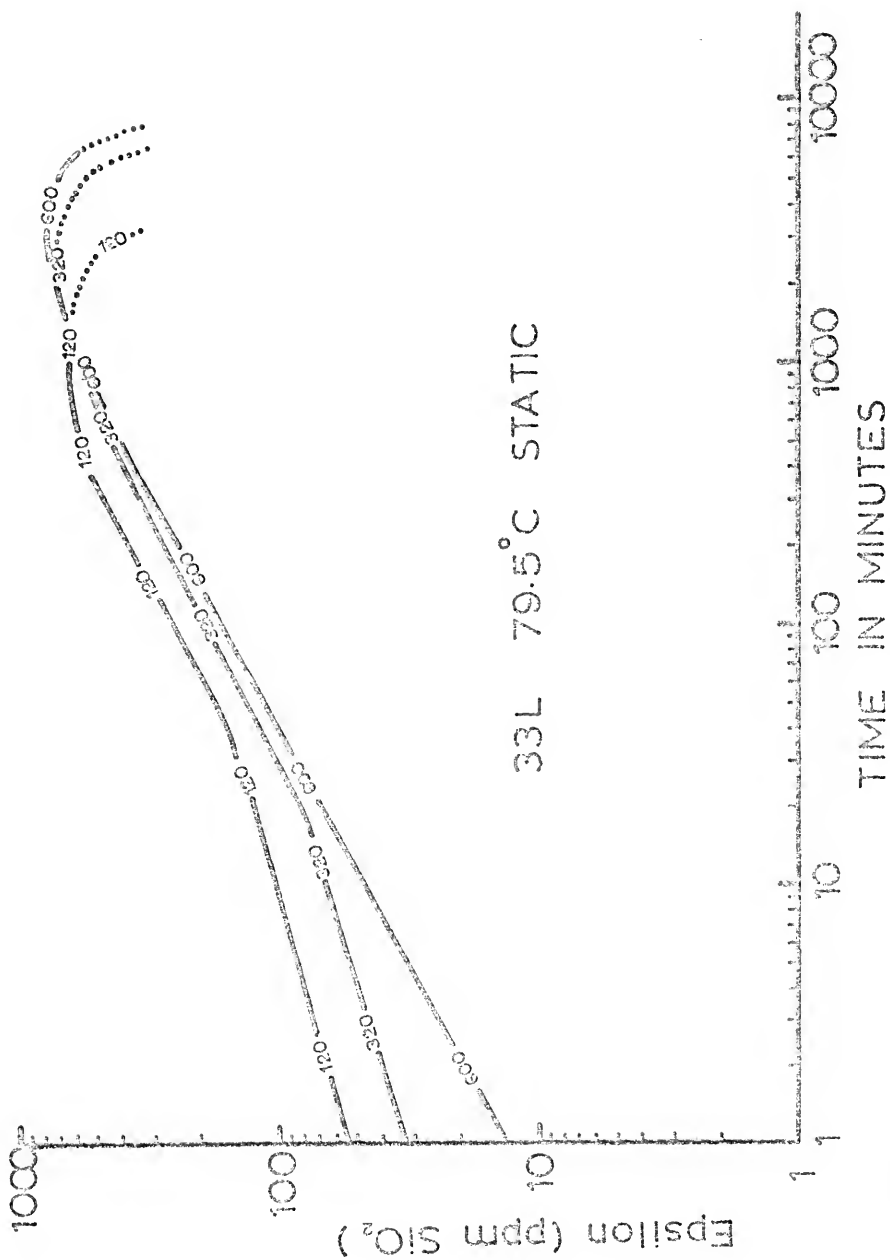
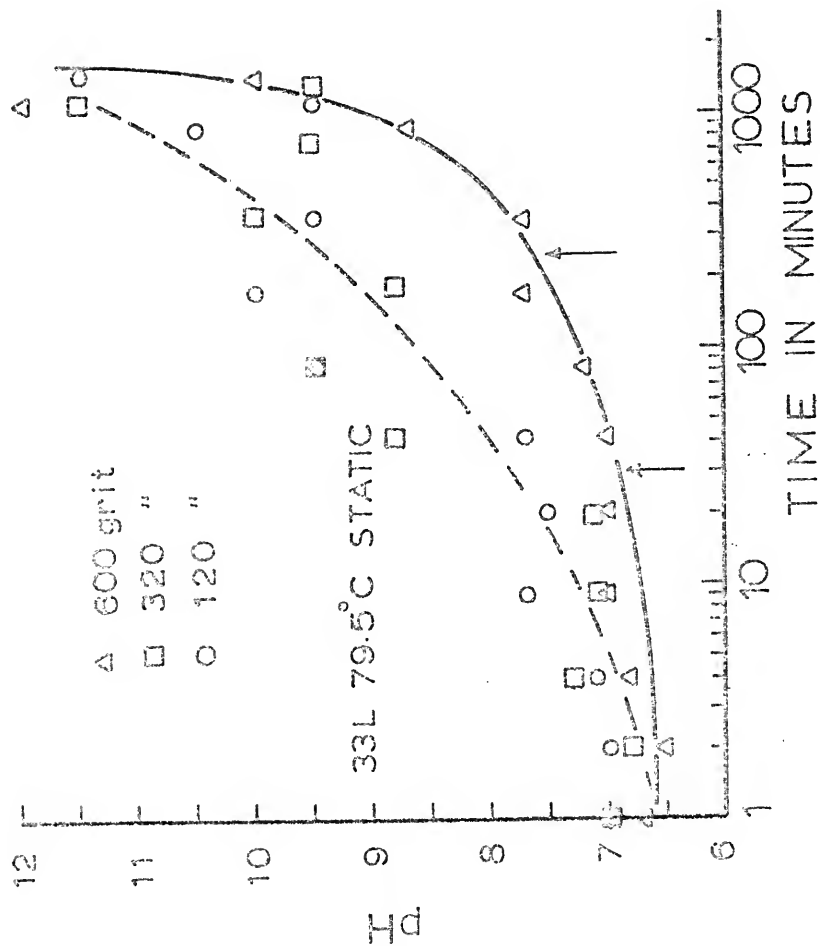


Fig. 41. Variation of pH with corrosion time for 33L glass abraded with dry 120, 320, and 600 grit SiC.

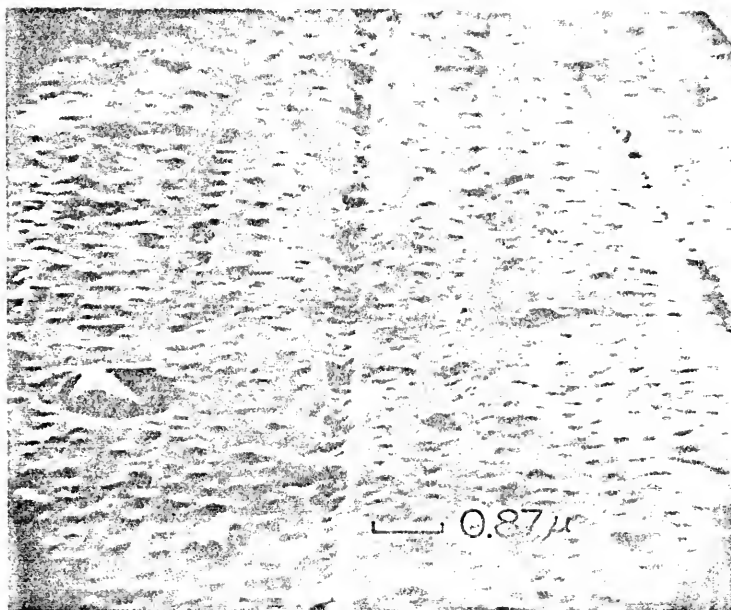


same extent in the 600 grit pH curve. This scatter is not seen in the corresponding 320 and 120 grit curves in Fig. 38 for solution silica and β .

The 600 grit curve of Fig. 41 can be divided into regions having boundaries corresponding to the breaks of the solution silica curves (Fig. 38). For corrosion times less than 20 minutes the pH is relatively independent of corrosion time. At roughly 20 minutes the pH increases slightly with corrosion time to 250 minutes when the rate of increase becomes much more rapid. The equilibrium pH for 33L is 12 and once this value is reached the pH remains constant with corrosion time. The large amount of scatter for the 120 and 320 grit curves does not permit the same division into corrosion regions to be made; however, these curves have consistently higher values than the 600 grit curve and reach the equilibrium pH of 12 in approximately the same time.

Figures 42, 43, and 44 are micrographs of corroded and freshly abraded samples for the three surface roughnesses. A nominal magnification of 10,000X was used for all samples. The polystyrene gage ball seen on the uncorroded 320 and 120 grit surfaces is 0.87 microns in diameter. The areas chosen for the corroded and non-corroded comparisons are not from the same sample, but from representative areas of different samples. The corrosion condition, 1,020 minutes at 79.5°C, corresponds to a time where the three ϵ curves of Fig. 40 intersect. In the corroded sample with the 320 grit

Fig. 42. S.E.M. micrographs of freshly abraded and corroded 33L glass. The initial surface was abraded with dry 600 grit SiC and the corrosion treatment was with static water at 79.5°C in a 0.9 ml cell.



FRESHLY ABRADED

CORRODED

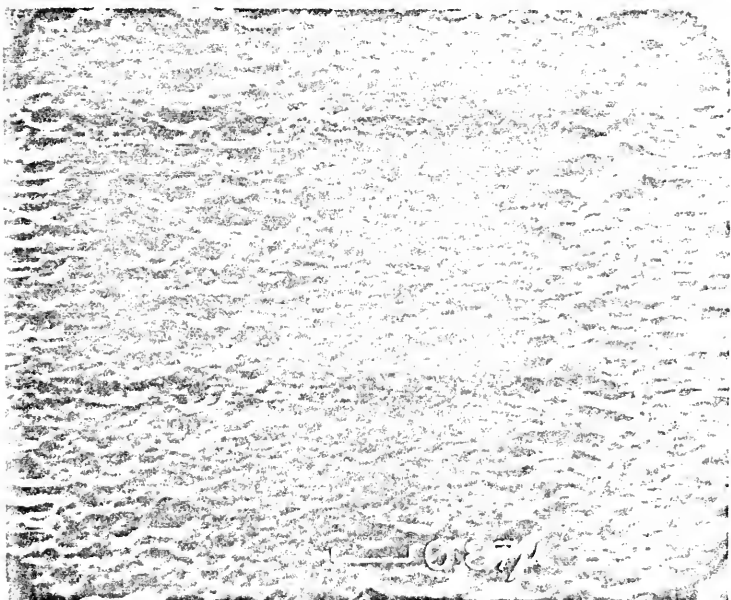


Fig. 43. S.E.M. micrographs of freshly abraded and corroded 33L. The initial surface was abraded with dry 320 grit SiC and the corrosion treatment was with static water at 79.5°C in a 0.9 ml cell.



FRESHLY ABRADED

CORRODED

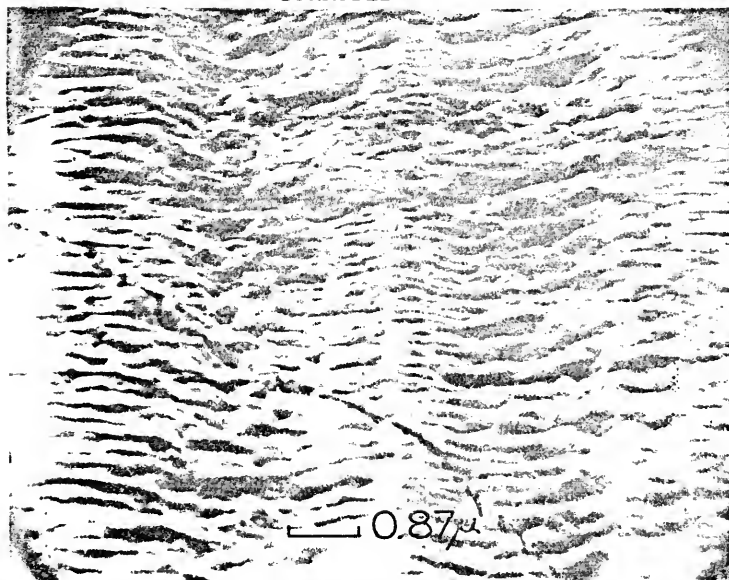
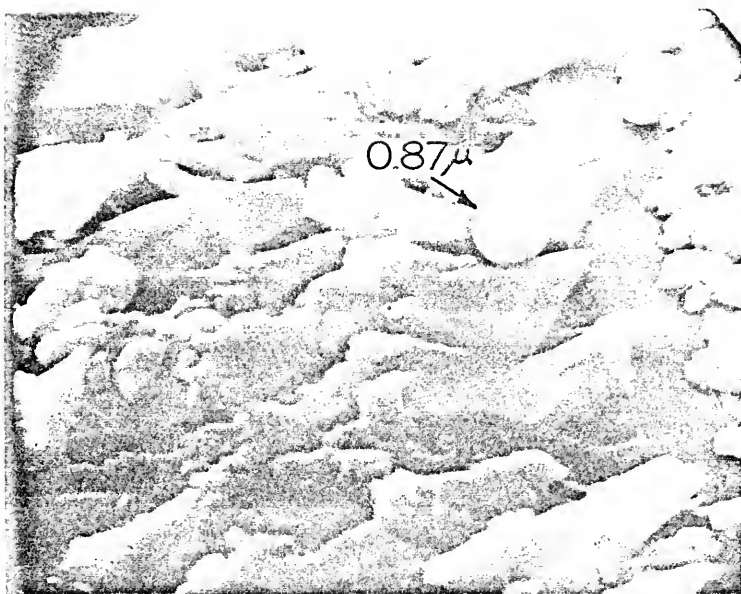
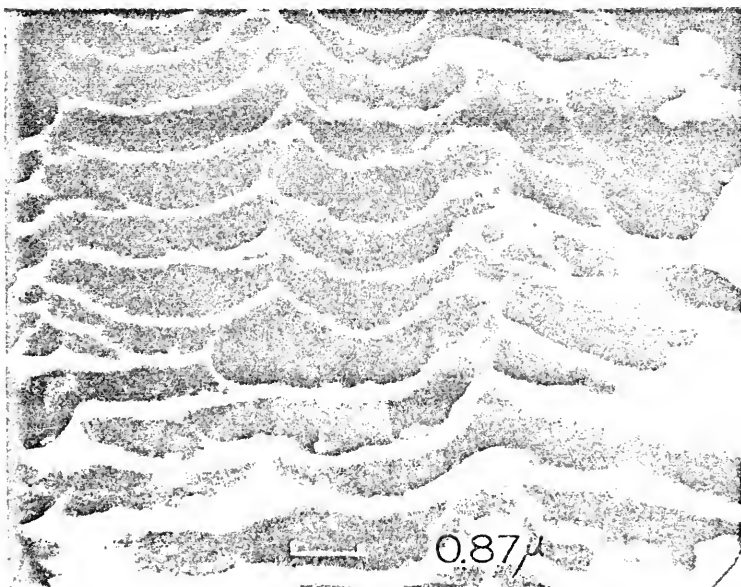


Fig. 44. S.E.M. micrographs of freshly abraded and corroded 33L glass. The initial surface was abraded with dry 120 grit SiC and the corrosion treatment was with static water at 79.5°C in a 0.9 ml cell.



FRESHLY ABRADED

CORRODED



surface (Fig. 43A), a drying crack is seen to transverse the micrograph. This is unusual behavior for 33L, but is quite common in soda-silica glasses.

The micrographs of the freshly abraded 320 and 120 grit surfaces (Figs. 43A and 44A) have protrusions along the scratches (running vertically), while the 600 grit surface (Fig. 42A) lacks this feature. During the corrosion process the protrusions break off, leading to the formation of holes (Figs. 43B and 44B) in the surface of the glass. Similar holes form in the 600 grit sample (see Fig. 42B), but both the protrusions and the holes formed are less pronounced.

Discussion of Results

The initial rate of silica release (Fig. 38) for corrosion times less than 3.5 minutes is greatest for the roughest surface (120 grit). However, the rate of release of lithium ions, determined by the slope of the β curve, was less for rougher surfaces even though the magnitude of lithium ion loss was greater. This behavior is due to the breaking and subsequent dissolution of the protuberances shown in Figs. 43A and 44A from the 320 and 120 grit surfaces. Since analogous protuberances are not seen in the sample freshly abraded with 600 grit (Fig. 42A), the dissolved silica behavior of the 600 grit surface seen in Fig. 38 is more regular with three regions of corrosion corresponding to the three regions of pH change. The initially slower

rate of increase of ϵ (Fig. 40) and faster rates of increase of α (Fig. 39) for rougher surfaces can also be explained by the gradual break-off of protuberances and their subsequent dissolution. As these protuberances are exhausted (after about 20 minutes), the ϵ and α behavior becomes more like that of the 600 grit surface.

As shown in Chapter IV, ϵ can be used to measure film thickness if the silica concentration at the film's surface is known. Thus a maximum in ϵ indicates the time when the rate of total dissolution of the glass surface exceeds the rate of selective leaching of alkali. In other words, at maximum ϵ the silica surface film begins to be destroyed rather than being formed. This maximum occurs most rapidly for the roughest surface (120 grit). In addition, the 120 grit maximum occurs at a lower value of ϵ than does the 600 grit maximum. This indicates that the maximum film thickness of the 120 grit surface is less than the maximum thickness of a finer polished surface.

The error in the pH curves from 120 and 320 grit surfaces is due to the irreproducibility of rougher surfaces compared to finer surfaces. Thus, the 600 grit surface yields optimal reproducibility in addition to providing the greatest ease of measurement of surface silica concentration. The lack of correspondence of pH and ion release for the coarser 120 and 320 grit surfaces is probably due to a localized solution concentration effect in the glass pores

coupled with the presence of undissolved glass fragments in the corrosion solution. Thus, under these conditions, pH does not appear to be a sensitive monitor of solution behavior.

Conclusions

A 600 grit SiC polish induces a heterogeneous corrosion attack of a glass surface. Rough surfaces produced by abrasion with coarse 120 and 320 grit SiC grains produce even rougher corroded structures during aqueous corrosion. This behavior was explained by the removal of protuberances from the freshly prepared 120 and 320 grit surface during the corrosion process. While the film-forming behavior is qualitatively similar for the three levels of abrasion studied (120, 320, and 600 grit), the variation of pH with exposure time shows a lack of reproducibility with the two rougher starting materials. This suggests that pH is not an ideal reaction coordinate for use with rough surfaces.

Solution analysis shows that the initial rate of silica-rich film formation is most rapid for the smoothest initial surface (600 grit). After 15 minutes of exposure the rates are similar for all sample preparations. The corrosion of the roughest surface produced the thinnest silica-rich corroded layer. This is due to a higher pH of the corrosion solution being present throughout most of the corrosion

process for 120 and 320 grit surfaces. Thus, the extent of roughness of glass exposed to water influences both the total and relative amount of removal of ions from the glass.

CHAPTER VII

CONCLUSIONS AND NEW STUDIES

The purpose of this study was to develop a systematic approach to be used for corrosion studies on many different glass compositions, with strong emphasis on the changes in physical and chemical structure of the corroded glass surface and its relationship to engineering properties. The information obtained from a complete study using this approach should permit one to better understand many of the results present in the corrosion literature which resist incorporation into a unified body of knowledge.

This purpose was accomplished by developing several new techniques and by applying a variety of established techniques to a single representative glass composition. The initial surface state and corrosion condition were systematically varied to determine the effects of roughness, flow, pH, temperature, relative humidity, and other variables on the kinetics and structures of glass corrosion. The techniques and theories developed to obtain and interpret data concerning the nature of the surface silica gel produced by the corrosion process are general and can be extended to any glass composition or state and any condition of corrosion where the corrosion process alters the infrared spectra.

The automated techniques described in Chapter II can be used as a basis for the design of on-line controls of the surface composition of glass bottles during their production. In addition, all of the techniques, with the exception of the S.E.M. and microprobe studies, require little measurement time per sample and are therefore applicable to systematic studies over wide ranges of corrosion conditions and glass compositions which would be of interest to the glass manufacturer. The infrared techniques can be made still more sensitive to surface reactions by taking spectra at grazing incidence and by ratioing the spectrum of the corroded glass with that of the freshly prepared glass surface.

The structural study described in Chapter III has produced applications which are more general than the area of glass corrosion per se. For instance, the finding that reflectance is proportional to the concentration of the species causing it suggests that infrared reflection spectroscopy could be used to study concentrations of specific bond types in samples which are too thick to permit traditional absorption spectroscopy. In addition, as discussed in Chapter III, both phase separation and the tendency toward phase separation can be detected by observing breaks in reflectance composition plots. The breaks can also be used to detect changes in the environment around a specific vibrational species (i.e., the lithium ion reflectance composition plot around 10 mole % Li_2O in Fig. 18) or the

specific composition of a vibrational species (i.e., the maximum in the NSL plot in Fig. 15).

The results presented in Chapter III permit the interpretation of spectral changes which occur during the exposure of silicate-based glasses to water. The linear relationship that was found between composition and reflectance allows one to follow the kinetics of these composition changes as a function of sample state and corrosion condition. This surface composition was used in conjunction with data obtained from solution analysis and with a model of an idealized silica composition profile to predict the structure of that layer and its effect on further reactions. From such an analysis the greater chemical resistance of 33L compared to 22N was rationalized in terms of a thicker and less coherent gel layer found in the latter. The approach can be extended to other binary and more complicated ternary glass compositions, but in the latter care must be taken to understand the effect of third components on the inherent chemical resistance of the glass apart from the presence of a silica gel layer. The effect could be better understood by a structural study of ternary glasses similar to that carried out in Chapter III on binary glasses. The extension of the work of Chapter IV to other binary and ternary glass compositions is therefore indicated.

Corrosion condition studies of Chapter V indicate that the gel formed on the glass surface during the corrosion

process has an alkali content which is strongly dependent on the concentration of alkali in the corrosion solution. This must be distinguished from the removal of alkali ion from the original glass structure which does not seem to be strongly influenced by the alkali concentration of the corrosion solution. Since the presence of residual alkali ion in the gel will cause a decrease in the chemical resistance and mechanical strength of the gel, the corrosion condition should be most important in determining many of the properties of the glass.

A complete knowledge of the static fatigue behavior of silicate glass would require an understanding of the variation of the mechanical properties of gel layers as a function of alkali ion concentration. In addition, the effect of various corrosion conditions on the structure of the gel layer would be required. A particularly useful aspect of the infrared technique is its sensitivity to both the removal of alkali ion from the original glass structure via the NSR plots and the removal of the alkali ion from the silica gel corrosion layer via the S plots. Since both can be monitored as function of corrosion time (as was done with the static water and 100% relative humidity studies), the formation of gel layers having silica concentrations identical to that of the original glass can be studied. These are the most probable gel structures to be found in the crack tips

of the glass surface where the equilibrium alkali concentration would be expected to be quite high.

In future work the effect of the corrosion conditions studied here on different glass compositions should be explored. In addition, other corrosion treatments designed to increase the chemical resistance of the glass could be studied such as TiCl_4 or SO_2 treatments. The effect of other metal ions on the structure of the silica gel formed during corrosion should also be of interest and could be carried out using the techniques outlined in this dissertation.

The results obtained in Chapter VI indicate that surface roughness will strongly influence the rate of dissolution, the rate of film formation, and the thickness and composition of the film formed. The large influence of roughness on corrosion behavior suggests that roughness must be closely controlled to explore the effects of other sample states and corrosion conditions on the corrosion process.

Since the mechanical behavior of glass should be influenced by the thickness and composition of any silica gel present at crack tips initiating fracture, and since surface roughness was found to influence silica gel formation, it appears that roughness may influence mechanical properties via its effect on gel formation. Gel formation may also be a mechanism for crack tip blunting and the relationships between mechanical properties and gel properties warrant

further study. Additional sample states which could be explored in future work are stress, phase separation, and crystallization.

Besides extending the techniques introduced to other glass compositions and corrosion conditions, other techniques would prove valuable in future corrosion studies. Radioactive tracer techniques⁽⁶⁹⁾ and carbon furnace absorption and emission spectroscopy⁽⁷⁰⁾ would significantly improve the sensitivity of the solution analysis and permit the automated techniques described in Chapter II to be used on glasses having higher chemical resistance. The thickness of the corroded films and the thickness of the glass removed by total dissolution of the glass could be measured using interference microscopy⁽⁷¹⁾ as done previously. Small angle x-ray scattering⁽⁷²⁾ and B.E.T. adsorption studies⁽¹⁶⁾ could be used to determine pore size distributions produced by the corrosion process. Finally, Auger spectroscopy⁽⁷³⁾ could be used to obtain the silica concentration within several atomic layers of the corroded glass surface.

BIBLIOGRAPHY

1. R. J. Charles and W. B. Hillig, Symposium on Mechanical Strength in Glass, Union Scientifique Continentale de Verre, Charboi, Belgium, 1962, p. 511.
2. W. A. Weyl and E. C. Marboe, The Constitution of Glasses: A Dynamic Interpretation, Vol. 3, Part 2, John Wiley, New York, 1967.
3. L. Holland, The Properties of Glass Surfaces, Chapman and Hall, London, 1964.
4. L. L. Hench, R. J. Splinter, W. C. Allen and T. K. Greenlee, J. Biomed. Mater. Res. Sympos., Vol. 2, Part 1, John Wiley, New York, 1971, pp. 117-141.
5. J. G. Vail, Soluble Silicates, Vols. 1 and 2, Reinhold, New York, 1952.
6. L. S. Yastrebova and S. P. Zhadanov, J. Appl. Chem. USSR, Consultants Bureau Transl., 37 [7], 1439 (1964).
7. C. R. Das and R. W. Douglas, Phys. and Chem. of Glasses, 8, 5 (1967).
8. L. Zagar and L. Hartmut, Glastech. Ber., 42 [3], 81 (1969).
9. Yu. V. Rogozhin and L. A. Saconts, Steklo, 1, 64 (1968).
10. F. L. Jones and H. J. Homer, J. Opt. Soc. Am., 31, 34 (1941).
11. W. Geffcken and E. Berger, Glastech. Ber., 16, 296 (1938).
12. W. C. Taylor and R. D. Smith, J. Am. Ceram. Soc., 19, 331 (1936).
13. M. A. Rana and R. W. Douglas, Phys. and Chem. of Glasses, 2 [179], 196 (1961).
14. R. J. Charles, J. Appl. Phys., 11, 1549 (1958).

15. T. M. El-Shamy and R. W. Douglas, Glass Technology, 13 [3], 77 (1972).
16. L. S. Yastrebova and S. P. Zhadanov, Zhurnal Prikladnoi Khimii, 37 [7], 1442 (1964).
17. A. H. Pfund, J. Opt. Soc. Am., 31, 679 (1941).
18. Sc. Anderson and D. D. Kimpton, J. Am. Ceram. Soc., 36, 175 (1953).
19. E. B. Wilson, J. C. Decius and P. C. Cross, Molecular Vibrations, McGraw-Hill, New York, 1955.
20. J. R. Sweet and W. B. White, Phys. and Chem. of Glasses, 10, 6 (1969).
21. W. Vogel, Structure and Crystallization of Glass, Pergamon Press, New York, 1971.
22. R. E. Mould and R. D. Southwick, J. Am. Ceram. Soc., 42, 582 (1959).
23. I. R. Beattie, J. Soc. Glass Technol., 36, 37 (1952).
24. G. Kortum, Reflectance Spectroscopy, Springer Verlag, New York, 1969.
25. N. J. Harrick, Appl. Opt., 10, 2344 (1971).
26. I. Simon, J. Opt. Soc. Am., 41, 336 (1951).
27. M. Born and E. Wolf, Principles of Optics, Pergamon Press, New York, 1965.
28. N. J. Harrick, Internal Reflection Spectroscopy, John Wiley, New York, 1967.
29. I. Simon, Modern Aspects of the Vitreous State, J. D. Mackenzie, ed., Vol. 1, Butterworths, London, 1960, p. 120.
30. G. Andermann, A. Caron and D. A. Dows, J. Opt. Soc. Am., 55, 1210 (1965).
31. C. R. Das, Trans. Indian Ceram. Soc., 24 [1], 12 (1965).
32. A survey of reflection spectra as a function of composition for the binary lithia-silica system has been given by E. F. Chorneva and V. A. Florinskaya in Structure of Glass, Vol. 7, E. A. Porai-Koshits, ed., Consultants Bureau Transl., New York, 1966.

33. J. Wong and C. A. Angell, Appl. Spec. Rev., 4 [2], 155 (1971).
34. J. R. Ferraro, Low-Frequency Vibrations of Inorganic and Coordination Compounds, Plenum Press, New York, 1971.
35. P. J. Hendra and P. M. Stratton, Chem. Rev., 69, 325 (1969).
36. R. J. Bell and P. Dean, "The Vitreous State," in Discussions of the Faraday Society, Butterworths, London, 1970, p. 50.
37. P. H. Gaskell, "The Vitreous State," in Discussions of the Faraday Society, Butterworths, London, 1970, p. 50.
38. D. L. Kinser and L. L. Hench, J. Am. Ceram. Soc., 51 [8], 445 (1968).
39. S. Kumar and A. K. Maitra, Trans. Indian Ceram. Soc., 27, 2 (1968).
40. I. R. Morrison and A. L. Wilson, Analyst, 88 (1963).
41. A. F. Pozubenkov and V. A. Florinskaya, Structure of Glass, 7 (1966).
42. V. A. Florinskaya, Zh. Strukt. Khim., 4, 850 (1963).
43. J. Bock and G.-J. Su, J. Am. Ceram. Soc., 53 [2], 69 (1970).
44. G.-J. Su, N. F. Borrelli and A. R. Miller, Phys. and Chem. of Glasses, 3 [5], 167 (1962).
45. E. F. Cherneva and V. A. Florinskaya, Structure of Glass, 7 (1966).
46. R. J. Charles, J. Am. Ceram. Soc., 51 [12], 631 (1967).
47. R. Hanna, J. Am. Ceram. Soc., 48, 595 (1965).
48. A. R. Tsatses, J. W. Reed and W. M. Risen, Jr., J. Chem. Phys., 55, 7 (1971).
49. G. J. Exarhos and W. M. Risen, Jr., Chem. Phys. Letters, 10, 4 (1971).
50. G. J. Exarhos and W. M. Risen, Jr., to be published in Solid State Communications.

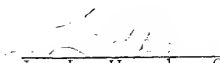
51. R. J. Charles, J. Am. Ceram. Soc., 49, 55 (1966).
52. L. Meites, H. C. Thomas and R. P. Baumann, Advanced Analytical Chemistry, McGraw-Hill, New York, 1958.
53. H. E. Simpson, J. Am. Ceram. Soc., 42, 337 (1959).
54. R. J. Charles in Modern Aspects of the Vitreous State, 1960, p. 23.
55. T. M. El-Shamy, J. Lewins and R. W. Douglas, Glass Technology, 13 [3], 81 (1972).
56. Yu. A. Shmidt, Stroenie Stekla, Inst. Khim. Silikatov Akad. Nauk. S.S.S.R., Leningrad, 1955, p. 319.
57. J. Zarzycki and F. Naudin, J. Chem. Phys., 58, 830 (1961).
58. H. Schroder, Glastech. Ber., 26, 91 (1953).
59. R. W. Douglas and J. O. Isard, J. Soc. Glass Technol., 33, 289 (1949).
60. R. M. Hakim and D. R. Uhlmann, Phys. and Chem. of Glasses, 12 [5], 132 (1971).
61. F. R. Bacon, The Glass Industry, 49 (1968).
62. W. Eitel, Silicate Science, Vol. 2, Academic Press, New York, 1965, p. 487.
63. G. W. Morey and C. N. Fenner, J. Am. Chem. Soc., 39, 1173 (1917).
64. D. L. Kinser and L. L. Hench, J. Mat. Sci., 5, 369 (1970).
65. S. M. Widerhorn, J. Am. Ceram. Soc., 50, 407 (1967); 54 (1970).
66. R. E. Mould in Fundamental Phenomena in the Materials Sciences, Bonis, Fuga and Gilman, eds., Vol. 4, Plenum Press, New York, 1967.
67. R. J. Charles, J. Am. Ceram. Soc., 47 [3], 154 (1964).
68. G. S. Khodakov, Uspekhi Khim., 32 [7], 860 (1963).
69. A. O. Long and J. E. Willard, Ind. Eng. Chem., 44, 916 (1952).

70. A commercial spectrometer of this type is available from Perkin-Elmer Corporation.
71. J. Loffler, Glass Technology, 2, 192 (1961).
72. The presence of small angle scattering in silica gels is demonstrated in the early work of B. E. Warren in J. Appl. Phys., 8, 645 (1937).
73. L. Berrin and R. C. Sundahl in Characterization of Ceramics, L. L. Hench and R. W. Gould, eds., Marcel Dekker, New York, 1971, p. 593.

BIOGRAPHICAL SKETCH

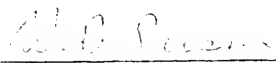
The author was born in Hershey, Pennsylvania, in 1947 and grew up in Rochester, New York, attending John Marshall High School. He was enrolled in Lafayette College for one year and transferred to Alfred University, completing his B.S. degree in ceramic science in June, 1969. While at Alfred, he married his wife, Marilyn. They now have a three-year old son, Brian. Since obtaining his bachelor's degree, the author has been pursuing his doctorate at the University of Florida. His interests include tennis, photography, and hiking.

I certify that I have read this study and that in my opinion it conforms to acceptable standards of scholarly presentation and is fully adequate, in scope and quality, as a dissertation for the degree of Doctor of Philosophy.



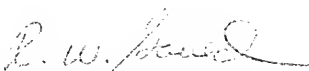
L. L. Hench, Chairman
Professor of Materials Science
and Engineering

I certify that I have read this study and that in my opinion it conforms to acceptable standards of scholarly presentation and is fully adequate, in scope and quality, as a dissertation for the degree of Doctor of Philosophy.



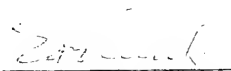
W. B. Person
Professor of Chemistry

I certify that I have read this study and that in my opinion it conforms to acceptable standards of scholarly presentation and is fully adequate, in scope and quality, as a dissertation for the degree of Doctor of Philosophy.



R. W. Gould
Associate Professor of
Materials Science and
Engineering

I certify that I have read this study and that in my opinion it conforms to acceptable standards of scholarly presentation and is fully adequate, in scope and quality, as a dissertation for the degree of Doctor of Philosophy.

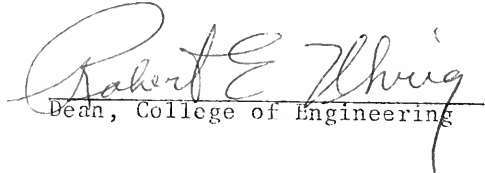


E. D. Verink, Jr.
Professor of Materials Science
and Engineering

This dissertation was submitted to the Dean of the College of Engineering and to the Graduate Council, and was accepted as partial fulfillment of the requirements for the degree of Doctor of Philosophy.

March, 1973

JONE


Dean, College of Engineering

Dean, Graduate School

UNIVERSITY OF FLORIDA



3 1262 08552 7868